GAS-AEROSOL MODEL FOR MECHANISM ANALYSIS: KINETIC PREDICTION OF
GAS- AND AQUEOUS-PHASE CHEMISTRY OF ATMOSPHERIC AEROSOLS

Joseph Lai-man Woo

Submitted in partial fulfillment of the
requirements for the degree of
Doctor of Philosophy
in the Graduate School of Arts and Sciences

Columbia University

2014

ABSTRACT

Kinetic Prediction of Gas-Aqueous-Aerosol Chemistry of Atmospheric Aerosols

Joseph L. Woo

Atmospheric aerosols are a major contributor to the total energy balance of the Earth's atmosphere. The exact effect of these aerosols on global climate is not well understood, due to poorly-characterized compositional variation that takes place over a given aerosol's lifetime. Organic aerosol (OA) species are of particular interest, forming through a myriad of gas- and aerosol-phase mechanisms and contributing to aerosol light absorbance, cloud formation properties, and overall particle lifetime. As different organic species will affect physical properties in different ways, proper prediction of these compounds forming in the aerosol phase is necessary to estimate the net physical properties of aerosols, and subsequently their effects on overall global climate.

Several previous models exist that attempt to predict organic components of aqueous-phase mass in aerosols, with varying degrees of scope of chemistry and range of applicability. Many of such simulations emphasize OA formation via oxidation of gas-phase organic species that results in low-volatility compounds that subsequently partition into aerosols. Other models focus on aqueous-phase processing of semi-volatile and non-volatile water-soluble organic compounds (WSOC's) under cloud water conditions. However, aqueous reactions that occur in atmospheric, deliquesced salt aerosols have recently also been found to be potentially important additional pathway for the creation of additional aerosol-phase organic mass, contributing different products due to the significantly higher inorganic concentrations present under these conditions. It is desirable to incorporate these reactions into analogous predictive simulations, allowing for

the chemistry taking place in small, deliquesced salt atmospheric aerosols to be more accurately represented.

In this work, we discuss a new photochemical box model known as GAMMA, the Gas-Aerosol Model for Mechanism Analysis. GAMMA couples gas-phase organic chemistry with highly detailed aqueous-phase chemistry, yielding speciated predictions for dozens of secondary organic aqueous aerosol-phase compounds under various atmospheric and laboratory initial conditions. From these studies, we find that isoprene-derived epoxides (IEPOX) and their substitution products are predicted to dominate aqueous-phase organic aerosol mass in conditions with low NOx in the atmosphere, representative of rural environments. The contribution of these epoxide species is expected to be high under acidic conditions, though our findings still estimate significant contribution to aqueous-phase organic mass under higher pH or under cloudwater conditions, when acidity is expected to be lower. Under high-NOx conditions typical of urban environments, glyoxal is seen to form the majority of evolved aqueous organic species, with organic acids comprising the bulk of the difference.

We then implement a series of physical property modules, designed to predict changes in aerosol absorbance and surface tension due to bulk concentrations of evolved OA species. Preliminary results from these modules indicate that bulk solution effects of aqueous-phase carbonyl-containing volatile organic compounds (CVOCs) and organic acids are insufficient to significantly affect net aerosol surface tension under any condition tested, implying that observed deviations from pure inorganic aerosol surface tension will arise from surface-aerosol partitioning rather than bulk compositional effects. Light absorption of aqueous aerosols is seen to be driven by dark glyoxal chemistry in deliquesced salt aerosols and organic acids in cloud droplets, though additional information about the absorbance properties of IEPOX and its

derivatives is required to accurately predict the net absorbance of aerosols where these species dominate OA mass.

The predictions as described by GAMMA are comparable to field observations, and give further credence to the significance of epoxide formation as a source of aqueous-phase organic aerosol mass. These results also suggest the relative importance of specific organic compounds in the aqueous phase of both deliquesced salt aerosols and cloud droplets in the atmosphere, which gives direction to the study of compounds whose impact on aerosol physical properties will matter the most. In turn, new kinetic and physical information can be directly applied into the groundwork laid here, allowing GAMMA to provide a continuously better understanding of the effect of organic material on aqueous aerosols and their implicit effect on the environment.

TABLE OF CONTENTS

LIST OF FIGURES

LIST OF TABLES

GLOSSARY OF SYMBOLS AND ACRONYMS USED

α_i	Accomodation coefficient of species i
A	Net aerosol absorbance
$\hat{A}_i$	Specific aerosol absorbance of species i
a_i	Fit parameter for Szyszkowski-Langmuir Equation
a_H^+	Activity of hydronium ion
A_i	Aerosol-Phase Concentration of compound i, as defined by MPMPO/CACM
aL	Fraction of aerosol liquid in the a given air parcel, units cm3/cm3
β	Branching ratio of IEPOX to organosulfate and tetrol substitution products as defined by Eddingsaas (2010)
b_i	Fit parameter for Szyszkowski-Langmuir Equation
BVOC	Biogenic Volatile Organic Compounds
C_i	Gas-phase concentration of species i as defined by Schwarz (1986), units moles/L solution
c_i	Aqueous-phase concentration of light-absorbing material as defined by Beer-Lambert's Law
CCN	Cloud Condensation Nucleus
CVOC	Carbonyl-containing Volatile Organic Compound
γ_i	Activity coefficient of species i in water
D_i	Deposition rate of species i as defined by Schwarz (1986)
$D_{g,i}$	Gas-phase diffusivity of species i
D_p	Particle Diameter
E_i	Emission rate of species i as defined by Schwarz (1986)
G_i	Gas-Phase Concentration of compound i, as defined by MPMPO/CACM
H:C	Hydrogen-to-carbon ratio
H_i^*	Effective Henry's Law Constant of species i
IEPOX	Isoprene-derived epoxydiol
$k_{mt,i}$	Mass transfer coefficient for species i (See Chapter 1)
k	Reaction rate constant of IEPOX-derived substitution products as defined by Eddingsaas (2010)
k_H^+	Acid component of the reaction rate constant of IEPOX-derived substitution products as defined by Eddingsaas (2010)
$k_{sulfate}$	Sulfate component of the reaction rate constant of IEPOX-derived substitution products as defined by Eddingsaas (2010)
$k_{bisulfate}$	Bisulfate component of the reaction rate constant of IEPOX-derived substitution products as defined by Eddingsaas (2010)
MAE	Mass Absorption Efficiency
M_o	Total aerosol-phase organic mass fraction of an aerosol, as defined by MPMPO/CACM
M_w	Molecular Weight of water
MW_{om}	Mean Molecular Weight of bulk organic phase compounds in an aerosol, as defined by MPMPO/CACM
n_s	moles of solute present in a particle
O:C	Oxygen-to-Carbon ratio
OS	Organosulfate species

P_i	Gas-phase concentration of species i as defined by Schwarz (1986), units molecules/cc
p_{Li}^0	Vapor pressure of species i
POA	Primary Organic Aerosol
R	Univeral Gas Constant
RH	Relative Humidity
R_p	Particle Radius
$r_{ij,gas}$	Consumption rate of species i through gas-phase reaction j, as defined by Schwarz (1986)
$r_{ik,aq}$	Consumption rate of species i through aqueous-phase reaction k, as defined by Schwarz (1986)
ρ_w	Density of water
σ	Aerosol surface tension, units dyn/cm
σ_s	Surface tension of aerosol without dissolved organics, units dyn/cm
T	Temperature
SOA	Secondary Organic Aerosol
VOC	Volatile Organic Compound
WSOC	Water-soluble Organic Compound
χ_i	Molality fraction of compound i out of total soluble carbon
ω_i	Thermal velocity of species i

For a complete list of abbreviations for chemical species used by GAMMA, see Appendix A.

CITATIONS OF PUBLISHED WORK

Chapter 2 was previously published as:

"Aqueous-phase Secondary Organic Aerosol and Organosulfate Formation in Atmospheric Aerosols: A Modeling Study" VF McNeill, JL Woo, DD Kim, AN Schwier, NJ Wannell, AJ Sumner, JM Barakat. *Environ. Sci. Technol.*, 46 (15), 8075–8081 (2012).

Chapter 3 was previously published as:

"Aqueous aerosol SOA formation: Impact on aerosol physical properties" JL Woo, DD Kim, AN Schwier, R Li and VF McNeill. *Faraday Discuss*., Advance Article, doi: 10.1039/C3FD00032J (2013).

ACKNOWLEDGEMENTS

To Wanyi, who gave me the push to take charge and trust in my own abilities.

To Andrew, whose boundless potential kept me on my toes and defied every undergraduate horror story I have ever heard.

To the rest of the denizens of McNeill Group that I've had the pleasure of working with, past and present - Coty, Joe, Lum, Zhi, Dame, Giuliana, Dhruv, Mark, Christine, Shitao, Alex, Hannah, and Yanyin - whom are all part of an academic family that was far greater than anything I could have ever dreamed of.

To the members of my committee - Alan West, Scott Banta, Vanessa Ortiz, and Arlene Fiore - for taking the time to help me complete the work written in this text, and for providing me with guidance and support in all of the time that I've known each of you.

To Ed Leonard, who took a chance on a wild card and spent nearly half a decade supplying me with sage advice and crazy stories, even long after I left his group.

To Michael Hill, who fostered my development as an educator and gave me a fantastic example of what great chemical engineering education should look like.

To Bob von Gutfeld, who showed me the light of science firsthand, even if it came from sparks and lasers.

To the other professors of the department - Sanat Kumar, Jeff Koberstein, Jingguang Chen, Venkat Venkatasubramanian, Chris Durning, Ben O'Shaugnessey, Jingyue Ju, and Alissa Park - for tolerating my presence and supporting me for nearly a decade without throwing me out a window.

To Teresa, Krystal, Kathy, Andrew, and Mary Ko, for making all the magic happen that saved my hide more times than I can count.

To my students, past and present, for constantly providing me with purpose in life and instilling me with drive to be the best I can be.

To Catherine, whose optimism and strength throughout her trials and tribulations as one of my students, then as a friend, reminded me to treasure every moment I have with people I love.

To Sara, whose amazing development as a student and fried has further bolstered my desire to try to make a difference with even more students who have that same potential for greatness.

To Roel, who was always there to share a drink, to share a story, to share any burden, and to just do everything he could to help make things better, no matter how bad the situation was for either of us.

To Shuo, who was never afraid to tell me when I was being a fool.

To Vi, who was always happy to partake in some foodie banter and get overcaffeinated with me.

To Helen, who forced me to grow up and learn from every experience, to acknowledge my mistakes while accepting and appreciating my successes.

To Dana, who reminded me that life is always a little better with a little music and laughter, when I had forgotten.

To Liz, Jin, and Candy, who helped me survive my first steps as a chemical engineer.

To the members of the GSA, or ChEGO, or whatever we choose to call it – Kevin, Beyza, Harun, Kristen, Lizzy, Ellie, Damla, Ben, Tushar, and Kevin Dooley – who shared my desire to make our department a better place, in our own way, and for countless happy hours to make things seem just a little less strenuous in the harder points of grad school.

To the other graduate students of the department whom I've had the pleasure of working with, hanging out with, or even just meeting once or twice – for being part of the community that I've loved and grown with for so long.

And most importantly of all, to my family – Mom, Ba, Kim, and my grandparents – without whom I would have never been able to come to Columbia, without whom I would have never have survived graduate school, and whom were always there to support me through every single decision I've ever had to make or any difficulty I've ever had to endure.

To everyone here, and anyone I may have forgotten, thank you. Thank you so much. I love you all.

~JLW

DEDICATION

"The road is ahead of us, so let's start out today.

Just, one more thing... the people and the friends that we have lost,
or the dreams that have faded...

Never forget them."

~ Kazushige Nojima (translated)

CHAPTER 1

INTRODUCTION

Aerosols are an important part of the Earth's environment and contribute strongly to the total global energy balance of the atmosphere. These contributions can arise from direct scattering and absorbing effects, or from indirect effects, such as altering cloud lifetimes and reflectivity. These forcing effects are poorly constrained due to the varied composition of aerosols. A large source of compositional uncertainty is the organic component of these aerosols, which can enter an aerosol through a variety of primary and secondary means. Here, we provide a brief review of atmospheric aerosols, the organic compounds that constitute them, and previous measures that have been taken to try to model these compounds' formation. This chapter then closes with an overview of this dissertation, outlining the purpose of the work herein and its context in the field of atmsopheric modeling at large.

1.1. Motivation to Study Atmospheric Aerosol

Aerosols, defined as small (2nm-20μm) particles in gaseous media, are a ubiquitous part of the Earth's atmosphere, existing in measurable quantities in every environment on the planet. Consisting of any combination of solid, liquid, or complex phases, aerosols can arise from nautral sources like dust storms, volcanic eruptions, or crashing waves, or from anthropogenic sources such as combustion processes or construction of roads and buildings. Due to their small size and propensity to follow air currents, aerosols can persist in the atmosphere as long as approximately seven days. Over the course of an aerosol's lifetime, its net composition and physical properties will change due to reaction, uptake, and volatilization of its constituent species. In turn, these properties subsequently play a factor in a given aerosol's ability to affect visibility (*1*), human health (*2*), and the total global energy balance (*3*).

1.2 Aerosols and the Global Energy Balance

The total global energy balance – the net sum of absorbed and emitted energy by the planet – has a number of contributors that affect its total accumulation. Some of these contributors, such as greenhouse gases, exhibit a positive (warming) forcing effect on the environment. Others, such as planetary surface albedo (the ability for highly light-reflective areas, like ice surfaces of the Arctic, to bounce light away from the planet) exhibit a negative (cooling) effect. The projected sums of these effects have been made by the Intergovernmental Panel of Climate Change, summarized in Figure 1-1. While the forcing effects of many atmospheric phenomena have been estimated with good certainty, the effect of aerosols remains poorly characterized and as a result contributes the largest source of inaccuracy to atmospheric models (Figure 1-1).

Aerosols contribute to radiative forcing in a number of ways. By absorbing or scattering solar radiation, aerosols in the atmosphere can *directly* affect the total amount of solar energy that reaches the planet. The sign and magnitude of this contribution are highly dependent on aerosol composition. Aerosols that are mostly sulfate, for instance, will be more prone to scattering and reflecting light (a net cooling effect), while black carbon aerosols from combustion of biomass and fossil fuels will be highly absorbing, contributing a warming effect on the atmosphere. In addition, non-soot "brown carbon" organic compounds that exist in aerosol phase can also add to the total absorbance of a given aerosol. These species include nitrogen-containing species, oligomeric species (*4–9*) and organic acids (*10*, *11*), varying in abundance based on aerosol origin and age.
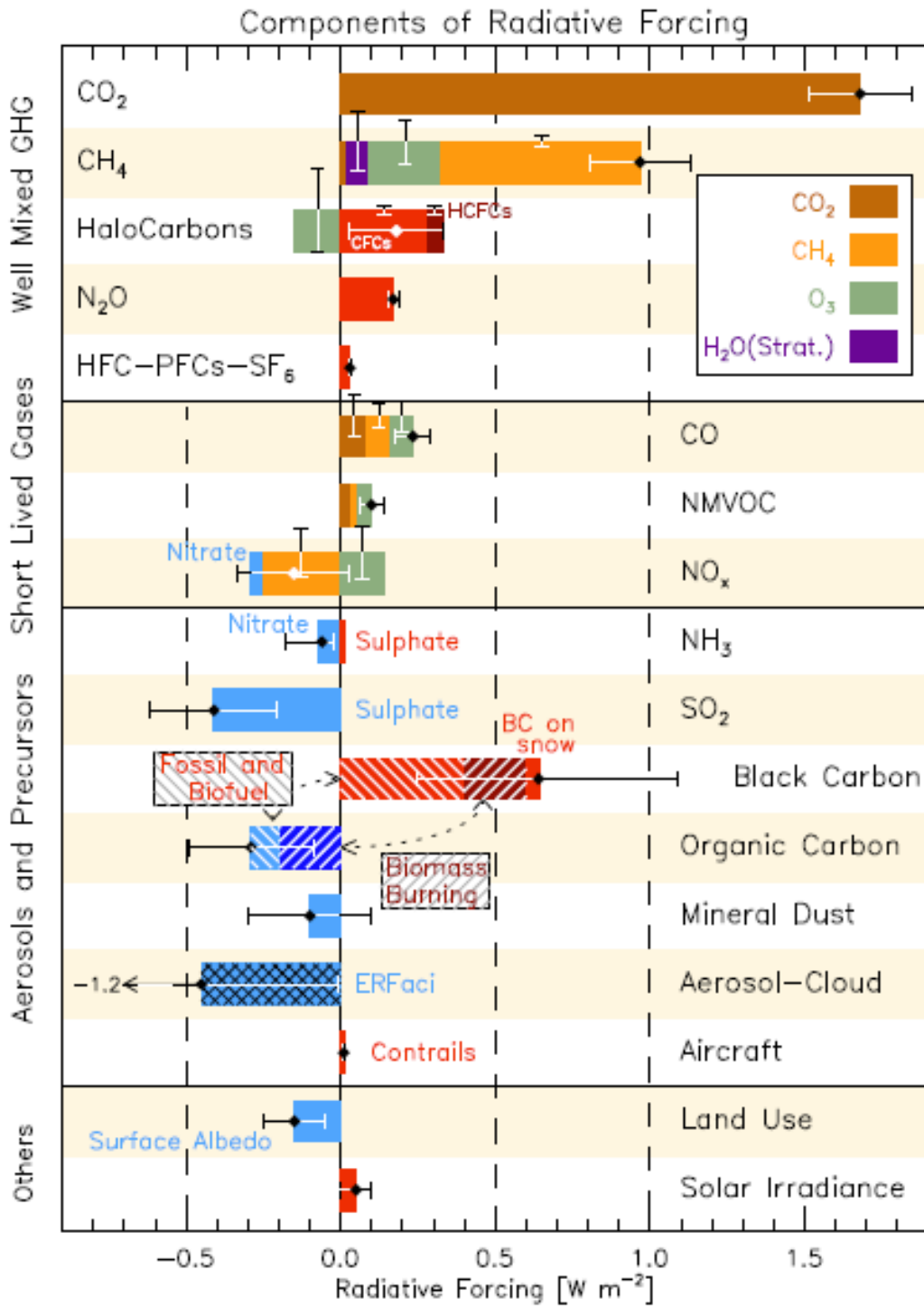
Figure 1-1 - Radiative forcing bar chart for 1750-2011. Aerosols contribute strongly to total radiative forcing, but with huge degrees of uncertainty. [From the Intergovernmental Panel for Climate Change's Fifth Assessment Report (12).]

Aerosols can also contribute *indirectly* to the global energy budget, by affecting the formation and properties of clouds. The material comprising a cloud seed particle will change how likely it is to uptake water, persist in the atmosphere, or reflect light (*13*). The effect of aerosols on clouds is not very well constrained and therefore leads to large amounts of uncertainty about cloud lifetime, albedo, and the net radiative forcing effect of clouds, as can be seen in Figure 1-1.

When an aerosol and its surrounding air are transported into conditions such that local water vapor is supersaturated, spontaneous condensation and uptake of water onto the aerosol will occur. The propensity of an aerosol to form cloud droplets as cloud condensation nuclei (CCN) can be described by Köhler theory (*14*):

$$S = \frac{A}{D_p} - \frac{B}{D_p^3}$$

Such that $A = \frac{4M_w\sigma}{RT\rho_w}$ and $B = \frac{6n_sM_w}{\pi\rho_w}$,

Where M_w is the molecular weight of water, R is the universal gas constant, T is the ambient temperature, ρ_w is the density of water, σ, is the total aerosol surface tension, and n_s is the number of solute moles present in the particle (*15*). Under a given supersaturation S, particles of diameter D_p or larger will activate and form into cloud droplets. As with light absorbance, the contents of the aerosol factors greatly into its net CCN properties; increasing n_s or decreasing σ can both lead to particles of a given diameter activating at a lower supersaturation. The high variability that comes into play here subsequently makes it extremely difficult to accurately predict the exact effect aerosols will have on cloud formation (and consequently its effect on the global energy balance,) thus underscoring the need to properly characterize and understand atmospheric aerosols and their composition.

1.2.1. Organic Aerosols and Aerosol Composition

The exact composition of atmospheric aerosols is highly variable based on season and location. Aerosols are emitted from both natural (wave crashing, dust storms, volcanic eruptions) or anthropogenic (combustion systems, agricultural processes) sources. Regardless of origin, inorganic and organic compounds will both be present in the aerosol phase, with the organic species contributing between 10-90% of total mass. (*16*, *17*) The exact compounds comprising organic aerosol (OA) mass are also extremely diverse, numbering in the hundreds to thousands, and are largely still unspeciated.

While OA can be emitted directly into the atmosphere through both biogenic and anthropogenic sources as primary organic aerosols (POA), the contribution of organics that evolve over the aerosol's lifetime though secondary formation pathways, or secondary organic aerosols (SOA), is also thought to be significant. SOA is usually thought to arise through the gas-phase oxidation of volatile organic compounds (VOCs), which results in lower-volatility organic species that subsequently partition into aerosols (*18*, *19*).
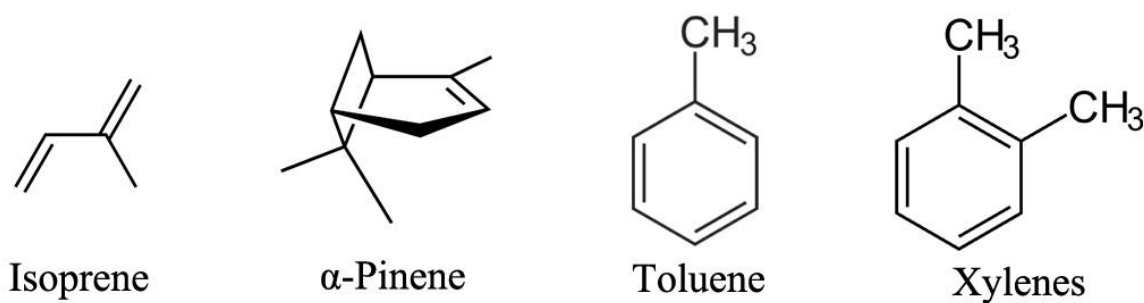
Figure 1-2 - Molecular structure of various volatile organic compounds (VOCs). These gases can be biogenic (isoprene, α-pinene) or anthropogenic (toluene, xylenes) in origin.

Like the compounds comprising POA mass, VOCs that are capable of undergoing these types of reactions can be both natural or man-made in origin. Isoprene is the most common non-methane hydrocarbon in the atmosphere, seen to be emitted in quantities as high as 660 teragrams per year. (*20–22*) Similarly, aromatic species, such as toluene or xylene, are the most prevalent gas-phase hydrocarbon byproducts of automotive fuel combustion, and therefore will be relevant in any urban environment. Many of these organics are highly unsaturated in structure (Figure 1-2), and therefore have several potential reactive sites for gas-phase chemistry.

More recent work has revealed that the semi-volatile oxidation products of these VOCs, as well as VOCs that directly enter into aerosol themselves, can continue to react via aqueous-phase aerosol processing. SOA generated via this family of reactions will also tend to have lower volatilities than their precursors and are expected to remain in the aerosol phase rather than re-partition back into the gas phase (*4–6, 23*). The partitioning of the VOCs that participate in these reactions can occur through both thermodynamic and kinetic mechanisms, which are later described in this chapter.

Exposure to sunlight causes photolytic reactions to occur in both inorganic and organic gas-phase species, leading to a constant presence of radicals in the atmosphere. (*24*) Of these, the hydroxyl (OH) and hydroperoxy (HO_2) radicals will readily interact with nearby organic species, leading to ring-opening, self-rearrangement, and addition of oxygen atoms to total structure. Other inorganic species, such as ozone or nitrogen oxides (NOx), can also participate in similar radical chemistry, although these compounds are more prevalent in urban environments where large amounts of motor vehicle combustion takes place. Radical chemistry can occur in both gas and aerosol phases, acting as a significant source of oxygenation and active group substitution of emitted organic gases and deposited, aqueous-phase semi-volatile organic species alike.
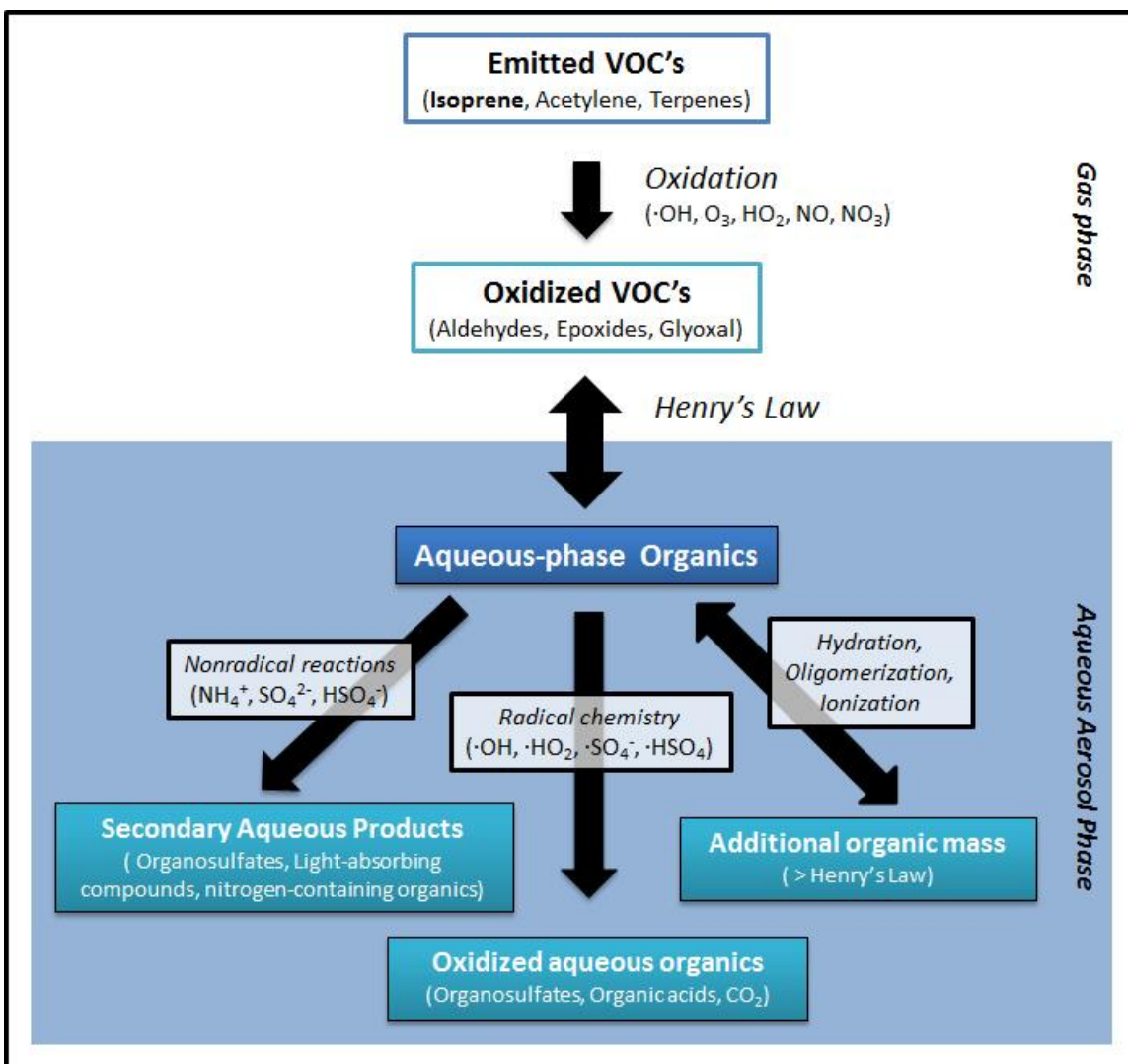
Figure 1-3 - An overview of some gas- and aerosol- phase chemistry that may occur over an aerosol's lifetime.

A major participant in this type of chemistry is glyoxal, as well as similar, small (<3 carbons) volatile carbonyl-containing organic compounds (CVOCs, seen in Figure 1-4). These species have been observed in high quantities in both urban and rural field studies, evolved from bond-breaking mechanisms of isoprene and aromatic compounds (*25*). These compounds are also thought to contribute significant amounts of aqueous aerosol mass, owing to their high solubility

in water and propensity to hydrolize or further oxidize once in the particle phase, facilitating reactive uptake. (*26*, *27*)
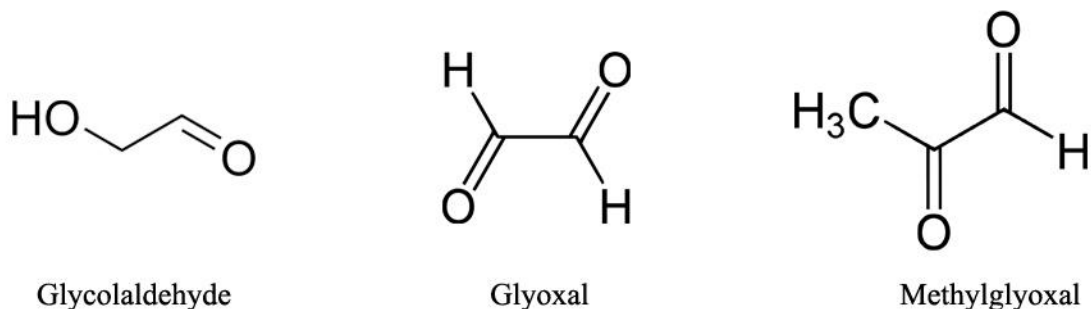
Figure 1-4 - Molecular structure of carbonyl-containing volatile organic compounds (CVOCs).

The chemistry of CVOCs in larger aqueous aerosols, ie. cloud droplets, has been extensively explored, in a number of field (*28*), laboratory (*29–32*), and modeling (*27*, *33–36*) studies. Glyoxal and methylglyoxal can take on additional oxygen and convert carbonyl groups to organic acids. Deviation from modeling results in laboratory studies also suggest the formation of oligomers of these low weight-species when dissociated in water. (*31*)

Our own research group has also performed work with aqueous aerosol mimics containing CVOC species, that suggest cross- and self-reactions between glyoxal and methylglyoxal are possible. (*4–6*) These oligomeric species were seen to be highly light-absorbing, though they were shown to revert to smaller, organic acid species with exposure to ozone or UV light. (*37*) Our group has also found through chamber laboratory studies that methylglyoxal changed the cloud activation properties of aerosols in their own right, without need of further oxidation or oligomerization. (*38*)

More recently, other laboratory studies focusing on photooxidation of isoprene and monoterpene gases have shown significant amounts of polyols (*39–41*) and organosulfate (OS) species (*40–44*) in the particle phase. OS compounds have been considered as potential tracers for SOA formation under acidic conditions, and may also have effects on aerosol surface tension and cloud activity due to their amphiphilic properties. While the formation of sulfate esters has historically been attributed to reactions between alcohols and sulfuric acid (*45*), NMR-based feasiblity studies for these reactions revealed that these mechanisms are negligible in aerosol conditions typical of the atmosphere. (*46*, *47*) Laboratory experiments using controlled photolysis with glycolaldehyde yielded mass spectra consistent with sulfate-substituted derivatives of a number of similar CVOC oxidation products (glyoxal sulfate, glycolic acid sulfate, etc.), suggesting that radical-radical addition of aqueous-phase sulfate and organic radicals also contributes to organosulfate formation (*48*, *49*). However, these products did not completely account for the total organosulfate mass observed, thus requiring other mechanisms to be occuring to completely account for their presence.
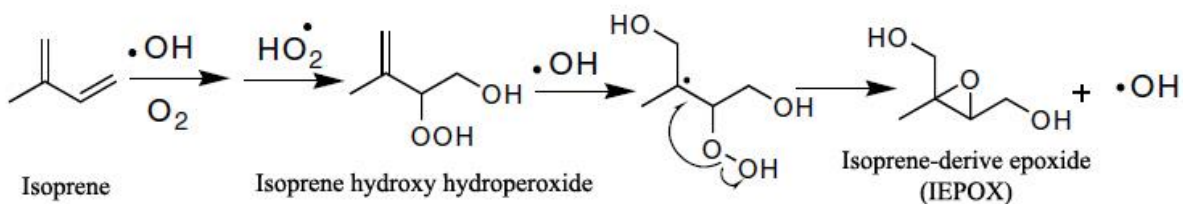
Figure 1-5 - Proposed mechanism for IEPOX formation. (From Surratt 2010 (50))

Under conditions with low amounts of nitrogen-based oxidant gases, the process for formation of larger isoprene-derived OS and polyol species was posited to rely on the reaction of an epoxide intermediate, formed upon exposure to hydroxyl radicals (OH·) and oxygen (Figure 1-5).

Addition of OH· to any of the double bonds on isoprene yields a series of high-yield, hydroxyhydroperoxide formation and decomposition reactions. (*51*) Consistent with OS-generating precursors, the resultant family of epoxides (IEPOX) absorbs readily into aqueous medium, accelerating with increasing aerosol acidity. Epoxide species derived from monoterpenes were also seen to yield increased uptake at higher acidity, through similar mechanisms. (*43*, *44*)
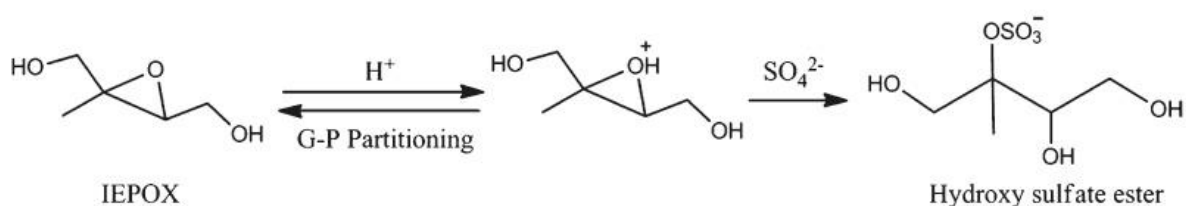
Figure 1-6 – Proposed mechanism for aerosol-phase, IEPOX-derived organosulfates. (From Hatch 2011 (52))

These epoxides, once formed, can then subsequently undergo nucleophilic substitution with sulfate or water and form the observed tetrol and organosulfate species. Given the necessity for a high acidity-environment for these reactions to take place, (*47*) it was posited that these reactions must be more prevalent in deliquesced inorganic seed aerosols rather than cloud droplets, where sulfate and hydronium ion activities are extremely high.

1.3. Prediction of OA Formation

Given the diverse range of chemical reactions occurring in both the gas and aerosol phases in the atmosphere, several mechanistic modeling approaches have been attempted to properly describe these phenomena, as well as the interphase transport of organic species into aerosols. Pankow and Oden developed early gas-aerosol models that used thermodynamic, physical adsorption to describe partitioning between the two phases. The Model to Predict Multiphase Partitioning of

Organics (MPMPO) also implemented this approach to semi-volatile partitioning of organic compounds to discern SOA growth. (*53*) For organic aerosols, the separation between gas and aerosol phase was defined using a partitioning coefficient , *K*, defined as: (*18*, *19*, *54*)

$$K_{om,i} = \frac{A_i}{G_i M_o} = \frac{RT}{MW_{om} 10^6 \gamma_i p_{L,i}^o}$$

Where A_i and G_i are the aerosol- and gas-phase concentrations of a given compound *i*, respectively, M_o is the total aerosol-phase organic mass concentration of the aerosol, MW_{om} is the average molecular mass of the bulk organic phase of the aerosol, γ_i is the activity coefficient of species *i*, and $p_{L,i}^0$ is the vapor pressure of species *i*. R and T are the gas constant and temperature of the system. These models were able to successfully track the evolution of high-mass organic compounds, but do not factor in further aerosol-phase reactions. MPMPO tracked the uptake of several lumped surrogate species for terpene-derived semi-volatile oxidation products based on common general structure and origin species. (*55*)

Later versions of MPMPO also implemented another, simple thermodynamic means of SOA accumulation for systems with aqueous aerosols, using Henry's Law: (*56*)

$$A_i = \frac{G_i a_L H_i}{\gamma_{aq,i}}$$

Here, a_L is the fraction of aerosol liquid in the atmosphere, H_i is the effective Henry's Law constant of species *i*, and $\gamma_{aq,i}$ is the activity coefficient of *i* in the aqueous phase.

The Caltech Atmospheric Chemistry mechanistic model (CACM) implemented several types of gas-phase oxidation reactions, focusing on terpene species and other large (4+ carbon) organics. (*55*, *57*, *58*) The reactions considered were a combination of the general mechanisms

11

implemented by the Statewide Air Pollution Research Center atmospheric chemistry model (SAPRC), which estimated reactions based on general active groups within given organic structures (*59*), and the nearly-completely explicitly defined mechanisms described by the Master Chemical Mechanism model (MCM), which took a brute-force method of approximating every possible iteration of radical oxidant reaction, bond by bond, (*60, 61*) at the cost of significantly high computational load. The gas phase chemistry in CACM has subsequently been coupled with the uptake mechanisms of MPMPO, to approximate SOA mass accumulation from terpene-derived semi-volatile products under laboratory conditions. (*55, 56*) However, reactions pertaining to isoprene and direct uptake of low-weight species into the aerosol phase are not captured in these studies.

The AqChem model compiled carboxylic acid formation reactions observed in cloud droplets (*27, 57*) with mechanisms from the coupled MPMPO/CACM model (*27, 36, 57, 62, 63*). In addition, aerosol-phase oxidation of aldehyde-containing surrogate species from MPMPO is considered. Like previous models, AqChem does not factor in the potential oligomerization effects of dicarbonyl compounds.

AqChem employs a kinetic model of inter-phase transport, first proposed by Schwartz. (*64*) With this approach, the time dependence of specific gas and aerosol species takes on the form:

$$\frac{dP_i}{dt} = -k_{mt,i}a_L P_i + \frac{k_{mt,i}a_L}{H_i^*}C_i + \sum_j r_{ij,gas} + E_i - D_i$$

$$\frac{dC_i}{dt} = \frac{k_{mt,i}P_i}{RT} - \frac{k_{mt,i}}{H_i^*RT}C_i + \sum_k r_{ik,aq}$$

Here, P_i and C_i are the concentration of species i in gas and aerosol phase, respectively. E_i and D_i are emission and deposition rates of species i, and $r_{i,j}$ and $r_{i,k}$ are the rates of formation or

consumption in the gas and aerosol phases. a_L is again the fraction of aerosol liquid in the atmosphere, and H_i^* is the effective Henry's Law constant for i,. The value $k_{mt,i}$ represents a mass transfer coefficient, dependent on aerosol radius, R_p:

$$k_{mt,i} = \frac{1}{\frac{R_p^2}{3D_{g,i}} + \frac{4R_p}{3\omega_i\alpha_i}}$$

$D_{g,i}$ is the gas-phase diffusivity, ω_i is the thermal velocity, and α_i is an accomodation coefficient for species i. R and T are the gas constant and temperature of the atmosphere. By handling uptake as a kinetic process rather than a thermodynamic equilibrium, dynamic effects such as reactive uptake are better represented, as equilibria between hydrated or oligomeric states can change over the lifetime of a simulation. For example, the rapid reversible hydration and oligomerization of glyoxal (*65*, *66*) leads to a disproportionately high level of partitioning for its size, which is then not accurately represented in its contribution to aerosol mass. This approach will yield a more accurate uptake mechanism than the thermodynamic ones used in the past, though it requires more information about the species being tracked.

The previously discussed models are all zero-dimensional, and therefore do not contain any convective or diffusive transport information about the aerosols they are representing. As there also exists a large amount of previously recorded meteorological and spatially defined emission data, the next logical step of progression with these models has been to superimpose their mechanisms into measured or predicted concentration distributions. For example, the EPA's Community Multiscale Air Quality model (CMAQ) is one of the most widely used air quality models, implemented by several agencies for air quality regulation (*67*). CMAQ couples several robust spatial advection, diffusion, and emission models to a suite of chemical transport and

13

reaction modules, yielding concentration profiles of particulate matter and air pollutants over wide ranges of time-scales.

CMAQ's built-in SOA predictions use relatively simplified gas- and aerosol-phase oxidation mechanisms compared to the previously mentioned zero-dimensional models. (*68*, *69*). Like previously mentioned models, lumped surrogate species were employed to represent chemistry, though the criteria for combined classification were somewhat more general by comparison. All long-chain alkanes were treated as a single class (as opposed to being segregated by number of carbons in MPMPO), as were 'high yield' aromatics such as toluene, and 'low yield' aromatics such as xylene, monoterpenes, and sesquiterpenes. Furthermore, gas-phase oxidation from one category of possible semi-volatile species to another (such as isoprene or aromatic species to CVOCs) are not considered, limiting the range of applicability of its implemented chemistry.

However, CMAQ's modular nature allows for easy interfacing of its meteorological information with other mechanistic atmospheric chemistry models. Application of CACM and MPMPO has shown strong improvements to the accuracy of spacial variance of predicted SOA, but still underpredict total measured OA mass compared to observed data. (*36*, *56*)

Similarly, the Geos-CHEM model uses compiled emission, deposition, and chemical information combined with meterological information from the Goddard Earth Observing System (GEOS) of NASA's Global Modeling and Assimilation Office, to create a 3-dimensional, global-scale atmospheric composition model. This model has shown accuracy in predicting and mapping inorganic particulate matter concentrations under a variety of applications, from health quality assessment to long-range forecasting and tracking of specific emission events. (*70–72*) Geos-CHEM emphasizes gas-phase reactions and inorganic inter-phase transport in its models and has

limited scope with respect to the organic chemistry that takes place within its modeled aerosols. The partitioning and SOA mechanisms employed by Geos-CHEM SOA modules (*73*, *74*) assume uptake of organic gas species into only organic-phase aerosols, as opposed to aqueous or mixed-phase particles. Gas-phase chemistry and aerosol uptake of epoxide and CVOC species is included in Geos-CHEM's gas-phase chemistry, but their subsequent aerosol-phase processing is not represented. Like CMAQ, Geos-CHEM can also readily couple with or integrate other chemistry models, to better represent the atmospheric systems they are modeling.

Given the advent of newer uptake and kinetic data pertaining to aqueous aerosol chemistry that is not covered in current models, **it is therefore desirable to develop a model that effectively captures aqueous chemistry and partitioning effects under a wide range of aerosol and atmospheric conditions**. Such a model would account for a wider range of relevant SOA in current multi-scale predictions and could eventually better represent the effect that aqueous-phase organic species have on net aerosol properties, improving predictions of forcing effects due the presence of these compounds.

1.4. Thesis Overview

This work presents a new mechanistic model developed by our research group, GAMMA, the Gas-Aerosol Model for Mechanism Analysis. Using a compiled library of explicit gas and aqueous aerosol phase reactions and a kinetic approach to gas-to-aqueous-aerosol interphase transport, we predict the formation of aqueous-phase SOA mass under a variety of conditions.

Chapter 2 introduces GAMMA and its application to describing the chemistry that occurs as gas-phase organic compounds uptake onto deliquesced ammonium sulfate aerosols. The governing equations and families of reactions implemented into GAMMA are described. Isoprene,

acetylene, toluene, and xylenes are used as precursor organic gas-phase species in these tests, simulating SOA formation over a variety of aerosol pH and ambient relative humidity (RH) conditions. Under rural, low-NOx conditions, we find that aqueous aerosol SOA (aaSOA) mass is mostly isoprene-derived epoxydiol (IEPOX) and its substitution products, occupying 69% or more of total evolved aaSOA over 12 hours of simulated daylight conditions. Under urban, high-NOx environments, where IEPOX is not expected to form, predicted aaSOA is dominated by reversible glyoxal uptake. Organosulfate formation is highest at low pH and RH conditions, when aerosol inorganic concentrations are higher, though its contribution is more significant under low-NOx conditions. As these mechanisms are expected to be important under conditions with high aerosol sulfate loading in rural areas, it is possible that IEPOX-derived organosulfate species (IEPOXOS) can therefore be used as an accurate tracer for aaSOA formation in field studies.

Next, Chapter 3 expands upon the functionality of GAMMA, introducing two modules that connect the formation of aaSOA species to changes in total aerosol surface tension and UV-visible light absorbance. Our results indicate that the formation of carbonyl-derived oligomers and organic acids in bulk aerosol liquid do not significantly affect surface tension, though adsorption of surfactant species at gas-aerosol interfaces may suppress surface tension more than their bulk phase concentration would suggest. Net aerosol light absorption in aaSOA is primarily driven by dark glyoxal chemistry. This chemistry is predicted to be highest under high humidity, high-NOx conditions, and yields highest total absorbance in early morning hours. The predicted wavelength dependence of these simulations is comparable to field data, and predicted mass absorption efficiencies imply that this modeled chemistry is a potential source for aerosol brown carbon in urban environments.

Chapter 4 applies the mechanisms compiled in GAMMA to cloudwater conditions, to compare its gas- and aqueous- phase chemistry to the numerous existing models that represent similar families of reactions. Under high-NOx conditions, cloud chemistry is dominated by glyoxal uptake and its subsequent processing to low-weight organic acids, consistent with findings and predictions of other groups. Under low-NOx conditions, the initial pH of the seed aerosol is seen to play a major factor in the ultimately prevailing chemistry, indicating that IEPOX chemistry can still contribute significant amounts of SOA mass if initial aerosol acidity is sufficiently high. Simulations that alternated between aerosol and cloudwater conditions revealed brief transient periods immediately after drying and activating as gas-aerosol partitioning re-equilibrates. IEPOX derived compounds remain a strong to dominating feature of aerosol SOA when cycled, due to high reaction rates of formation when in aerosol and the high molecular mass of its contributing species. This pathway of OA formation is largely ignored in cloudwater simulations, but can still contribute potentially large amounts of aqSOA mass if a droplet reverts back to a seed aerosol state at any point in its lifetime. This phenomenon will occur even in less acidic conditions and may account for some of the underprediction of OA in cloud chemistry simulations compared to observed data.

Chapter 5 introduces a reduced version of GAMMA, intended for interfacing with other existing atmospheric models, that reduces the number of tracked aerosol-phase organic species while maintaining accurate prediction of total aaSOA mass. This version of GAMMA tracks only aqueous IEPOX, its derivatives, and glyoxal, which, as shown in Chapter 2, dominate aaSOA mass. Agreement between simpleGAMMA and the version of GAMMA containing complete suite of aqueous reactions is maintained within 25% for all conditions tested.

The discussion then moves to ideas for development of GAMMA. Expansion of GAMMA's coverage of chemistry is considered through the improvement of the number of relevant precursor gases tracked, or through the further addition of relevant aerosol-phase formation mechanisms. A candidate precursor gas must have both significant contribution to gas-phase emissions and generate water-soluble oxidation products. Low-weight, oxidized biogenic VOCs (BVOCs) are low in individual concentrations but can contribute high local emissions, with oxidation mechanisms similar to those already modeled by GAMMA. Similarly, monoterpenes are extremely common biogenic emission with interesting aerosol-phase chemistry, though their relatively low aqueous phase solubility must be considered before its inclusion. Gas-phase oxidation of phenolic compounds are a branch of gas-phase chemistry not yet tracked by GAMMA, that yields a suite of water-soluble organic species and can be used to more accurately track combustion products in both rural and urban environments. Reactions that can lead to strongly light-absorbing materials, such as formation of imidazoles or other nitrogen-containing compounds, are also of interest as they will contribute to the future accuracy of GAMMA's physical property modules.

This work ends with a short recap of the conclusions drawn in previous chapters and a few closing remarks about the long-term goals for GAMMA.

CHAPTER 2

PREDICTION OF AQUEOUS-PHASE SOA AND ORGANOSULFATE FORMATION IN ATMOSPHERIC AEROSOLS

2.1. Introduction

Internal mixtures of organic and inorganic material are typical in atmospheric aerosols. Inorganic aerosols may acquire an organic component via *in situ* interactions with volatile organic compounds (VOCs), a family of processes known as secondary organic aerosol (SOA) formation. Pathways for aqueous-phase SOA formation have been identified in which water-soluble VOCs dissolve into cloud droplets or wet aerosols, followed by aqueous-phase reactions (e.g. oxidation and/or oligomerization) which lead to the formation of SOA material (*1-4*). The carbonyl-containing VOCs (CVOCs) glyoxal and methylglyoxal have been studied intensively as potential precursors for this SOA formation pathway (*3-14*). Recently, aqueous-phase reactions of isoprene-derived epoxydiols have also been shown to be efficient pathways to SOA formation in the aerosol aqueous phase (aqueous aerosol SOA, or aaSOA) (*15-18*).

In-particle reactions between organic and inorganic material can lead to the formation of functionalized secondary organic products such as organosulfates (OS). OS is a ubiquitous component of continental tropospheric aerosols (*19-29*), comprising up to 5-10% of organic aerosol mass over the continental US (*30*). Lukács et al. observed that OS mass concentrations were highest for submicron aerosol size fractions, suggesting a link between OS formation and aerosol heterogeneous chemistry (*27*). Tolocka and Turpin found OS aerosol mass fractions at IMPROVE sites peaked in the summer and fall, when photochemical activity was at a maximum(*30*). Due to their low vapor pressures, the formation of OS from volatile organic

precursors is a pathway for secondary organic aerosol (SOA) production in aerosol water. OS are often amphiphilic, making them surface-active (*31*).

OS species are formed in the particle phase via reactions of organic species with sulfate or bisulfate, or their radicals, or sulfuric acid. Below we describe the two most significant mechanism types which have been investigated for their relevance to atmospheric aerosols: epoxide mechanisms and photochemical (radical) mechanisms. Alcohol sulfate esterification has also been investigated as a source of aerosol OS, but it was found to be very slow compared to the other OS formation mechanisms under tropospheric aerosol conditions (*32*); therefore it will not be considered further here.

2.1.1. Epoxide mechanisms (nucleophilic substitution)

Gas-phase epoxides derived from oxidation of VOCs such as isoprene and α-pinene are likely a significant source of SOA mass and OS species in aerosols. Epoxides such as isoprene-derived epoxydiol (IEPOX) are highly soluble in water and form stable sulfate esters in the aqueous phase (*15-17,19*). Field studies in the recent literature suggest that epoxide-derived OS are the most abundant OS type in aerosols and make up a significant fraction of SOA mass (*19,20,28,29*).

Sulfate or bisulfate ions may also add nucleophilically to protonated carbonyl groups. Sareen et al. tentatively identified of an OS species in nonirradiated methylglyoxal-ammonium sulfate solutions and proposed this mechanism (*33*). Organosulfates observed in nonirradiated ammonium sulfate aerosols exposed to glyoxal may be formed via this pathway (*34*).

2.1.2. Photochemical (radical) mechanisms

Sulfate (SO_4^-) and bisulfate (HSO_4) radicals are formed by reactions of bisulfate and sulfuric acid with OH in aqueous media according to (*35,36*):

$$HSO_4^- + OH \rightarrow SO_4^- + H_2O \qquad k^{II} = 3.5 \times 10^5 \ M^{-1}s^{-1} \qquad (2\text{-}1)$$

$$H_2SO_4 + OH \rightarrow HSO_4 + H_2O \quad k^{II} = 1.4 \times 10^7 \ M^{-1}s^{-1} \qquad (2\text{-}2)$$
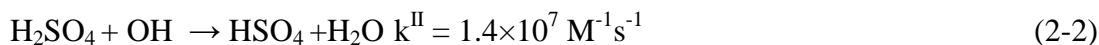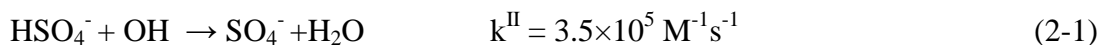
SO_4^- and HSO_4 can participate in many of the same reactions as OH in the aqueous phase, performing hydrogen abstraction (*37*), adding to C=C double bonds (*31*), or adding to radical species (*38*). The last two classes of reactions may result in OS formation.

Galloway and coworkers exposed ammonium sulfate aerosols to glyoxal in an aerosol chamber. They detected the formation of an OS species under irradiation, which they identified as glycolic acid sulfate (*7,39*). Glycolic acid sulfate may form from the reaction of the glycolic acid radical with SO_4^- or HSO_4. Glyoxylic acid sulfate and other acid sulfates are also expected to form via this pathway.

Numerical models of SOA formation in cloud water (*1,4,40-42*) have been developed previously and their use has improved predictions of SOA mass in air quality models (*41*). Due to the higher solute concentrations in deliquesced aerosols, the dominant SOA formation reactions are thought to differ in aerosol water as compared to cloud water (*2,43*). We have developed a new photochemical box model that couples gas-phase chemistry with detailed aqueous aerosol chemistry, enabling predictions of aaSOA and OS formation in atmospheric aerosols under ambient conditions. The detailed aqueous-phase mechanism presented here allows us to evaluate the relative contributions of recently proposed reaction pathways to aerosol mass and identify potential tracer compounds for aqueous aerosol chemistry.

21

2.2. Model Description

We used a newly developed photochemical box model, GAMMA (Gas Aerosol Model for Mechanism Analysis) to predict aerosol composition under different atmospheric and laboratory test conditions. Following Schwartz (1986), the temporal evolution of the partial pressure of species i in the gas phase (P_i) is given by (44):

$$\frac{dP_i}{dt} = -k_{mt,i}a_L P_i + \frac{k_{mt,i}a_L}{H_i^*}C_i + \sum_j r_{ij,gas} + E_i - D_i \tag{2-3}$$

where $k_{mt,i}$ is the gas-aerosol mass transfer coefficient for species i, a_L is the aerosol aqueous liquid volume fraction (cm^3 cm^{-3} of air), C_i is the aerosol-phase concentration of species i, H_i^* is the effective Henry's Law constant, $r_{ij,gas}$ is the rate of gas phase reaction j that species i participates in, and E_i and D_i are the emission and deposition rates of species i, respectively. Henry's Law applies to dilute, ideal aqueous solutions, however, the aqueous phase of aerosol is a highly concentrated, nonideal electrolyte solution. Kroll et al. have shown via aerosol chamber studies that glyoxal uptake by deliquesced ammonium sulfate aerosols depends linearly on gas phase glyoxal concentration, i.e. Henry's Law is applicable (14). We use the Henry's Law constant empirically determined by Kroll et al. for glyoxal. For other species for which such aerosol uptake data are not available, we have applied effective Henry's Law constants measured for electrolyte solutions, or when nothing else is available, the Henry's Law constant for uptake to pure bulk water (Appendix A).

The gas-aerosol mass transfer coefficient for species i, $k_{mt,i}$, is given by:

$$k_{mt,i} = \frac{1}{\dfrac{R^2}{3D_{g,i}} + \dfrac{4R}{3\omega_i\alpha_i}} \tag{2-4}$$

22

where R is the aerosol particle radius, $D_{g,i}$ is the gas-phase diffusion coefficient, ω_i is the thermal velocity, and α_i is the accommodation coefficient. The aerosol-phase concentration of species i is described by:

$$\frac{dC_i}{dt} = \frac{k_{mt,i}}{\mathbf{R}T} P_i - \frac{k_{mt,i}}{H_i^* \mathbf{R}T} C_i + \sum_k r_{ik,aq} \qquad (2\text{-}5)$$

where $\mathbf{R}$ is the gas constant, T is temperature, and $r_{ik,aq}$ is the rate of aqueous-phase reaction k that species i participates in. Full details of the chemical mechanism are available in Appendix A, but an overview is provided below.

2.2.1. Gas-phase chemistry

The model considers the gas-phase oxidation of isoprene, acetylene, toluene, and xylenes. These primary VOCs were chosen because they form glyoxal, methylglyoxal, epoxides, and other water-soluble VOCs upon oxidation. Please see the Appendix A for a complete listing of reactions, rates and references. The isoprene oxidation mechanisms under low-NOx (*45*) and high-NOx (*46*) conditions from Paulot and coworkers are used. Condensed mechanisms for the oxidation of toluene and xylenes under low- and high-NOx conditions were derived from the Master Chemical Mechanism (MCM) version 3.2 (*47-49*). Chemistry of acyl peroxynitrates follows La Franchi et al. and Paulot et al. (2009b) (*46,50*). Photolysis rates follow the Master Chemical Mechanism (*51*). The gas-phase output of the low-NOx mechanism agrees well with the experimental data of Paulot et al. (2009a) (Appendix A).

2.2.2. Aqueous-phase chemistry

Aqueous-phase oxidation of organic species in GAMMA follows the work of Turpin and coworkers (*1,38,40,43*). The effective Henry's Law constant was used where available for

carbonyl-containing VOCs (*14,52*). Therefore, hydration and self-oligomerization of these species were not separately represented in the model, to avoid double counting. This use of Henry's Law implies that the equilibrium between gas phase monomers and the monomers, hydration products, and oligomers in the aqueous phase is assumed to be reached instantaneously. Note that, in aerosol reaction chamber studies, equilibrium between gas phase glyoxal and deliquesced ammonium sulfate aerosols is reached under dark or irradiated conditions on a timescale of 1-10 hours (*7,12,14,53*).

The photochemical organosulfate formation mechanisms described in the previous section are included (*7,31,38,39*). Hydrolysis and organosulfate formation reactions from IEPOX are also represented (*15-18*). The mechanism, from Eddingsaas et al. (*16*), is as follows:

$$\text{IEPOX(aq)} \rightarrow (1\text{-}\beta) \text{ tetrol} + \beta \text{ IEPOXOS} \tag{2-6}$$

The branching ratio, β was observed in that study to depend on sulfate concentration in bulk solutions. We adopt $\beta = 0.4$, which the value for the most concentrated bulk solution (3.0 M SO_4^{-2}) studied by Eddingsaas et al. The rate constant is a function of H+ activity and the concentrations of sulfate and bisulfate:

$$\boldsymbol{k} = k_H^+ a_H^+ + k_{\text{sulfate}}[SO_4^{-2}]a_H^+ + k_{\text{bisulfate}}[HSO_4^-] \tag{2-7}$$

Here a_H^+ is the activity of H$^+$, $k_H^+ = 5\times10^{-2}$ s^{-1}, $k_{\text{sulfate}} = 2\times10^{-4}$ M^{-1}s^{-1}, and $k_{\text{bisulfate}} = 7.3\times10^{-4}$ M^{-1}s^{-1}.

It is assumed that epoxides formed by toluene and xylenes oxidation under high-NOx conditions are hydrolyzed and form OS. The thermodynamic and kinetic feasibility of these reactions was confirmed using density functional theory calculations (see Appendix A for details). Due to a lack of experimental rate data for these processes, it is assumed that the mechanisms and rates

for hydrolysis and organosulfate formation from these species are the same as those for IEPOX. Alcohol sulfate esterification was not included in the model since it is expected to be very slow compared to the other organosulfate formation mechanisms at the conditions considered here, as discussed in the previous section (*32*).

We note that insufficient data are available regarding the oxidative aging of oligomeric aqueous-phase SOA species such as glyoxal dimers, 2-methyltetrol or organosulfate species, so these mechanisms are not represented in the model at this time. Additionally, with the exception of the rate constant in the Eddingsaas (2010) mechanism for SOA formation from IEPOX, the influence of ionic strength on the reaction rates is not considered in the current version of GAMMA due to a lack of necessary thermodynamic data.

2.2.3. Test Conditions

Initial gas-phase conditions for the model, as well as emissions and deposition rates, were adopted from the general urban and rural conditions of CAPRAM 3.0 (*54*). The full list of test conditions can be found in the Supporting Information. The model currently considers only ammonium sulfate aerosols. Ammonium and sulfate are the most abundant ions found in continental aerosols, and therefore ammonium sulfate is expected to be a reasonable model of deliquesced aerosol in our test locations of choice (Yorkville, GA and Atlanta, GA) (see, for example,(*55*)). Other aerosol types will be incorporated in future versions of the model. The sulfate aerosol size distribution from Whitby (1978) is used: a constant mass-weighted mean diameter of 480 nm with a geometric standard deviation of 2.0 is used, giving a surface-area weighted mean diameter of 297 nm (*56,57*). Prescribed relative humidity and aerosol pH were input into the Extended *AIM* Aerosol Thermodynamics Model, *E-AIM* (http://www.aim.env.uea.ac.uk/aim/aim.php) in order to infer the aerosol liquid water content (*58*)

using measurements of sulfate mass loadings in representative test locations. 4.0 ug m^{-3} of sulfate mass was taken as representative of the rural Yorkville, GA region (*59*) and 20 ug m^{-3} was used for urban Atlanta, GA conditions (*60*). Aerosol pH was varied between 1 and 4, typical of continental aerosols (*61,62*). The calculated liquid aerosol content, a_L, varies on the order of ~10^{-12} to 10^{-11} cm^3 cm$^{-3}_{air}$ depending on RH and pH.

2.3. Results

Figures 2-1 and 2-2 summarize the results of our simulations for low-NOx and high-NOx conditions for a 12 h sunlit period. A full listing of the SOA species along with their molecular weights, H:C, and O:C ratios can be found in Appendix A.

2.3.1. Low-NOx conditions

SOA and OS formation in deliquesced ammonium sulfate (AS) aerosol under low-NOx conditions is dominated by IEPOX pathways: 69-100% of aaSOA mass is composed of IEPOX, 2-methyltetrol, and 2-methyltetrol sulfate ester after 12 hours of sunlight (Figure 2-1B and 2-1D). Low-NOx aaSOA and OS formation is highly dependent on RH and aerosol pH. As much as 0.9 μg m^{-3} SOA is predicted after 12 h of sunlight at 40% RH and aerosol pH=1 (Figure 2-1A). At 65% RH and pH = 4, only 17 ng m^{-3} aaSOA is predicted (Figure 2-1C). The dependence on aerosol pH can be traced to the pH-dependent rate constant for IEPOX hydrolysis and organosulfate formation (eq 2-6) (*16*). While all of the aerosol chemistry studied here requires the AS aerosol to be deliquesced in order to proceed, the optimum range for aqueous aerosol-phase SOA formation under low-NOx conditions is RH<60%.
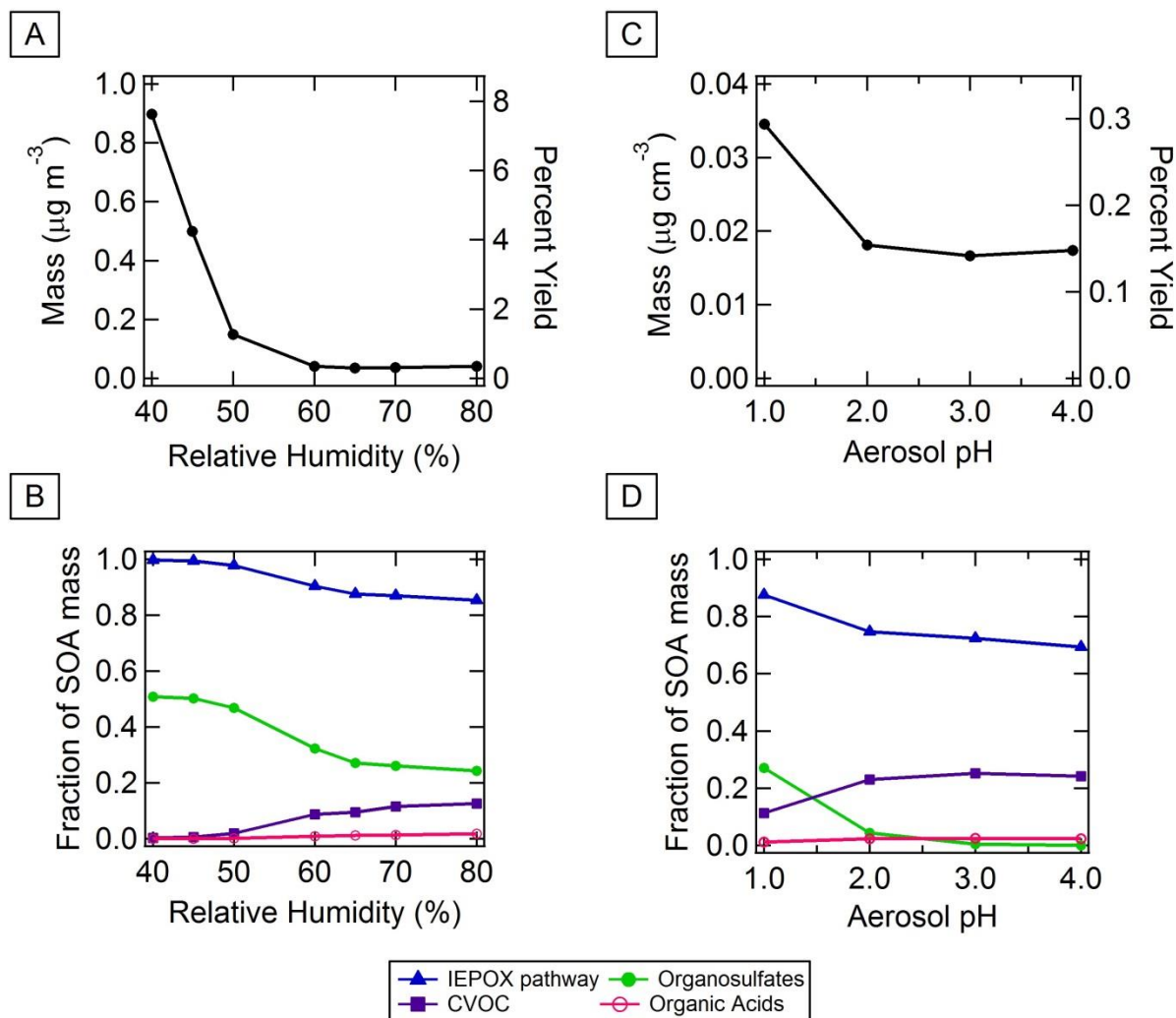
Figure 2-1 - GAMMA simulation results, low-NOx conditions, after 12h of sunlight as a function of relative humidity with an aerosol pH of 1 (panels A and B) and as a function of aerosol pH at 65% RH (panels C, D). In panels (A) and (C), predicted aaSOA mass is shown along with SOA yield with respect to all precursors (isoprene, acetylene, toluene, and xylenes). Panels (B) and (D) depict the fractional contributions to SOA mass. "IEPOX pathway" refers to aqueous-phase IEPOX, 2-methyltetrol, and 2-methyltetrol sulfate ester. "Organic acids" is the sum of succinic, oxalic, formic, glyoxylic, pyruvic, malonic, and glycolic acids and their ionized forms. "CVOC" refers to SOA from the uptake of glyoxal, methylglyoxal, glycolaldehyde, formaldehyde, acetaldehyde, and other aldehydes.

27

In addition to the fact that the second order SOA formation processes occur more efficiently under more concentrated conditions, the rate constant for SOA formation from IEPOX is sensitive to the activity of H^+ (see eq (7)). At pH = 1, this decreases to a low value above 60% RH until 100% RH is approached. We note that, in the current version of GAMMA, particle size does not change with relative humidity (in reality, the diameter of a pure ammonium sulfate particle can be expected to vary roughly 20% over the range of relative humidities studied here (*57*).). Therefore, changes in partitioning can be conclusively ruled out as contributing to this observation.

2-methyltetrol sulfate ester comprises >99% of OS mass (66 ng m^{-3} at 40% RH and pH 1). Figure 2-3 considers the relative contributions of each of the photochemically-derived organosulfate species under low-NOx conditions. Note that concentration is shown on a log scale, and the absolute concentration of each of these species is very small. Glyoxal sulfate is predicted to be the most abundant photochemically derived OS species. Note that, due to their very small Henry's Law constants, isoprene, MVK, and MACR concentrations are too low in the particle phase for significant direct OS formation (*31*).
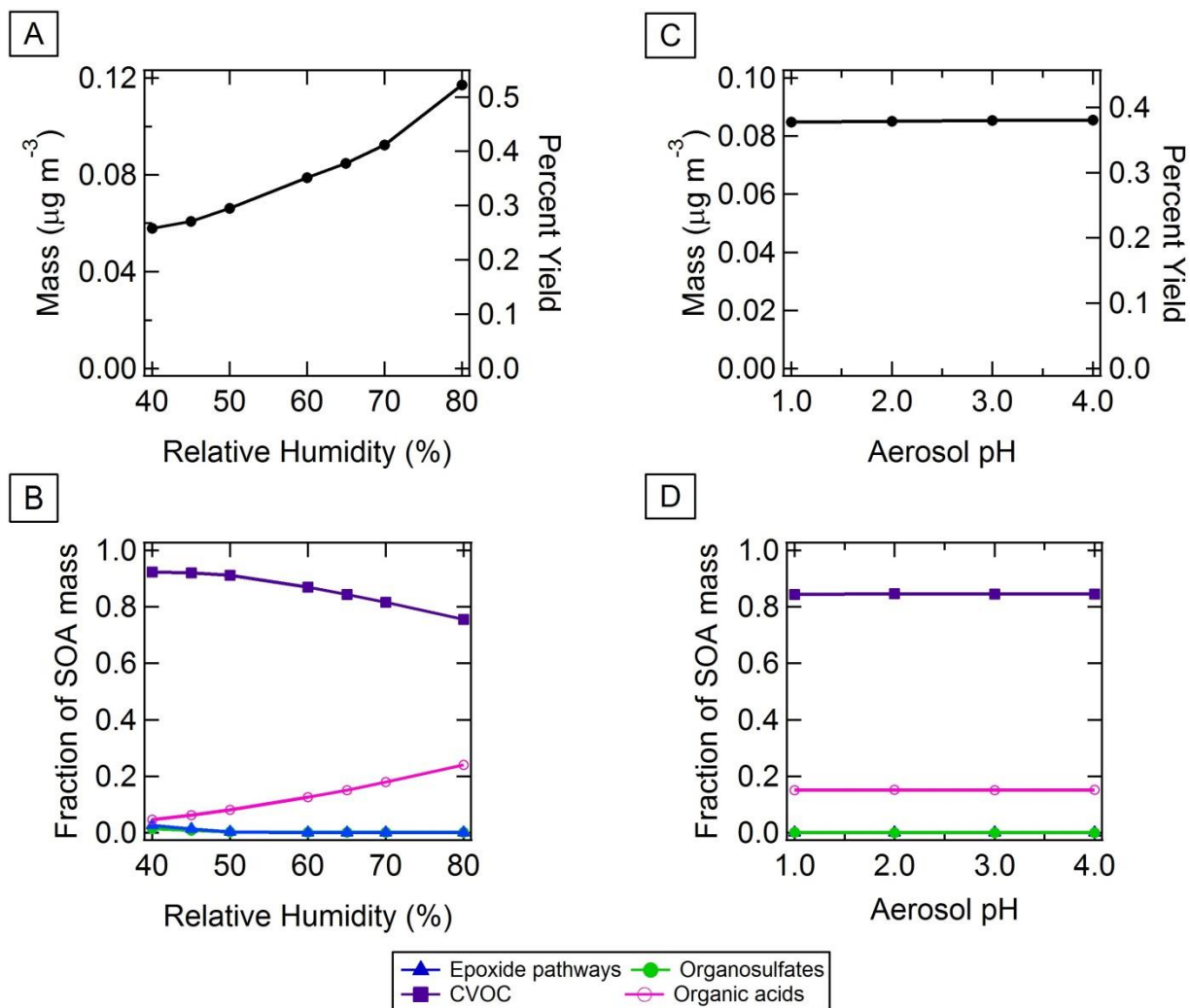
Figure 2-2 - GAMMA simulation results, high-NOx conditions, after 12h of sunlight as a function of relative humidity with an aerosol pH of 1 (panels A and B) and as a function of aerosol pH at 65% RH (panels C, D). In panels (A) and (C), predicted aaSOA mass is shown along with SOA yield with respect to all precursors (isoprene, acetylene, toluene, and xylenes). Panels (B) and (D) depict the fractional contributions to SOA mass. "Epoxide pathways" refers to TOL_EPOX, XYL_EPOX, EPXC4DIAL, and EPXMC4DIAL, as well as diols and diol sulfate esters formed from them. "Organic acids" is the sum of succinic, oxalic, formic, glyoxylic, pyruvic, malonic, and glycolic acids and their ionized forms. "CVOC" refers to SOA from the uptake of glyoxal, methylglyoxal, glycolaldehyde, formaldehyde, acetaldehyde, and other aldehydes.

2.3.2. High-NOx conditions

Glyoxal uptake dominates aaSOA formation under high-NOx conditions (i.e., when IEPOX is not expected to be formed from isoprene oxidation(*45,46*)) (Figure 2-2B and 2-2D). As a result, in contrast to the low-NOx scenario, aqSOA formation is insensitive to pH and increases with increasing relative humidity (Figure 2-2A and 2-2C). Mass of aaSOA predicted after 12h ranges from 58 to 120 ng m^{-3} at 40% and 80% RH, respectively (Figure 2-2A). OS does not contribute significantly to aaSOA mass under high-NOx conditions (maximum 0.8 ng m^{-3} at 40% RH and pH = 1). OS formed from toluene and xylenes-derived epoxides may comprise anywhere from 6%-89% of OS formed depending on pH and RH, with the remainder being formed via radical pathways.

2.4. Discussion

In contrast to what has been predicted for SOA generated in cloud water (*1,3*), organic acids were predicted to contribute less than 2% of aaSOA mass under low-NOx conditions and under 25% under high-NOx conditions. Total SOA mass generated in the aqueous aerosol phase is predicted to be highest under low-NOx conditions where aaSOA formation from IEPOX is favorable (i.e., low pH and low RH).

For low-NOx conditions with aerosol pH = 1, aaSOA O:C ratio was 1.08 ($\pm$ 0.04) after 12 h of simulation, with a mild dependence on relative humidity, while H:C = 2.39 ($\pm$ 0.008). For high-NOx conditions, O:C varied from 2 to 1.8 and H:C varied from 3 to 2.75 over an RH range of 40-80%. In all cases, the O:C values are higher at a given H:C ratio for aaSOA than what is typical for oxidized primary organic aerosol or "traditional" SOA derived from the condensation of semivolatile oxidized VOCs reported by Heald et al. (*63*). This is consistent with the notion

that aqueous-phase aerosol chemistry may be a source of highly oxidized, low volatility organic aerosol (LV-OOA) (*64,65*).
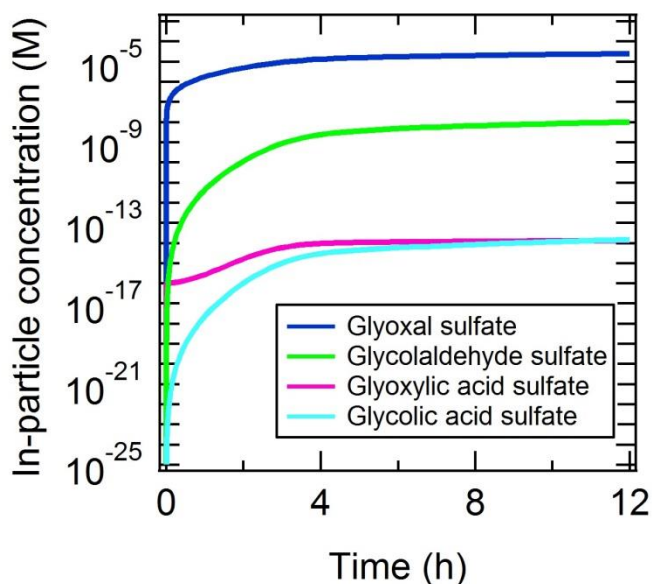
Figure 2-3 - In-particle concentrations of organosulfate species formed via radical mechanisms under low-NOx conditions (65% RH, pH = 1) as a function of time after sunrise.

Although the emissions and initial gas-phase conditions used in the model were not tailored to any specific location, comparing GAMMA model output to measurements made at representative locations in the Southeast USA can provide some insight into the potential significance of aqueous aerosol SOA formation pathways. Tanner et al. reported OC values of 3.15-3.53 µg m^{-3} from the SEARCH rural site at Yorkville, GA during summer months in 2002-2004 (*59*). Based on the results in Figure 2-1 and the predicted O:C ratio, our aaSOA mass predictions comprise within 0.2-11.25% of this value after 12 h of simulation, depending on aerosol RH and pH. This is consistent with the observations of Lin et al., who reported that IEPOX tracers comprised 7.9% of OC in Yorkville in summer 2010 (*66*). They reported the average mass concentration of 2-methyltetrol to be 330 ng m^{-3} during that time period. GAMMA

31

reproduces this observed mass concentration after 12 h of simulation at 40-45% RH and pH = 1. Lin et al. also observed 72 ng m^{-3} organosulfates derived from 2-methyltetrol, suggesting a branching ratio of 21.8%. This is lower than that suggested by the bulk phase laboratory studies of Eddingsaas et al. (2010) and used in this model. This difference suggests that this chemistry may proceed differently in the concentrated aerosol environment as compared to a bulk laboratory solution. Our predictions of aaSOA mass generated under high-NOx conditions after 12 h represent approximately 1% of the WSOC measured by Hennigan et al. in Atlanta (3-4 µgC m^{-3}) (*67*).

In a control simulation we found that changing the urban isoprene initial concentrations and emissions rates to match the rural case (roughly 10x increase in both emissions and initial concentration) resulted in a 10% increase in overall aaSOA mass (9% increase in mass due to CVOC and 17% increase in organic acid SOA mass).

2.5. Atmospheric Implications

The results of these simulations using our newly developed model, GAMMA, shed light on aaSOA and OS formation in aerosol water. The maximum aaSOA was formed under conditions where the IEPOX SOA formation pathways are active (low NOx, low pH and low RH). At high pH and RH, although the total aaSOA mass is lower, more is formed under urban/high NOx conditions because the greater sulfate aerosol loadings lead to higher aqueous aerosol volume, and also because gas-phase glyoxal concentrations are higher under urban conditions. Aqueous SOA formation is believed to be particularly important in the Southeastern United States (SE USA), where aerosol sulfate concentrations, humidity, and biogenic volatile VOC emissions (especially isoprene) tend to be high during photochemically active periods (*20,67*). Formation of both SOA and organosulfates in the aqueous phase is favored under low pH conditions,

therefore the formation of biogenic SOA may be enhanced due to anthropogenic emissions of acid precursors such as SO_2. All OS formation mechanisms studied here are second-order processes, and therefore they are more efficient at lower relative humidities, i.e. when the aerosol is more highly concentrated. This makes organosulfate species particularly good tracers for aqueous aerosol-phase SOA formation (vs. cloud water processing, or condensational SOA formation) in the field. Because of its relatively large mass contribution, IEPOXOS in particular could serve as an excellent tracer for aqueous aerosol-phase SOA formation when sufficient isoprene is present under low-NOx conditions (i.e., when the isoprene oxidation mechanism of Paulot et al. (2009a) dominates). Several groups have demonstrated that this species is readily detected in the field (*19,20,28,29,66*). Radical-derived OS are not expected to be produced in significant quantities, but detection using highly sensitive techniques (*39*) could be another indicator for chemistry occurring in aerosol water. If epoxides derived from anthropogenic volatile organic compounds (VOCs) such as the toluene-derived 2,3-epoxy-6-oxo-heptenal undergo analogous chemistry to IEPOX, the OS formed may serve as tracers for anthropogenic aaSOA.

2.6. Suggestions for future work

Significant uncertainties remain in the chemical mechanisms for isoprene oxidation in the gas phase and the subsequent formation of SOA. It has been proposed that 2-methylglyceric acid may form via aqueous-phase reactions of the isoprene oxidation products methacrolein and methacrylic acid in the presence of sulfuric acid and hydrogen peroxide (*68*), however, recent laboratory evidence suggests that the OH oxidation of methacryloylperoxynitrate (MPAN) may be responsible for its formation under high-NOx conditions (*15*). Lin et al. recently demonstrated that reactive uptake of IEPOX onto wet acidified sulfate seed aerosol yields several other

compounds in addition to the 2-methyltetrols and 2-methyltetrol sulfate ester, including C5-alkene triols, dimers of IEPOX, and 3-methyltetrahydrofuran-3,4-diols, as well as organosulfate derivatives of the dimers (*66*). Based on their field measurements, the contribution of IEPOX products to total SOA as predicted by GAMMA may be underestimated as much as 45% due to these unaccounted for formation pathways. GAMMA will be updated with these new products and mechanisms as rate data become available.

More experimental data describing the physical uptake of organic species to aqueous aerosol are needed. In general the accommodation coefficients of gas-phase species on deliquesced aerosols differ from those on pure water or sulfuric acid surfaces due to the differences in solubility, which may be particularly pronounced for organic species ("salting-in" or "salting-out"). Some empirically determined Henry's Law coefficients for aqueous aerosol exist in the literature, but more are necessary. In the case of glyoxal partitioning to ammonium sulfate aerosol, these values are considerably higher than for water or bulk electrolyte solutions (which are less concentrated than aerosol at <100% RH) (*7,14,69*).

34

CHAPTER 3

USAGE OF GAMMA TO PREDICT AEROSOL PHYSICAL PROPERTIES

3.1. Introduction

Atmospheric aerosols impact Earth's climate via interactions with solar radiation, or by acting as nuclei for cloud droplet formation. Organic matter, a typical component of tropospheric particulate matter (*75*), can affect the physical properties of aerosols which determine their influence on climate, such as optical properties (*4–7, 9, 76, 77*) and surface tension. (*4, 5, 38, 78, 79*) One recently identified source of organic matter in tropospheric aerosols is aqueous aerosol secondary organic aerosol (aaSOA) formation. In this mechanism, water-soluble volatile organic compounds are absorbed into aerosol water, where they may react to form low-volatility secondary organic aerosol (SOA) material. (*23, 29, 34, 80*) Aqueous aerosol SOA formation is likely to be significant in regions where aerosol sulfate concentrations, humidity, and volatile organic compound (VOC) concentrations tend to be high, such as the Southeastern United States. (*81–83*) However, the magnitude of the contribution of this pathway to total aerosol mass and its influence on aerosol physical properties is still uncertain.

The ability of a particle to act as a CCN a given supersaturation condition depends on its dry diameter (i.e., solute content) and chemical composition. This is described by the Köhler equation: (*84*)

$$S = \frac{A}{D_p} - \frac{B}{D_p^3} \tag{3-1}$$

with

$$A = \frac{4M_w \sigma}{T \rho_w} \quad \text{and } B = \frac{6 n_s M_w}{\pi \rho_w}$$

where D_p is the diameter of the aqueous droplet, p_w is the water vapor pressure over the droplet of diameter D_p, p^0 is the water vapor pressure over a flat surface, M_w is the molecular weight of water and ρ_w is its density, R is the gas constant, T is temperature, σ is the surface tension of the droplet at the point of activation, and n_s is the number of moles of solute. Surface-active organic species can enhance aerosol CCN activity by lowering surface tension, thus affecting the Kelvin term (A) of the Köhler equation, but they can also affect the Raoult term (B) by altering n_s when surface-bulk partitioning of solute is taken into account. Methylglyoxal, acetaldehyde, and formaldehyde, all species which have been suggested as aaSOA precursors, have been demonstrated to supress surface tension in bulk solutions with compositions mimicking aqueous aerosols. (*4*, *5*, *8*, *85*) Small organic acids such as succinic acid and oxalic acid, typical aaSOA products, are also known to be surface-active. (*78*) Finally, aaSOA formation is thought to be an efficient pathway for the production of organosulfates, which may also be surface-active. (*86*)

The chemical composition of an aerosol particle can also influence its direct effects on climate. There is evidence from field studies of non-soot light-absorbing "brown carbon" in aerosols associated with biomass burning and pollution plumes. (*87*) The absorption of UV radiation by atmospheric brown carbon has the potential to perturb tropospheric photochemistry. (*88*) The formation mechanisms, prevalence, and physical properties of brown carbon in aerosols are poorly understood. Our recent laboratory studies showed that particle-phase chemical reactions between absorbed volatile organics and inorganic salts can lead to secondary products which absorb light in the UV and visible. (*4–6*, *8*) We characterized the mechanisms and kinetics of changes in the light absorption spectrum for bulk solutions containing glyoxal and/or methylglyoxal with $(NH_4)_2SO_4$. We found that, even in cross-reacting mixtures of glyoxal and

methylglyoxal, light absorption by the reaction mixture could be modelled as a linear combination of the contribution of each reaction pathway in parallel. (*5*)

We recently developed a new photochemical box model, GAMMA (Gas-Aerosol Model for Mechanism Analysis), (*80*) that couples gas-phase chemistry with detailed aqueous phase chemistry, enabling speciated predictions of aqueous-phase SOA formation in atmospheric aerosols under ambient conditions. Besides allowing calculations of changes in aerosol mass due to aqueous SOA chemistry, these detailed, speciated SOA calculations enable a bottom-up prediction of aerosol surface tension based on parameterizations for complex inorganic-organic mixtures. Surface-active species tracked by the model include several organic acids, dicarboxylic acids, aldehydes, methylglyoxal, and organosulfates. We have also developed a method to simulate the aaSOA brown carbon absorption spectrum based on predicted aerosol composition from GAMMA. Mechanisms for the dark formation of light-absorbing organics from methylglyoxal, glyoxal, and acetaldehyde which were been recently identified in laboratory studies are represented. Here we demonstrate the use of this module with GAMMA to evaluate the contribution of aqueous pathways of brown carbon formation to total observed loadings.

3.2. Model Description

3.2.1. GAMMA – Gas Aerosol Model for Mechanism Analysis

GAMMA is a photochemical box that simulates coupled gas and aqueous-phase chemistry in order to predict aerosol composition under different atmospheric and laboratory test conditions. A complete, detailed description of the model, the parameters and initial conditions, and its application to modeling chemistry in deliquesced ammonium sulfate particles is available in Chapter 2. (*80*) The model currently follows over 160 species participating in over 260 reactions.

The general urban and rural conditions from CAPRAM 3.0 are used for initial gas-phase conditions and emissions and deposition rates. (*89*) Daytime conditions were simulated by scaling the photolysis rate constants semi-sinusoidally over 12 hours. For nighttime conditions, photolysis reactions and isoprene emissions were disabled. Only ammonium sulfate aerosols are treated in the model; this aerosol type is a typical representative for deliquesced aerosols over continental regions. The size distribution from Whitby (1978) is used. (*90*) Aerosol liquid water content is calculated based on RH and aerosol pH using the Extended *AIM* Aerosol Thermodynamics Model, *E-AIM* (http://www.aim.env.uea.ac.uk/aim/aim.php). (*91*) For comparisons with the field data of Hecobian et al. (2010), (*92*) an aerosol sulfate mass of 4.0 ug m^{-3} was taken as representative for Yorkville, GA, USA (*93*) and 20 ug m^{-3} was used for S. DeKalb, GA, USA.(*94*)

3.2.2. Surface tension module

Droplet surface tension is a key physical parameter determining the critical supersaturation for CCN activation, and therefore is an important input parameter for models of cloud droplet formation. We predict particle surface tension based on the aerosol composition results from GAMMA. We follow the approach outlined in Schwier et al. (2013). (*85*) In that study, surface tension depression by complex mixtures of organic material in aqueous solutions containing 3.1 M ammonium sulfate was parameterized using a fit to a modified form of the semi-empirical Szyzskowski-Langmuir equation(*95*) which was first proposed by Henning et al. (2005): (*96*)

$$\sigma = \sigma_w(T) - \sum_i \chi_i a_i T \ln(1 + b_i C) \qquad (3\text{-}2)$$

Here, σ and σ_w are the surface tension of the solution with and without organics, respectively, T is temperature (K), C is the molality of the organic carbon (mol carbon (kg water)$^{-1}$), a_i and b_i are

fit parameters of the ith organic compound (alone) in water, and χ_i is the molality fraction of compound i out of the total soluble carbon concentration in solution ($\chi_i = C_i\,C^{-1}$). Among the surface-active species for which parameterizations are available, those tracked by GAMMA include methylglyoxal, formaldehyde, oxalic acid, succinic acid, and acetaldehyde. Parameters a_i and b_i for those species are listed in Table 3-1.

Species Name	a_i	b_i
Methylglyoxal	0.0185	140
Formaldehyde	0.0119	50.23
Oxalic Acid	0.01297	1.0583
Succinic Acid	0.0349	0.74884
Acetaldehyde	0.02601	8.9282

Table 3-1 – List of Szyzskowski-Langmuir constants for surface-active species traced by GAMMA, from Schwier et al. (2013) Acetaldehyde is treated as a proxy for all multicarbon (C>2) aldehydes.

3.2.3. Light absorption module

We previously observed and quantified changes in the absorption spectrum for reactive aqueous mixtures of glyoxal (*6*) and/or methyglyoxal (*4*, *5*) with ammonium sulfate. Nozière and coworkers made similar observations for acetaldehyde. (*7*) Changes in aerosol absorbance due to these reactive processes are tracked in GAMMA (see Appendix A for details). These reactions are not included in the mass balance for the precursor species since dark oligomerization is assumed to be accounted for via the use of the effective Henry's Law constants to describe uptake. (*80*) Other light-absorbing organic species tracked by GAMMA for which absorption

data are available include oxalic acid and succinic acid, (*11*) as well as pyruvic acid. (*10*) Specific absorption data for each species are shown in Appendix A.

Despite significant cross-reactions between methylglyoxal and glyoxal in aqueous ammonium sulfate solution, we showed that the increases in light absorption in a reactive mixture of the two could be modelled as if each precursor were reacting in parallel.(*5*) Therefore, in GAMMA we treat these processes as independent, and a composite UV-Visible absorption spectrum for the aerosol is calculated based on a linear combination of the contribution of each reactive pathway (in the case of glyoxal, methylglyoxal, and acetaldehyde) or individual organic species (for oxalic, succinic, and pyruvic acids) as follows:

$$A = \sum_i c_i \hat{A}_i \qquad\qquad (3\text{-}3)$$

where $\hat{A}_i$ is the specific absorbance of the ith species per molar concentration (L mol^{-1}) and c_i is the concentration of the ith species (mol L^{-1}).

We recently studied the aerosol-phase photochemical aging of light-absorbing material formed by methylglyoxal in aqueous ammonium sulfate solutions. (*37*) We observed that the lifetimes of these species are controlled by fast photolysis ($k^I = 0.0167\text{s}^{-1}$) which leads to volatilization. This process is represented in GAMMA as a first-order decrease in the absorption associated with the glyoxal, methylglyoxal, and acetaldehyde reactive pathways.

3.3. Results and Discussion

36-hour simulations were performed, starting with sunrise at t = 0, for a variety of aerosol pH (1 ≤ pH ≤ 4) and RH (45%-80%) conditions, for urban (high-NOx) and rural (low-NOx) scenarios.
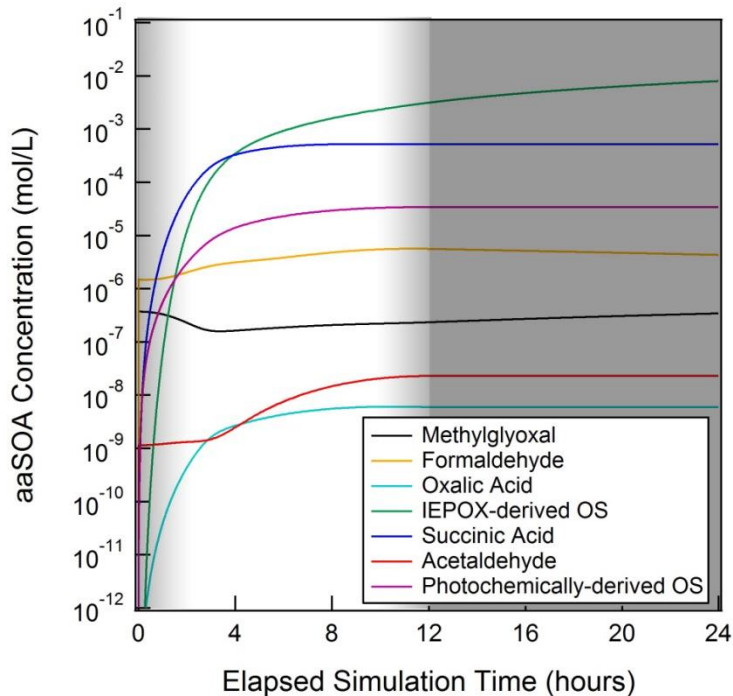
Figure 3-1. Surface-active aqueous SOA concentrations vs. Time, pH1 RH 65%, low-NOx mode. Shaded regions indicate night-time conditions.

3.3.1. Aerosol surface tension

As we reported previously, aaSOA mass as predicted by GAMMA under simulated urban conditions is dominated by glyoxal uptake. (*80*) Glyoxal and its self-reaction products have not been found to depress surface tension in aqueous solutions. (*6*) Succinic acid was the largest contributor to surface tension depression, however total surface-active organic mass (i.e. the combined mass of the species listed in Table 1) did not exceed carbon concentrations of 2.2×10^{-3} kgC/kg water. Predicted changes to net aerosol surface tension were therefore negligible ($< 1\%$ of the initial value).
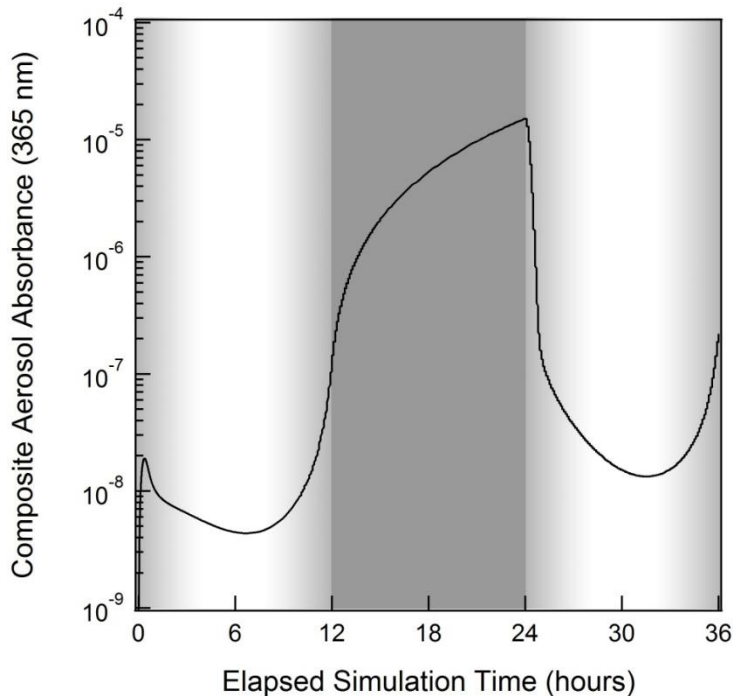
Figure 3-2 – Composite absorbance at 365nm vs. Time, 65% RH, pH1, High NOx mode. Shaded regions (12-24 h) indicate night-time conditions.

Under low-NOx conditions, isoprene-derived epoxide (IEPOX)-derived tetrol and organosulfate species are predicted to comprise over 60% of the total formed SOA under all conditions tested (Figure 3-1). (*80*) Succinic acid and the other species listed in Table 1 were again formed in quantities too small to significantly impact surface tension.

IEPOX-derived organosulfate species may depress aerosol surface tension, but to our knowledge this has not been characterized experimentally to date. In general, data for surface tension depression by organosulfates are sparse. (*78*) Noziére and coworkers studied surface tension depression by organosulfates generated by irradiating isoprene, methyvinylketone, methacrolein, or α-pinene in aqueous solutions containing sulfate salts. (*86*) For experiments initiated with 11 mM of isoprene, the minimum solution surface tension observed (after 200 min of reaction) was roughly 75% of the original value. Note that photochemically generated organosulfates of this

type are formed in negligibly small quantities in our simulations (Figure 3-1). (*80*) If we assume similar surface tension depression by IEPOX-derived organosulfate species, under conditions where their formation is predicted to be high, significant surface tension depression (~18% at pH 1, 65% RH) may occur.

3.3.2. Aerosol light absorption

The computed composite absorption spectra were dominated by the reactive uptake of glyoxal under all conditions studied. Therefore the absorbance exhibited a diurnal cycle, increasing in the evening and night-time and decreasing to low levels in the early morning hours due to photolysis (Figure 3-2). The baseline daytime absorption level was low, but increased with time due to the buildup of oxalic and pyruvic acids. While methylglyoxal oligomers are more strongly absorbing than those formed by glyoxal (*4–6*) the relatively low effective Henry's Law constants for methylglyoxal and acetaldehyde made their contributions to the composite absorption negligible compared to glyoxal.
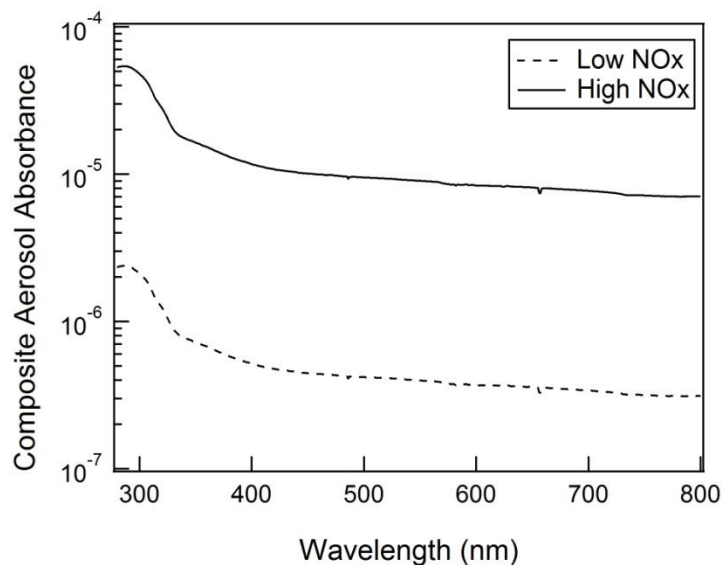
Figure 3-3 – Composite Aerosol Absorbance as predicted by GAMMA, pH 4, RH 65%.

Figure 3-3 shows the composite absorption spectra at maximum absorbance (24 h after the simulation was initiated) for low-NOx and high-NOx conditions. A peak is apparent in the spectra at roughly 280 nm, consistent with light absorption by carbonyl-containing glyoxal oligomer species. (6) The maximum mass absorption efficiency (MAE) is predicted to be roughly 6.5 times higher under high-NOx conditions (0.13 m^2gC^{-1}) than low-NOx conditions (0.02 m^2gC^{-1}) (see Supporting Information for details of the MAE calculation). This is to be expected since, as previously mentioned, glyoxal uptake dominates SOA mass under high-NOx conditions. Under low-NOx conditions, IEPOX-derived species dominate total SOA. Their potential contribution to aerosol absorption is unknown, and therefore is not included in our calculations.

3.4. Conclusions and Atmospheric Implications

We have performed detailed simulations of organic chemistry in the aerosol aqueous phase in order to predict changes in aerosol surface tension and light absorption due to the uptake and reaction of water-soluble volatile organic compounds.

We found that, under all conditions studied, the bulk concentrations of species known to depress surface tension (methylglyoxal, formaldehyde, acetaldehyde, succinic acid, oxalic acid, and photochemically-generated organosulfates) are so small that their predicted effects on aerosol surface tension are negligible. Based on our recent aerosol chamber studies of the effects of gas-phase methylglyoxal and acetaldehyde on the CCN activity of aqueous ammonium sulfate particles, adsorption of these species at the gas-aerosol interface may be sufficient to depress aerosol surface tension and therefore affect aerosol CCN activity.(38) Relatively little is known about this phenomenon at this time; additional experiments are needed so that it may be parameterized for the model.

We predict significant brown carbon formation via aqueous aerosol-phase pathways, especially under urban conditions. Our predictions of a build-up of absorbing species throughout the night, followed by a decrease in absorption in the early morning hours due to photobleaching, (*37*) is consistent with field observations of high brown carbon absorption in the early morning. (*97*) In Figure 4, we compare the wavelength dependence of our predicted composite absorption spectra to the measurements of Hecobian et al., who performed UV-Vis spectrophotometry on aqueous filter extracts (Figure 3-4). (*92*) Note that the data from Hecobian et al. (2010) were reported as absorption per volume of air sampled, and particle loading data for the sample period are not available, so normalized spectra are shown.
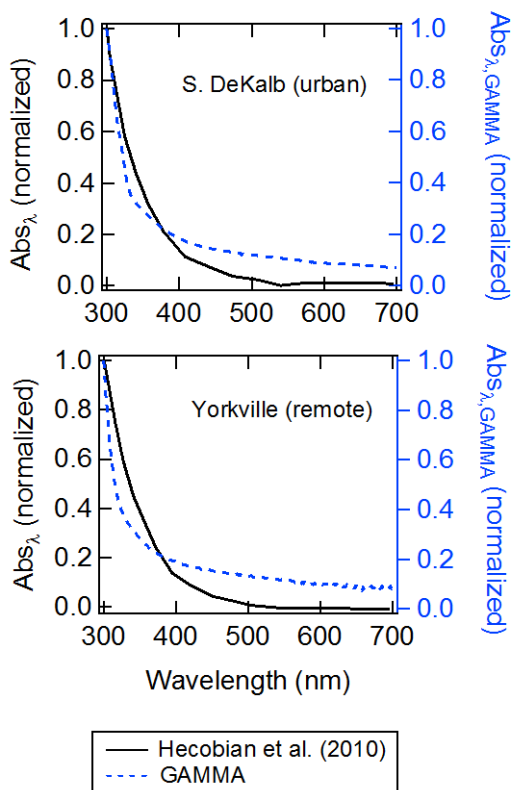
Figure 3-4 – Wavelength dependence of composite absorption spectra predicted by GAMMA (dashed line, right axis) compared to measurements of Hecobian et al. (2010) (solid line, left axis) for aqueous extracts of aerosol filter samples collected during periods with low biomass burning influence at representative urban and rural locations in Georgia, USA.

The featureless spectra with absorption increasing with decreasing wavelength reported by that group is reproduced well by our model. They reported an MAE of 0.31 m^2gC^{-1} at the S. Dekalb (urban) site, similar in magnitude to our predicted maximum MAE (0.12 m^2gC^{-1}) under high-NOx conditions. However, they reported a similar value of 0.29 m^2gC^{-1} at the Yorkville (rural) site, whereas we predict significantly less absorbance under low-NOx conditions. We note that our model does not account for primary sources of brown carbon such as biomass burning. (*87*) Furthermore, other reactive sources of brown carbon exist other than aqueous aerosol chemistry, such as reactions of condensationally formed monoterpene SOA with nitrogen-containing compounds such as ammonia, ammonium sulfate, or amines,(*98*, *99*) or the nitrate functionalization of aromatic species.(*88*, *100*, *101*) These processes are expected to occur in the aerosol organic phase rather than in the aqueous phase, and thus are not represented in GAMMA at this time.

Since IEPOX-derived tetrol and organosulfate species are predicted to contribute significantly to aqueous aerosol mass under low-NOx conditions, experimental data are needed so that we can quantify their potential impacts on aerosol surface tension and light absorption.

CHAPTER 4

USING GAMMA TO ESTIMATE CLOUDWATER PROCESSING

As has been previously discussed, GAMMA can be used to predict the concentrations and physical property changes due to the formation of secondary organic species in deliquesced ammonium sulfate aerosols, which contain high sulfate, ammonium, and hydrogen ion activities. We now explore GAMMA's capabilities to simulate chemistry occurring in cloud droplets, another ubiquitous family of atmospheric particles that has both significant gas-aqueous uptake and aqueous-phase processing.

4.1. Introduction

Of the many effects that contribute to the total radiative forcing of the atmosphere, the contributions of aerosols are the least understood and therefore represent the largest source of uncertainty in current climate models (*12*). Aerosols can contribute through direct forcing effects via scattering or absorption of sunlight, or through indirect effects, by which their properties implicitly change cloud lifetimes and reflectivity.

In the presence of sufficient gas-phase water supersaturation, atmospheric aerosols spontaneously uptake water to form cloud droplets. This effect is achieved when air parcels at RH ≤ 100% are transported to lower temperature areas, such as at higher altitudes. Water vapor content is constant in this process and can therefore subsequently exceed its local vapor pressure at the new, colder temperature. This results in condensation of liquid water onto aerosol particles that are present within the air parcel. Once activated, cloud droplets become significantly larger than atmospheric aerosols from which they are derived, ranging on the order of 10-50 μm (*102*).

The vast compositional majority of a cloud droplet is water, implying low aqueous-phase concentrations for inorganic and organic species alike. Cloud droplets may also revert back to deliquesced salt configurations multiple times within their lifetime (*103*), thus necessitating proper accounting of the formation of semi-volatile and non-volatile species that evolve in one or both regimes. It is likely that the different inorganic activities and surface-area-to-volume ratios between aerosol seed particles and cloud droplets will lead to different prevailing organic chemistry in the aerosol phase.

Organic acids have been observed to be ubiquitous in cloud droplets, regardless of particle age, location, and size (*28*, *104*). In particular, dicarboxylic acids have been observed to be internally mixed with inorganic material of collected sulfate particles, suggesting efficient aerosol-phase formation in addition to or in place of deposition via gas-aerosol partitioning (*105*). Oxalic acid, as the smallest and simplest of these acids, is commonly attributed with this branch of aqueous aerosol processing, due to its high prevalence in cloud droplet samples and multiple known formation pathways via both anthropogenic and biogenic precursors (*28*, *105*). Structurally similar organic acids, both dicarboxylic (malonic acid, succinic acid) and monocarboxylic (acetic acid, glycolic acid, glyoxylic acid, etc.), have also been measured in collected particles, in varying relative quantities depending on sampling location and time (*34*). Several of these acids have been observed to be surface-active (*78*), potentially affecting heterogeneous chemistry and a deliquesced aerosol particle's propensity to convert into a cloud droplet, or vice versa.

As mentioned in Chapter 1, small (< 3 carbon) carbonyl containing volatile organic compounds (CVOCs) are a ubiquitous contributor to organic mass in cloud water, and are known to oxidize with OH radicals present in the aqueous phase to form organic acids. (*62*) The gas- and aerosol-phase processing of these species under cloudwater conditions has been examined numerous

times, from both experimental (*4*, *5*, *28*, *31*, *32*, *49*, *105*, *106*) and modeling (*27*, *33*, *57*) approaches. As mentioned in Chapters 2 and 3, CVOCs are also relevant in deliquesced aerosol conditions as well, forming SOA in significant quantities under high-NOx conditions and contributing to changes in overall aerosol light absorbance and surface tension properties.

It has been proposed that the discrepancy between previous cloud water model SOA predictions and observed values arises from SOA that forms in the time spent as an aerosol. (*34*) Recent studies on common biogenic and anthropogenic precursor gases have indicated epoxide-derived organic compounds as a potential additional source of OA. (*41*, *51*, *107*) Although the high Henry's Law constant of IEPOX would lead to significant physical uptake into cloudwater, the formation of IEPOX organosulfate and tetrols require the participation of H^+ or NH_4^+, and as such are less likely in cloud droplet due to their high liquid water content. These compounds can be expected to contribute to SOA mass by forming in aerosol particles before activating into cloud droplets.

It is desirable to develop a model that can operate in both deliquesced aerosol and cloud droplet conditions, to track the aqueous chemistry of particles that exist in one or both of the two regimes over its lifetime. We now discuss the implementation of cloud conditions into GAMMA, as well as its coupling to deliquesced salt aerosol conditions to approximate the aqueous phase chemistry of a salt aerosol that is converted into a cloud droplet after several hours of aerosol-mode processing.

4.2. Methods

As mentioned in previous chapters, GAMMA has been used to predict the formation of aqueous aerosol SOA (aaSOA) mass for a variety of ambient starting conditions. By applying intial

inorganic concentrations and particle sizes of cloud droplets, GAMMA can also be used to predict the formation of cloudwater SOA (cwSOA) and total aggregate aqueous-phase organic aerosol mass (aqSOA) formed when alternating between cloud and aerosol regimes of chemistry.

Conditions for cloud particles were approximated using droplet diameters and liquid water fraction values from Lim 2005 (*27*), set to 10μm and 10 g/cm^3, respectively. Cloud droplet inorganic concentrations were approximated as if an aerosol particle of 297nm-diameter were diluted to 10μm diameters with pure water, with initial concentrations based off of calculations using the Extended AIM Aerosol Thermodynamics Model, E-AIM (*91*). Given the extremely low resultant concentrations due to the extremely high amount of water compared to its original 'seed' form, activity coefficients were set to unity. Water concentration was approximated to be 55.6 mol/kg-H$_2$O, that of pure water.

Photolysis reaction rates, tracked species and reactions, and all other aerosol properties were kept identical to the diurnal build of GAMMA described in Chapter 3 and Appendix A. Initial gas-phase concentrations, emissions, and deposition rates were approximated using the rural and urban conditions from CAPRAM 3.0 (*89*). As previous studies have indicated weak dependence of SOA formation on ambient droplet relative humidity and temperature (*36*), these values were kept constant over simulation. Formation and evolution of secondary species were tracked over 12 hours of daytime chemistry, followed by 12 hours of night-time chemistry. Aerosol pH and relative humidity in aerosol mode ranged from 1-4 and 40%-80%, respectively.

Simulations of particles switching from deliquesced aerosol to cloud droplet regimes were made by resetting aqueous-phase concentrations, activity coefficients, and particle diameters at set points during simulation. Particles were tracked as aerosols for up to 6 hours, upon which they

were converted to cloud droplets and allowed to continue reacting for a full diurnal cycle, ending at 24 hours of total simulation time.

4.3. Results

4.3.1. Low-NOx conditions

Under low-NOx conditions, the initial conditions of the seed aerosol are expected to have a profound effect on the amount and quantity of generated cwSOA. At higher ambient relative humidities and seed aerosol pH values, organic acids (oxalic, glycolic, and acetic acids), as well as glyoxal, comprise the majority of predicted cwSOA mass. Epoxide pathway species comprise a smaller but relevant amount of mass in these systems, contributing via non-reactive uptake of IEPOX. Formation of CVOC and acid species accelerate at higher pH and RH values, increasing nearly a full order of magnitude between seed aerosol pH's 1 and 4. Total estimated cwSOA mass reaches as high as 9 μg/m^3 air after 24 hours of simulation, showing similar diurnal trends but slightly higher overall production than similar predictions by Chen et al., which estimate ~8.7 μg/m^3 after 48 hours. (*36*)In low-pH seed aerosol systems, the higher H$^+$ activities result in fast production of IEPOX-derived organosulfates and tetrols, which subsequently dominate predicted SOA mass (vis Figure 4-2). The accelerated formation of these epoxide substitution products at low pH values, coupled with the high molecular weight of these species, results in significant increase of total cwSOA under these conditions, despite the higher predicted amounts of CVOC and acid compounds at higher seed aerosol pH.
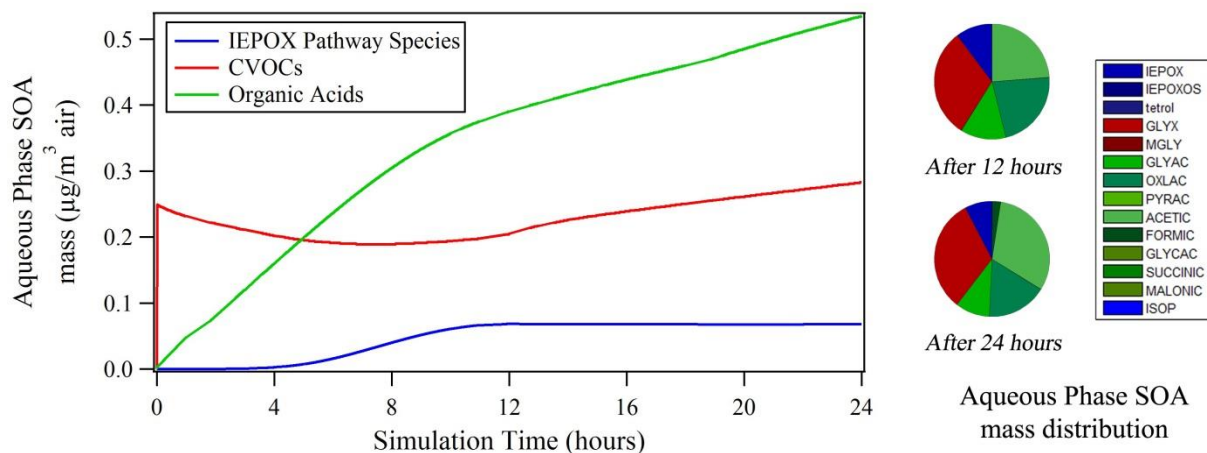
Figure 4-1 – Time dependence of different classes of cwSOA at RH 65%, pH4, under low NOx cloud conditions. "IEPOX pathway" refers to aqueous-phase IEPOX, 2-methyltetrol, and 2-methyltetrol sulfate ester. "Organic acids" is the sum of succinic, oxalic, formic, glyoxylic, pyruvic, malonic, and glycolic acids and their ionized forms. "CVOC" refers to SOA from the uptake of glyoxal, methylglyoxal, glycolaldehyde, formaldehyde, acetaldehyde, and other aldehydes.

The total rate of cwSOA formation decelerates under nighttime conditions (simulated hours 13-24), biasing slightly towards uptake of CVOC species. In the absence of radicals generated by gas-phase photooxidation, the formation of organic acids via aqueous processing is predicted to stop while uptake of CVOCs continues to occur, reflected by the slight increase of relative mass contribution of these species after 12 hours of night-time chemistry. These processes are seen to resume if simulations are run longer than 24 hours, and photochemistry is reintroduced. Non-photolytic processes that generate organic acids, such as the formation of acetic and formic acid via ozonolysis of first-generation isoprene oxidation products, continue to occur in night and contribute to overall cwSOA mass through non-reactive, gas-aerosol partitioning.

Similarly, the drop in radical concentrations, as well as the lack of isoprene under nighttime conditions, also results in a halt in the production of gas-phase IEPOX, subsequently leading to a stabilization of aerosol-phase concentrations in conditions where IEPOX is relatively unreactive.

Under low pH conditions, the acid-catalyzed production of organosulfate and tetrol species is unaffected by day or nighttime conditions and reactive uptake of IEPOX pathway species into the aerosol phase continues.
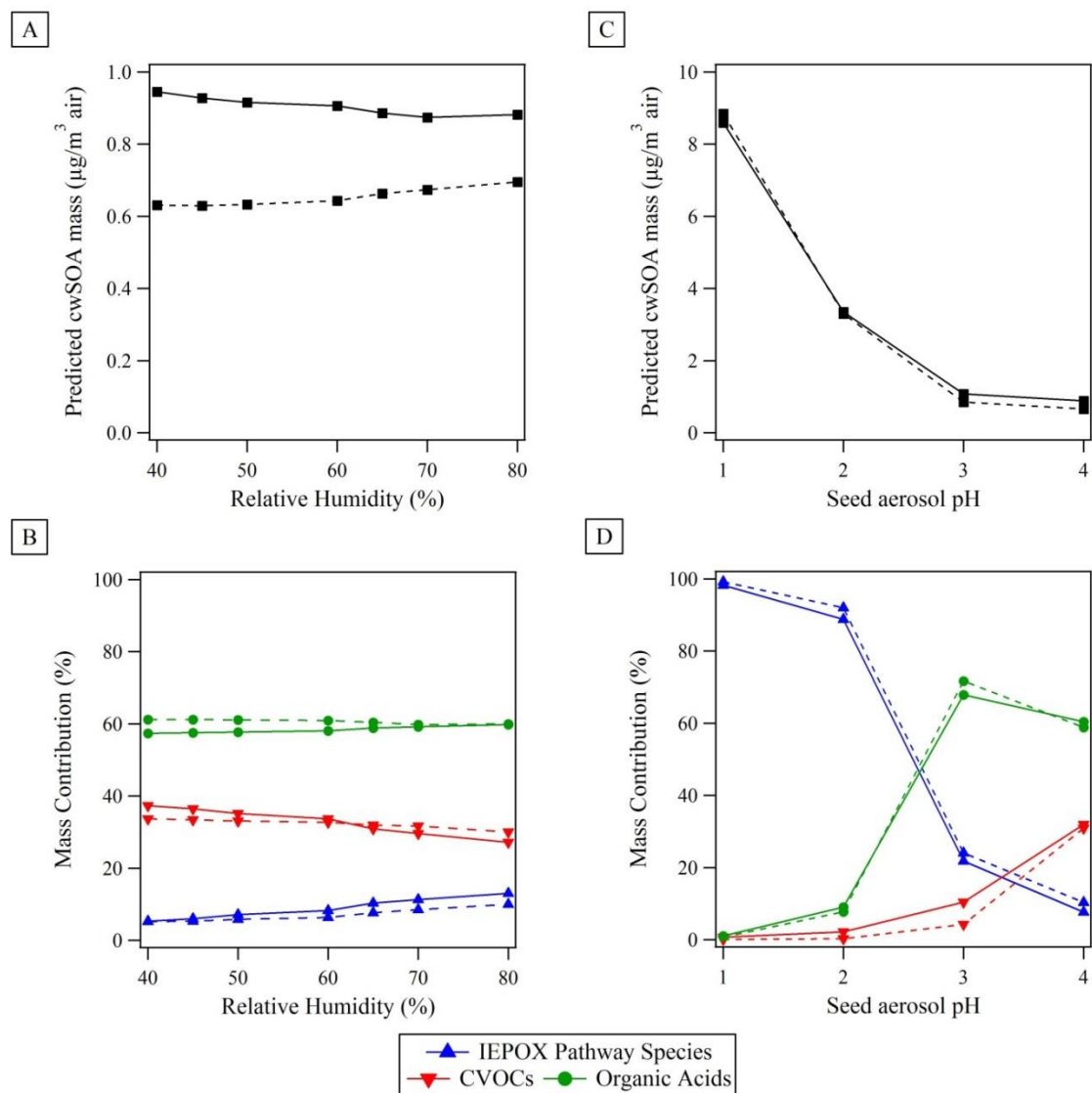
Figure 4-2 - GAMMA simulation results after 24 hours, low-NOx conditions, as a function of relative humidity with a seed aerosol pH of 4 (Panels A and B) and as a function of pH with an initial surrounding relative humidity of 65% (Panels C and D) after 12 hours of daytime simulation (dotted lines) and 24 hours of day-to-night simulation (solid lines). Panels A and C indicate total predicted formed cwSOA after simulated time. Panels B and D show relative contributions of different classes of organic species to total cwSOA mass.

4.3.2. High-NOx conditions

In urban, high-NOx conditions, IEPOX formation mechanisms are not expected to occur (*51*), resulting in a predicted prevalence of glyoxal and organic acid species. Estimated cwSOA ranges between 6-10 μg/m^3 after 24 hours of simulation, depending on seed aerosol pH and ambient relative humidity, also within general agreement with Chen et al, which estimated ~6.2 μg/m^3 after 24 hours of simulation under similar conditions (*36*).
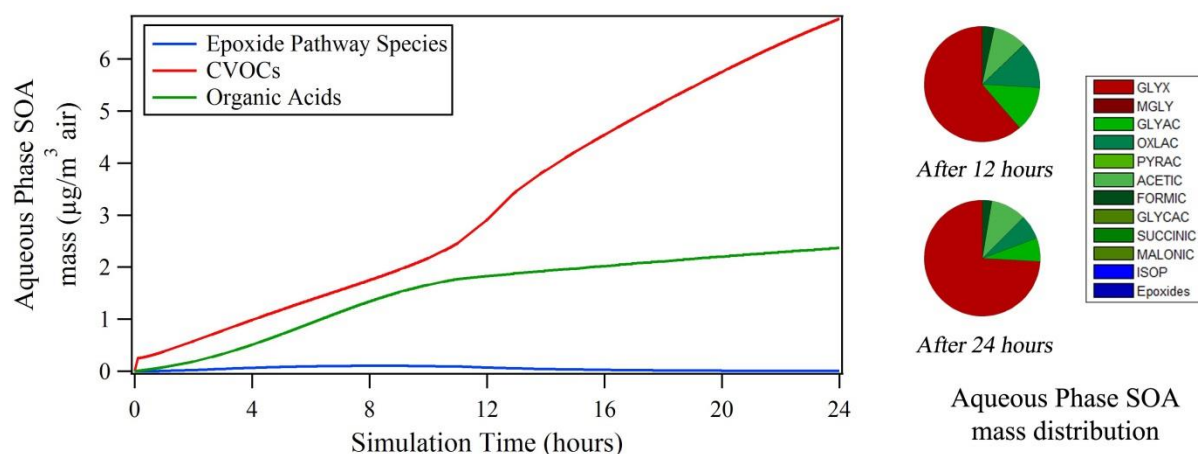
Figure 4-3 – Time dependence of different classes of cwSOA at RH 65%, pH4, under high NOx conditions. "Epoxide pathways" refers to TOL_EPOX, XYL_EPOX, EPXC4DIAL, and EPXMC4DIAL, as well as diols and diol sulfate esters formed from them. "Organic acids" is the sum of succinic, oxalic, formic, glyoxylic, pyruvic, malonic, and glycolic acids and their ionized forms. "CVOC" refers to SOA from the uptake of glyoxal, methylglyoxal, glycolaldehyde, formaldehyde, acetaldehyde, and other aldehydes.

cwSOA mass contribution from epoxide species is nearly negligible under all conditions after 24 hours of simulation. These epoxide compounds, derived from the photochemistry of emitted gas-phase aromatic VOCs, are seen to accumulate in the aerosol phase over day-time-hours via non-reactive uptake under higher-pH conditions. Upon entering the nighttime chemistry regime, ozone that persists in the gas phase will continue to react with these epoxide species (forming a

variety of CVOC and acid species), causing existent aerosol-phase epoxides to re-partition back

into the gas phase.
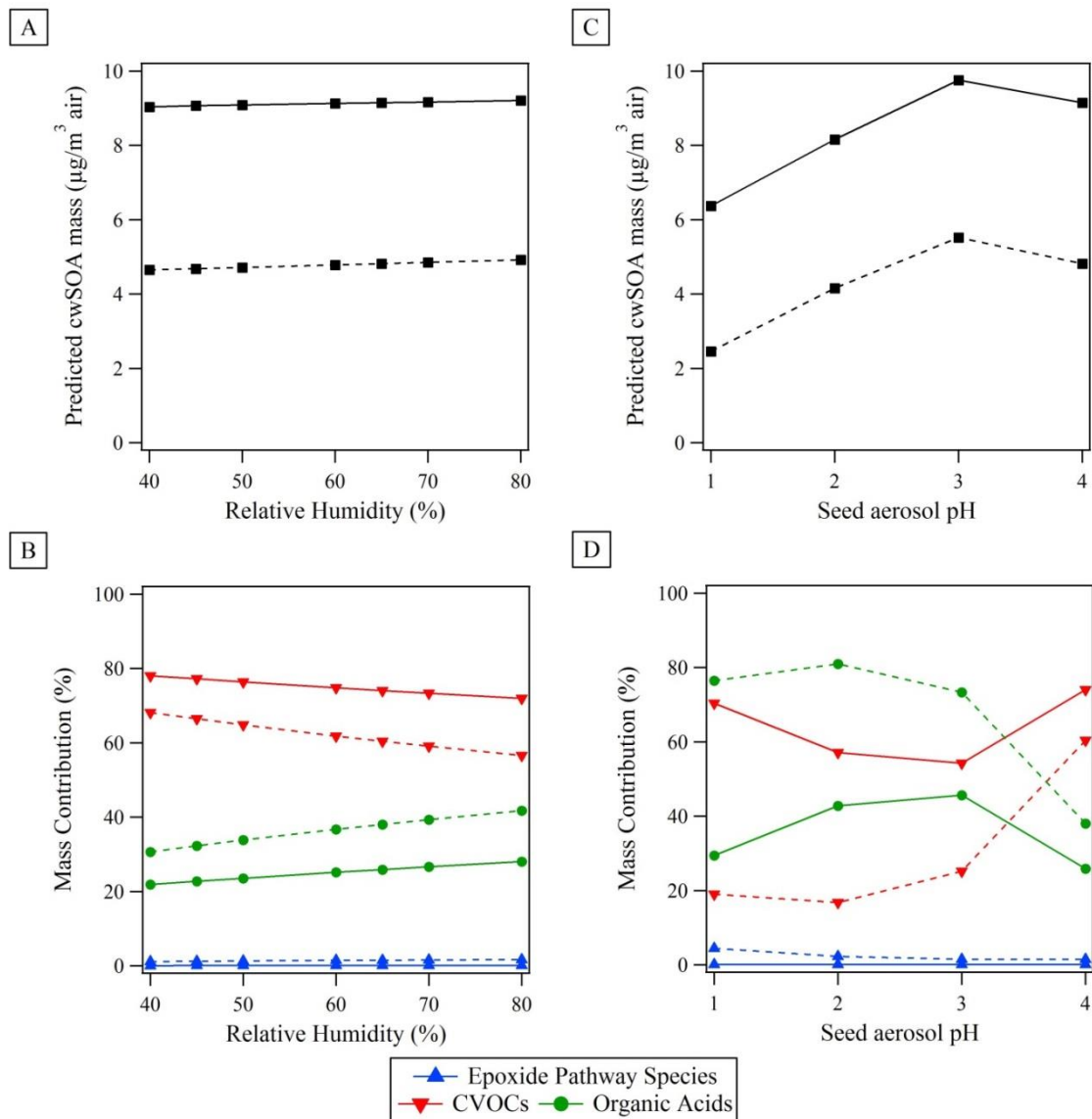
Figure 4-4 – GAMMA simulation results after 24 hours, high-NOx conditions, as a function of relative humidity with a seed aerosol pH of 4 (Panels A and B) and as a function of pH with an initial surrounding relative humidity of 65% (Panels C and D) after 12 hours of daytime simulation (dotted lines) and 24 hours of day-to-night simulation (solid lines). Panels A and C indicate total predicted formed cwSOA after simulated time. Panels B and D show relative contributions of different classes of organic species to total cwSOA mass.

55

Like in low-NOx mode, the diurnal cycling of OH radical-generating reactions is reflected in the shifts of predicted relative abundances of acids and carbonylic species between night and day. However, predicted total cwSOA formation rate remains roughly constant, regardless of simulation time. Additionally, total organic mass is not expected to change significantly at different ambient RH and seed aerosol pH values.

4.3.3. Cycling from aerosol to cloud conditions
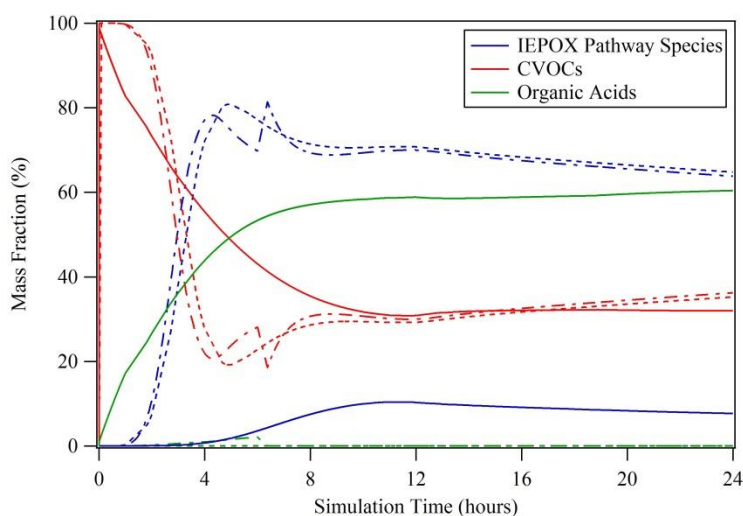
Figure 4-5 - Relative aqSOA mass contributions of IEPOX pathway products, CVOC products, and organic acid products when converted from aerosol to cloud droplet modes at 0 hours (solid lines), 1 hour (dot-dash lines), and 6 hours (dotted line). Low NOx mode, RH 65%, pH4.

Under low-NOx conditions, it can be seen that aging particles in aerosol mode will lead to large contributions from IEPOX pathway species. The mechanisms from which IEPOX products are derived are highly dependent on the activity of H^+ ions present in solution (*108*), and therefore do not dominate cwSOA formation as it did with aqueous aerosol SOA (aaSOA). By contrast, organic acids do not form in large quantities under aerosol conditions, and those that do are different from the predominating species observed in cloud samples. If the initial aerosol is sufficiently acidic to form tetrol and organosulfate substitution products, the production of these

species will halt upon conversion to cloudwater concentrations due to the sudden decrease in droplet-phase H^+ activity, leading to equilibrium partitioning of IEPOX as the only source of aqSOA mass via this pathway. Aqueous-phase CVOC species such as glyoxal are present in both cloud and aerosol particles and will be generated in both regimes.

Simulated particles that initially spent at one hour or more in aerosol mode were not seen to form organic acids upon conversion to cloud droplet chemistry. The beginning gas-phase chemistry taking place under aerosol conditions preferentially leads to rapid formation of IEPOX from isoprene, the most prevalent gas-phase precursor gas species at the beginning of simulation. This formation leads to dampened OH radical concentration in both gas and aqueous phases compared to cloud conditions, preventing further propagation of the radical species required to generate organic acids from CVOC species. This radical depletion, coupled with the high contribution of IEPOX to total aqSOA mass after as little as one hour of initial aerosol conditions, suggests that the initial lifetime of these particles as deliquesced salt aerosols must be negligible compared to their time as cloud droplets, to achieve the high organic acid content as predicted by GAMMA, when operating in cloud chemistry mode only.

Under simulated urban (high NOx) conditions, the predicted ending droplet composition shows a significantly weaker dependence on the duration of time spent as an aerosol compared to low-NOx systems. After the intial concentration perturbations caused by re-equilibration of gas-aerosol partitioning of semi-volatile species, the relative contributions of reaction pathways to overall aqSOA approach similar values after 24 hours of total simulation time, regardless of duration as a seed aerosol. CVOC contributions remain wholly comprised of glyoxal at all conditions. As a particle spends more time as a deliquesced aerosol versus a cloud droplet, organic acid contributions shift slightly towards lower-weight compounds that are formed in the

gas phase (formic and acetic acids), compared to larger species (oxalic acid and glycolic acid) that form through aqueous-phase radical processing of CVOCs.
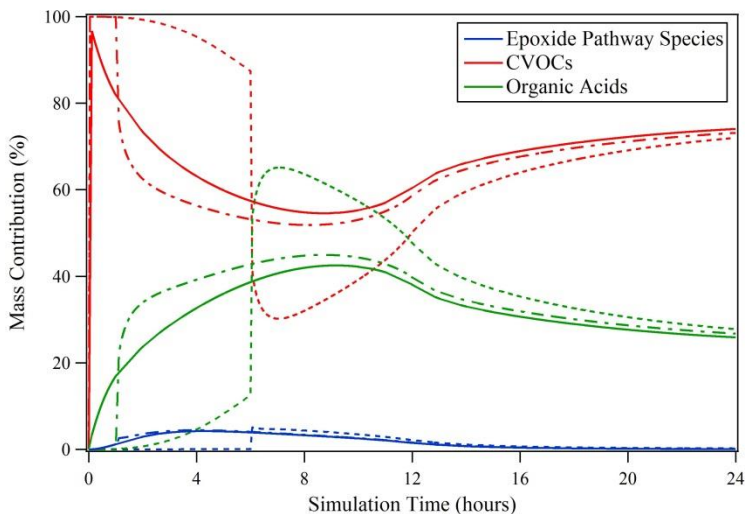
Figure 4-6 - Relative aqSOA mass contributions of epoxide pathway products, CVOC products, and organic acid products when converted from aerosol to cloud droplet modes at 0 hours (solid lines), 1 hour (dot-dash lines), and 6 hours (dotted line). High NOx mode, RH 65%, pH4.

4.3.4. Prediction of bulk aerosol property changes from cwSOA formation

Changes in surface tension and light absorbance due to SOA formation were estimated using physical property modules described in Chapter 3 and Appendix A. Composite light absorbance was approximated as a linear combination of the specific absorbance values for methylglyoxal, glyoxal, and acetaldehyde oligomers, as well as oxalic and pyruvic acid. Bulk surface tension depression was estimated using Szyszkowski-Langmuir values for methylgloxal, formaldehyde, oxalic acid, succinic acid, and acetaldehyde.

As the absolute concentrations of all organic compounds in cloud droplets are assumed to be low, and therefore yield negligible results with respect to property changes, the effect of cloud droplet chemistry on physical properties was examined by considering organic concentrations of a 10μm

droplet that was allowed to react for a given time, then subsequently dried to a diameter of 297nm, assumed to be that of a deliquesced salt aerosol, as in Chapters 2 and 3.
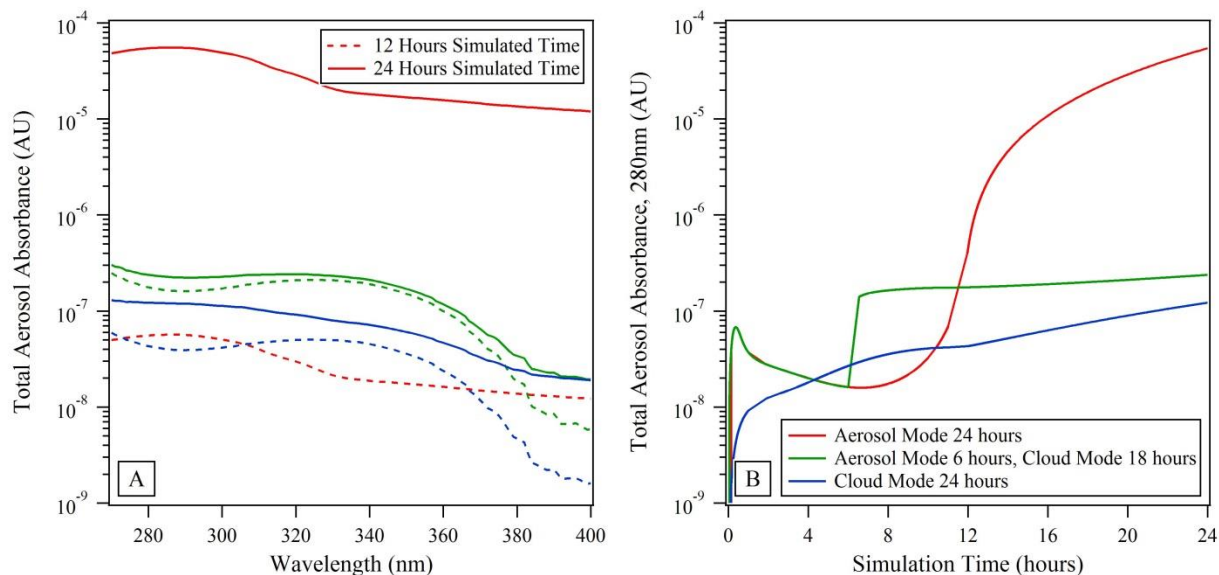
Figure 4-7 – Total aerosol light absorbance as a function of wavelength and simulation time, high-NOx mode, RH 65%, pH 4.

Despite this extra concentration effect, the predicted amount of surface-active cwSOA mass was insufficient to appreciably affect total surface tension of aerosols under any RH and pH conditions tested, for both high- and low-NOx conditions. The major contributors to surface activity in these systems were oxalic acid and formaldehyde, with negligible predicted mass formation of aqueous-phase succinic acid, methylglyoxal, and acetaldehyde.

The lower concentrations of NH_4^+ and H^+ ions lead to slower formation of light-absorbing glyoxal, methylglyoxal, and acetaldehyde oligomers compared to deliquesced aerosols, resulting in a lower contribution of these species to total aerosol light absorbance, despite the large concentrations of CVOCs present in the aerosol phase. The greater amounts of organic acids in

predicted cwSOA also results in relevant light absorbance effects from tracked acids, though still in significantly smaller values than in aerosol mode.

While oxalic acid is the more prevalent of the tracked acid species present in cwSOA, the higher specific absorbance of pyruvic acid leads to a total aerosol absorbance spectrum closer to that of pyruvic acid than oxalic acid. As this formation is not subject to the same photobleaching phenomena observed for CVOC-derived oligomers, the total light absorbance of predicted cwSOA is also not subject to the same diurnal dependence as aaSOA species, and will expect to increase over the lifetime of the particle as additional acid species are evolved. Simulations that switched between cloud droplet and aerosol modes yielded absorbance values between the two individual regimes (Figure 4-7), and were mostly dependent on the formation of pyruvic acid in total aqueous-phase organic mass.

4.4. Atmospheric Implications and suggestions for future work

The usage of GAMMA to predict cwSOA and aqSOA provide some insight on the importance of initial aerosol pH and ambient relative humidity on evolved OA mass and composition. Under low-NOx conditions, IEPOX mechanisms are seen to contribute significant amounts of SOA mass in cloud droplets, owing to the relatively high molecular mass of these species. Under high-NOx conditions, where IEPOX formation does not occur, prevailing cloud chemistry remains consistent with previous modeling and experimental studies, with the added note that initial lifetime as an aerosol does not strongly affect terminating cwSOA composition. The predictions by GAMMA for less acidic cloud droplets show consistent diurnal dependence and estimated cwSOA values compared to other kinetic models (*27*, *36*). GAMMA's initial emission and gas-phase conditions are not specific to any particular location, but are expected to be most comparable to environments where sulfate occupies a relevant portion of inorganic aerosol mass.

Crahan and coworkers observed marine cloud-phase oxalate concentrations that were 0.14 μg/m^3 air in excess of below-cloud measurements during the CARMA I campaign in California over the summer of 2002, attributing this discrepancy to cloud droplet-phase processing of biogenic, volatile precursor organics transported into measured areas (*109*). GAMMA is able to replicate these values when scaled to the sulfate loading observed in this study, estimating cloud droplet oxalate masses of 0.156 μg/m^3 air after five days of simulated time as a cloud droplet in low-NOx mode at 65% RH and pH=4. The predicted differences in prevailing aerosol-phase SOA chemistry in the cloud droplet and aerosol modes of GAMMA imply that the relative masses of dominant products in total aqueous organic aerosol mass, aqSOA, can be used to infer information about the amount of time an aerosol spends as a deliquesced salt or as a cloud droplet. Under high-NOx conditions, the amount of formed light-absorbing organic acids can be compared to glyoxal oligomers evolved via dark chemistry under deliquesced salt aerosol conditions, as droplets that spend time in both regimes are expected to have absorption spectra that lie between predicted values of the two modes individually. As mentioned, the ability for IEPOX-derived substitution products to rapidly overtake total aqSOA mass for acidic aerosols in low NOx conditions implies that the amount of time a cloud droplet spent as a deliquesced salt aerosol over its entire lifetime must be extremely short.

The conversion between cloud and aerosol regimes in GAMMA is accomplished by altering initial conditions while conserving gas and aerosol mass between iterations; as a result, the activation and deactivation of particles is assumed to be instantaneous. While uptake of water is assumed to be rapid and uninhibited under trace solute concentrations, this process is still inherently kinetic and therefore can be expected to have a transient period between cloud droplet and aerosol modes. The duration required to convert between the two regimes, extent of drying

between cycles, and propensity to reactivate upon exposure to supersaturation, will change as the aqSOA is formed. Under low-NOx conditions, the effects of IEPOX and derived tetrol or organosulfate species are potentially relevant as they occupy a large fraction of aqSOA under acidic conditions. However, as mentioned in Chapter 3, the physical properties of these compounds have not been characterized and are therefore not represented in GAMMA.

Given the prevalence of glyoxal in the aqueous phase under both cloudwater and aerosol conditions, its physical properties are especially important to properly represent its uptake and overall effect on aqSOA composition. The effective Henry's Law constant for glyoxal has been observed to vary greatly between studies based on ambient temperature, RH, and aerosol liquid water content (*49*, *110*, *111*). As the equilibrium between glyoxal and its hydrated states are likely to shift between cloud and aerosol conditions, the value of H* is also expected to also change, altering both extent and speed of partitioning as a particle converts from one mode to the other.

With these caveats in mind, GAMMA can be used to provide some insight into the primary mechanisms of SOA formation due to aqueous-phase processing in aerosols that exist in both cloud and deliquesced salt particles. As more information about physical uptake paramters and hydration mechanisms become available and subsequently implemented into GAMMA, the effect of these organic species on gas-aerosol uptake, and consequently total aerosol composition, will continue to be predicted more accurately.

CHAPTER 5

FUTURE DIRECTIONS OF GAMMA

Earlier, Chapter 2 discussed some of the limitations and preliminary ideas of future work for GAMMA, focusing on the IEPOX-based chemistry and obvious improvements to the library of physical constants required to represent gas-aerosol uptake. We now discuss other long-term directions that can be taken to further enhance the relevance, scope, and range of GAMMA in the future.

5.1. simpleGAMMA - An abridged version of GAMMA for inter-model coupling

Results from GAMMA simulations indicate that, under low-NOx conditions, organosulfate and aqueous-phase SOA formation is dominated by IEPOX ring-opening chemistry. In urban (high-NOx) environments, aaSOA is primarily formed via reversible glyoxal uptake. This suggests that it is possible to model the great majority of aqueous aerosol-phase SOA mass using a highly simplified reaction scheme which is computationally efficient and suitable for coupling with larger-scale atmospheric chemistry models.

We have therefore developed an abridged version of GAMMA, simpleGAMMA, which reduces the total number of tracked aqueous species from ~75 to 5 and the number of species partitioning between the gas and aqueous aerosol phases to 2 (glyoxal and IEPOX). The aqueous-phase organic species followed by simpleGAMMA were chosen based on relative contributions to total SOA mass predicted by the complete version of GAMMA after 12 hours of simulation.

The aqueous species tracked by simpleGAMMA are listed below:

> Low-NOx:
> - o [IEPOX] – Isoprene-derived dihydroxyepoxide

- o [IEPOXOS] – Organosulfate species from sulfate nucleophilic substitution in IEPOX
- o [tetrol] –Tetrol species from nucleophilic hydration of IEPOX
- o [GLYX] – Glyoxal.

High-NOx:

- o [GLYX] – Glyoxal.

The gas phase mechanism of GAMMA has not been changed for simpleGAMMA, since it is expected that gas-phase chemical composition fields will be adopted from the large-scale model (CMAQ, Geos-CHEM, etc.) being interfaced with GAMMA.

General agreement (to within 40% of predicted SOA mass) between simpleGAMMA and the full version of GAMMA described in Chapter 2 is observed under all conditions tested (between pH 1-4 and RH 40-80%), after 12 hours of simulation. Under low-NOx conditions, simpleGAMMA consistently overestimates SOA mass formation compared to its complete version. This discrepancy likely has to do with the CVOC and acid species that are formed and uptake into the aqueous phase in the complete version of GAMMA; upon formation, these species drive down the concentration of OH radicals in the gas phase, which are responsible for both the generation and gas-phase decomposition of IEPOX. The apparent result is an increase in gas-phase IEPOX at all times, which then results in over-predicted SOA mass. After 3 hours of simulation, the relative contribution of this excess IEPOX drops to between 15-20% deviation from the complete version of GAMMA (Figure 5-1), increasing with lower RH and pH values.

Conversely, under high-NOx conditions, the simplified build of GAMMA maintains nearly perfect agreement to its complete version until roughly three hours into simulation (vis Figure 5-2). At this stage, glyoxal-derived radical species accumulate in the aqueous phase in the complete version, and the lack of aqueous-phase oxidation chemistry introduces more error. As

glyoxal soon becomes the dominant SOA species as the simulation continues, the discrepancy between the two remains relatively constant as the total SOA mass builds. Deviation between the two versions maximizes at 24%, roughly 8 hours into simulation.
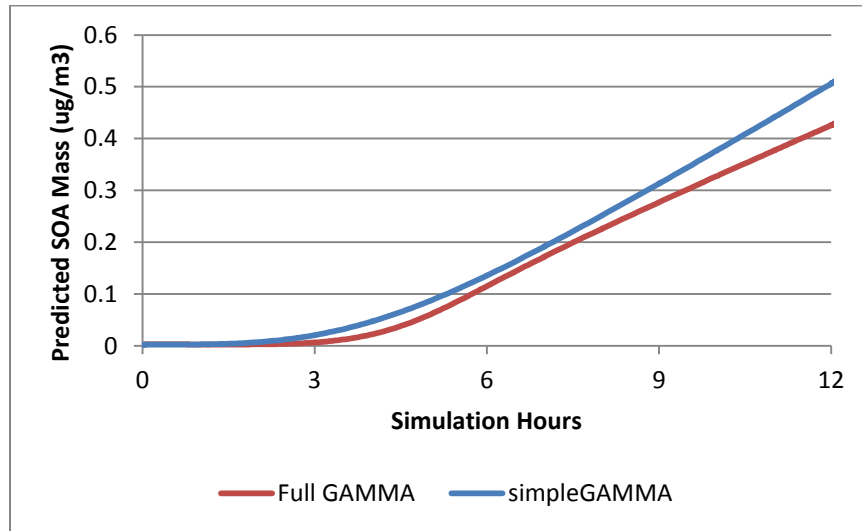
Figure 5-1 - Comparison of low-NOx simpleGAMMA and the full low-NOx GAMMA, pH1, RH45.
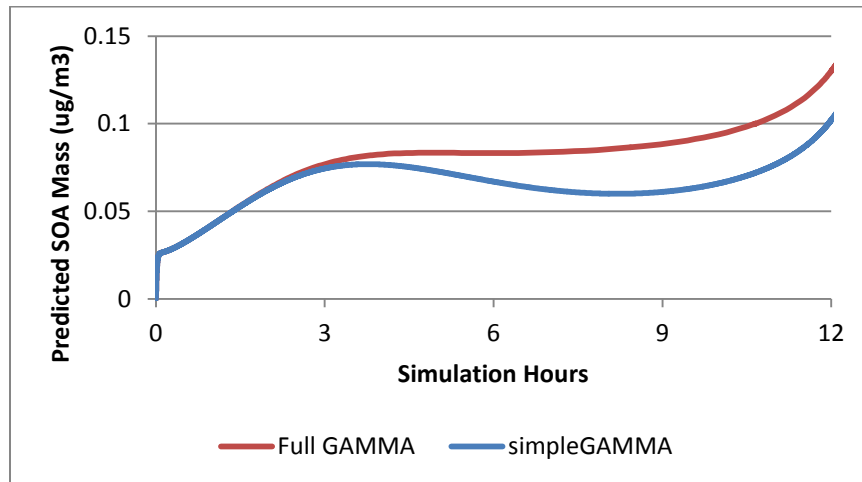
Figure 5-2 - Comparison of high-NOx simpleGAMMA and the full high-NOx GAMMA, pH1, RH80.

5.2. Implementation of Other Organic Precursors

The gas-phase precursors currently tracked by GAMMA (acetylene, isoprene, toluene, and xylenes) were chosen due to their ability to form water-soluble SOA and their presence in rural or urban environments. In rural environments, non-oxidized biogenic volatile organic compounds (BVOC) such as isoprene comprise the bulk of these precursors. As previously mentioned, emissions of these species can reach up to 660 teragrams of carbon per year (*20–22*), justifying their inclusion into GAMMA.

As mentioned in Chapter 1, the formation of organosulfates is a particularly interesting branch of aerosol-phase chemistry in these environments, due to their contributions to observed SOA mass (*52*, *81*, *112*, *113*) and potential effects on surface tension and cloud condensation nuclei formation, due to their amphiphilic nature. In addition, "brown carbon" species, which include nitrogen-containing or carbonyl-derived oligomeric compounds, have been shown to change the light-absorbing properties of the aerosol in which they reside, therefore affecting their contributed total direct radiative forcing effects to the atmosphere. We now discuss potential avenues of future development to GAMMA, based upon their prominence in the atmosphere as a whole, and the relevance of their chemistry to aqueous aerosols.

5.2.1. Low-weight Biogenic Oxidized VOCs

Apart from isoprene, oxidized BVOCs (such as aldehydes, alcohols, or ketones) can also be directly emitted into the atmosphere, in smaller but still significant quantities. (*114*, *115*) Collective global emission rates are predicted to be as high as 22% of the total biogenic compounds emitted annually. (*22*)

Isoprene (ISOP)   2-methyl-3-buten-2-ol (MBO)
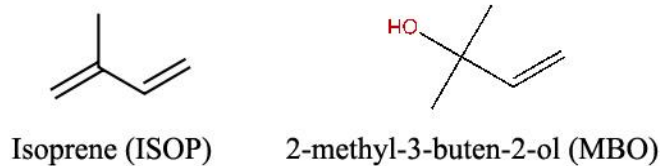
Figure 5-3 – Molecular structures of isoprene and 2-methyl-3-buten-2-ol (MBO).

One such compound, 2-methyl-3-buten-2-ol (MBO), is very similar in structure to that of isoprene (Figure 5-3). MBO has been seen to form many photo-oxidation products similar to those produced by isoprene under low and high-NOx conditions. (*116*, *117*) It has also recently been proposed by Chan et al. that MBO undergoes epoxide formation mechanisms analogous to those that evolve IEPOX from isoprene, suggesting the formation of potentially surface-relevant organosulfate compounds. (*118*)
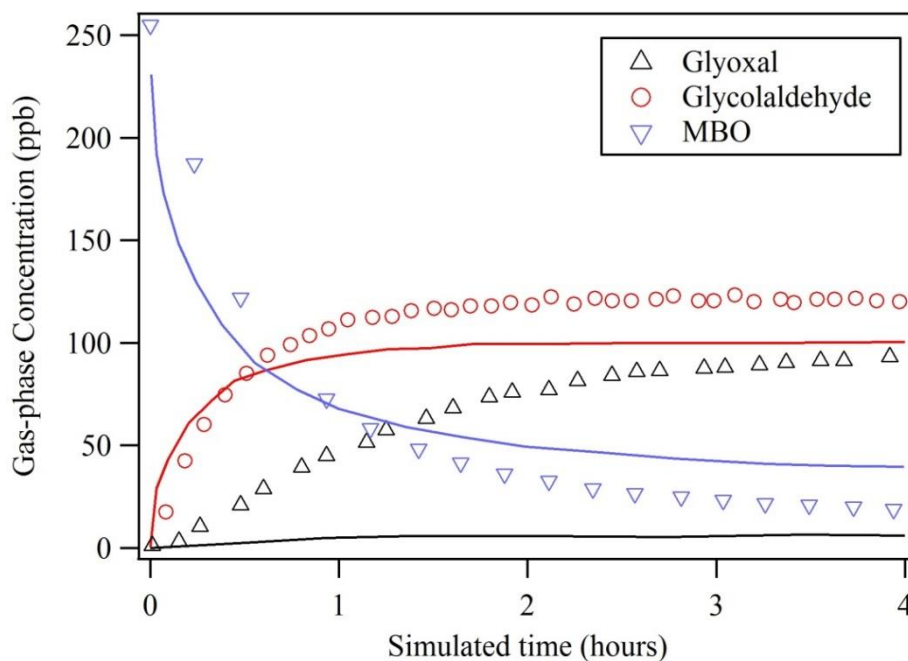
Figure 5-4 - Comparison of data from Chan 2009 (data points) to GAMMA simulations (solid line), for MBO photo-oxidation under similar high-NOx conditions.

While global emission rates of MBO are generally seen as negligible compared to isoprene, observations in the western United States also indicate that local emissions of MBO can often match or surpass isoprene during the summer (*119*). Therefore, it is necessary to implement this branch of chemistry into GAMMA to maintain proper accounting of gas-phase OH (and subsequently prevailing gas-phase photochemistry under those conditions.)

Preliminary work to implement gas-phase oxidation mechanisms of MBO into GAMMA is able to replicate gas-phase chemistry observed in laboratory chamber studies within an order of magnitude. These reactions can be added or removed from GAMMA's main library of reactions to minimize computational load, if these precursors are not a major source under the conditions being tested.

5.2.2. Monoterpenes

Monoterpenes, a class of organic molecules defined by their general structure of two linked isoprene backbones, also exist in large quantities in the atmosphere, collectively reaching emission rates on the same order of magnitude as isoprene, as high as 127 teragrams of carbon per year. (*20*, *22*) The most common of the monoterpenes, α-pinene, readily converts to α–pinene oxide (αPO) when exposed to gas-phase oxidants (OH/HO$_2$ radicals, ozone, etc.) αPO, as an epoxide species, also has the potential to form organosulfate or diol compounds under acidic conditions. (*40*, *43*, *47*, *107*, *120*, *121*)
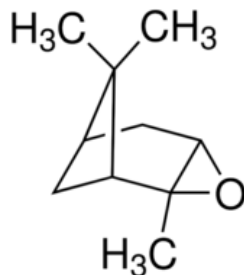
Figure 5-5 - Molecular structure of alpha-pinene oxide.

The low O:C ratio of αPO and other terpene-derived species suggests that uptake of such species may lead to the formation of a second, organic-rich liquid phase, rather than dissolution into aerosol water. Work by our own group observed self-limiting uptake of αPO in chamber studies, with liquid-liquid phase separation between αPO and sulfate in bulk solution mimics. (*122*)

Special care must therefore be taken when considering the applicability of monoterpene oxidation products in aqueous aerosols; the solubility limit for these species is significantly lower compared to that of isoprene-derived products, and as such will be more prone to yielding predicted aqueous concentrations that are not realistic. That said, the formation of terpene-derived organosulfate species has been shown to be dependent on total aerosol acidity, with negligible uptake except under extremely acidic (pH < 1) aerosol conditions, (*39*, *40*, *43*, *120*, *122*) so it is possible that this concentration limit will not be reached under normal atmospheric conditions. As high bulk concentrations are not necessary for surfactant species to affect net aerosol properties, (*38*) the aqueous chemistry taking place may still be in teresting   to   track regardless of its accuracy as predicted by GAMMA's current surface tension modules.

5.3. Mechanisms of Future Interest

Due to the largely bottom-up design to GAMMA's modeled gas- and aerosol-phase chemistry, the accuracy of its prediction of aaSOA and aqSOA mass is dependent on the ability of implemented mechanisms to properly represent the dominating chemistry taking place in the environment being tested. This accuracy is dependent on two factors: the ability of GAMMA to track prevailing observed species in the tested environment, and the existing library of modeled reactions compiled within GAMMA itself. We now discuss some preliminary work that has been done on both of these fronts, and suggest new directions that can be taken to improve the accuracy and robustness of GAMMA on a whole.

5.3.1. Phenolic Chemistry

Partially oxygenated VOCs can also be emitted into the atmosphere through anthropogenic sources, such as combustion. The vast majority of OA mass generated through combustion mechanisms arises from biomass burning such as residential wood burning or deforestation. (*123*) Aerosol formation of these gas-phase combustion species may be of relevance as local concentrations are likely to surpass otherwise prevailing organic emissions during major biomass burning events in rural areas. It is desirable to capture relevant chemistry within GAMMA's library of reactions, particularly if water-soluble oxidation products are generated in significant quantities.

Phenols and methoxyphenols are major pyrolysis products of lignin (a central component of plant tissue), comprising as much as 21% and 45% of total OA in samples of collected wood smoke particulate matter, respectively. (*124*) These species can also arise from photooxidation of other gas-phase aromatic compounds. (*125*)

Exposure to radicals in both the gas and aqueous phase can lead to ring opening or cleavage reactions, resulting in a host of several semi-volatile products. Previous work with smog chamber photooxidation of guaiacol and catechol resulted in observed concentrations of lactones, esters, carboxylic acids, and carboxylic anhydride-containing species, (*126*, *127*) several of which already exist in GAMMA (eg. Pyruvic acid and glyoxal). Reactivity appears to increase with the addition of methoxy groups, making syringol a more likely candidate for interesting aerosol-phase chemistry compared to guaiacol or phenol; however, all of the mentioned species have the ability to form epoxide species upon ring opening, thus making them attractive as possible candidates for organosulfate formation. (*127*) Other studies with similar oxidized aromatic species have observed rearrangement and isomerization products.(*125*, *128*, *129*) Furthermore, oligomerization reactions are also possible with these species under photolytic conditions, with cleaved methoxy groups breaking off to form formic and oxalic acids. (*130*)
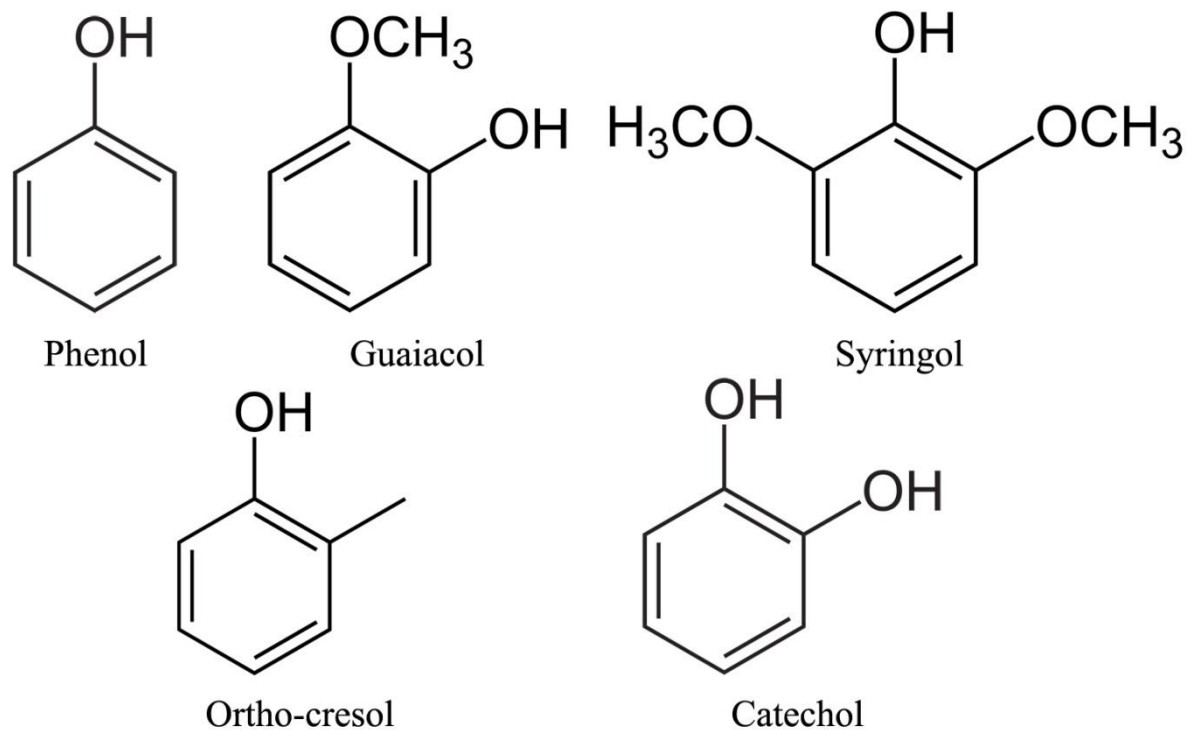
Figure 5-6 - Molecular structures of phenol and methoxyphenols.

While several oxidation products of phenolic species have been identified, limited kinetic information exists for many of these oxidation mechanisms. As more data with these mechanisms becomes available, this branch of chemistry will be a high-interest target for implementation into GAMMA.

5.3.2. Photosensitizers

As mentioned in Chapters 1 and 3, carbonyl containing compounds such as glyoxal and methylglyoxal have the ability to form light-absorbing compounds once absorbed into aerosol phase. Previous work from several groups, including our own, has indicated the presence of nitrogen containing compounds arising from organic uptake onto ammonium salt aerosols. (*6*, *49*, *106*, *131*)
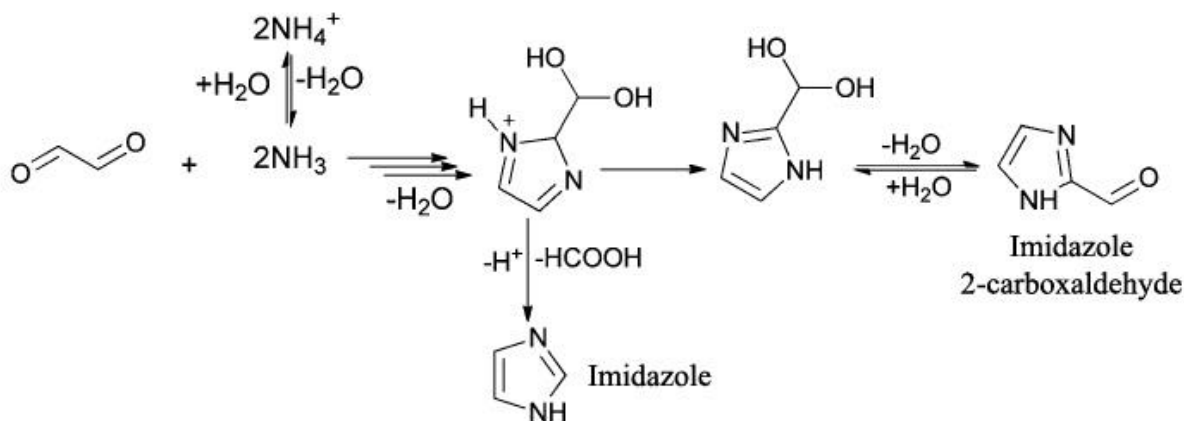
Figure 5-7 - Glyoxal can react with ammonium ions to form light-absorbing, nitrogen-containing compounds such as imidazoles. (Mechanisms from Yu 2011 and Kampf 2012, figure modified from Aregahegn 2013.)

These light-absorbing compounds are expected to be forming from ammonium ion interactions with dicarbonyl compounds; Galloway and coworkers first discovered imidazole-2-carboxaldehyde as a product of glyoxal in ammonium sulfate (*49*), which was later expanded upon by Yu to include imidazole and glyoxal-substituted imidazole derivatives. (*106*) These compounds are absorptive at 280nm, consistent with aged aerosol mimic studies performed by our group. (*4*, *6*) These imidazole compounds are photosensitizing species, reversibly forming radicals and facilitating further aerosol-phase chemistry under irradiated conditions. Experimental work by Aregahegn indicates increased SOA mass accumulation of SOA derived from several terpene and aromatic precursor gases in the presence of these imidazole species, biasing towards unsaturated tertiary carbons. (*132*)

Currently, GAMMA does not cover this family of reactions, instead lumping light-absorbing products of glyoxal, methylglyoxal, and aldehyde species into a single proxy term with absorption properties based upon work by our group and Noziére et al. (*5*, *6*, *76*) As the

photosensitizing behavior of imidazole species is not properly represented in GAMMA, implementing the kinetics of these reactions will be beneficial for more accurate accounting of both glyoxal-derived SOA products, as well as the mechanisms that are boosted by the presence of these photosensitizing species.

REFERENCES

(1)   Malm, W. C. Atmospheric haze: Its sources and effects on visibility in rural areas of the continental United States. *Environ. Monit. Assess.* **1989**, *12*, 203–225.

(2)   Pope, C. A.; Dockery, D. W. Health Effects of Fine Particulate Air Pollution: Lines that Connect. *J. Air Waste Manage. Assoc.* **2006**, *56*, 709–742.

(3)   Isaksen, I. S. a.; Granier, C.; Myhre, G.; Berntsen, T. K.; Dalsøren, S. B.; Gauss, M.; Klimont, Z.; Benestad, R.; Bousquet, P.; Collins, W.; Cox, T.; Eyring, V.; Fowler, D.; Fuzzi, S.; Jöckel, P.; Laj, P.; Lohmann, U.; Maione, M.; Monks, P.; Prevot, A. S. H.; Raes, F.; Richter, A.; Rognerud, B.; Schulz, M.; Shindell, D.; Stevenson, D. S.; Storelvmo, T.; Wang, W.-C.; van Weele, M.; Wild, M.; Wuebbles, D. Atmospheric composition change: Climate–Chemistry interactions. *Atmos. Environ.* **2009**, *43*, 5138–5192.

(4)   Sareen, N.; Schwier, A. N.; Shapiro, E. L.; Mitroo, D.; McNeill, V. F. Secondary organic material formed by methylglyoxal in aqueous aerosol mimics. *Atmos. Chem. Phys.* **2010**, *10*, 997–1016.

(5)   Schwier, A. N.; Sareen, N.; Mitroo, D.; Shapiro, E. L.; McNeill, V. F. Glyoxal-methylglyoxal cross-reactions in secondary organic aerosol formation. *Environ. Sci. Technol.* **2010**, *44*, 6174–6182.

(6)   Shapiro, E. L.; Szprengiel, J.; Sareen, N.; Jen, C. N.; Giordano, M. R.; McNeill, V. F. Light-absorbing secondary organic material formed by glyoxal in aqueous aerosol mimics. *Atmos. Chem. Phys.* **2009**, 2289–2300.

(7)   Nozière, B.; Dziedzic, P.; Córdova, A. Inorganic ammonium salts and carbonate salts are efficient catalysts for aldol condensation in atmospheric aerosols. *Phys. Chem. Chem. Phys.* **2010**, *12*, 3864–72.

(8)   Li, Z.; Schwier, A. N.; Sareen, N.; McNeill, V. F. F. Reactive processing of formaldehyde and acetaldehyde in aqueous aerosol mimics: Surface tension depression and secondary organic products. *Atmos. Chem. Phys.* **2011**, *11*, 11617–11629.

(9)   Nozière, B.; Dziedzic, P.; Córdova, A. Formation of secondary light-absorbing "fulvic-like" oligomers: A common process in aqueous and ionic atmospheric particles? *Geophys. Res. Lett.* **2007**, *34*, 1–5.

(10)   Rincón, A. G.; Guzmán, M. I.; Hoffmann, M. R.; Colussi, a J. Optical absorptivity versus molecular composition of model organic aerosol matter. *J. Phys. Chem. A* **2009**, *113*, 10512–20.

(11) Lund Myhre, C. E.; Nielsen, C. J. Optical properties in the UV and visible spectral region of organic acids relevant to tropospheric aerosols. *Atmos. Chem. Phys. Discuss.* **2004**, *4*, 3013–3043.

(12) Stocker, T.; Qin, D.; Plattner, G.-K. *Contribution of Working Group I to the Fifth Assessment Report of the Intergovernmental Panel on Climate Change*; Cambridge, UK, 2013.

(13) Albrecht, B. A. Aerosols, cloud microphysics, and fractional cloudiness. *Science* **1989**, *245*, 1227–30.

(14) Köhler, H. The nucleus in and the growth of hygroscopic droplets. *Trans. Faraday Soc.* **1936**, *32*, 1152.

(15) Seinfeld, J. H.; Pandis, S. N. *Atmospheric Chemistry and physics: from air pollution to climate change*; 2nd ed.; Wiley: New York, 1998.

(16) Kanakidou, M.; Seinfeld, J. H.; Pandis, S. N.; Barnes, I.; Dentener, F. J.; Facchini, M. C.; Van Dingenen, R.; Ervens, B.; Nenes, A.; Nielsen, C. J.; Swietlicki, E.; Putaud, J. P.; Balkanski, Y.; Fuzzi, S.; Horth, J.; Moortgat, G. K.; Winterhalter, R.; Myhre, C. E. L.; Tsigaridis, K.; Vignati, E.; Stephanou, E. G.; Wilson, J. Organic aerosol and global climate modelling: a review. *Atmos. Chem. Phys.* **2005**, *5*, 1053–1123.

(17) Zhang, Q.; Jimenez, J. L.; Canagaratna, M. R.; Allan, J. D.; Coe, H.; Ulbrich, I.; Alfarra, M. R.; Takami, a.; Middlebrook, a. M.; Sun, Y. L.; Dzepina, K.; Dunlea, E.; Docherty, K.; DeCarlo, P. F.; Salcedo, D.; Onasch, T.; Jayne, J. T.; Miyoshi, T.; Shimono, a.; Hatakeyama, S.; Takegawa, N.; Kondo, Y.; Schneider, J.; Drewnick, F.; Borrmann, S.; Weimer, S.; Demerjian, K.; Williams, P.; Bower, K.; Bahreini, R.; Cottrell, L.; Griffin, R. J.; Rautiainen, J.; Sun, J. Y.; Zhang, Y. M.; Worsnop, D. R. Ubiquity and dominance of oxygenated species in organic aerosols in anthropogenically-influenced Northern Hemisphere midlatitudes. *Geophys. Res. Lett.* **2007**, *34*, L13801.

(18) Pankow, J. F. An absorption model of gas/particle partitioning involved in the formation of secondary organic aerosol. *Atmos. Environ.* **1994**, *28*, 189–193.

(19) Odum, J. R.; Hoffmann, T.; Bowman, F.; Collins, D.; Flagan, R. C.; Seinfeld, J. H. Gas/Particle Partitioning and Secondary Organic Aerosol Yields. *Environ. Sci. Technol.* **1996**, *30*, 2580–2585.

(20) Guenther, A.; Hewitt, C. N.; Erickson, D.; Fall, R.; Geron, C.; Graedel, T.; Harley, P.; Klinger, L.; Lerdau, M.; Mckay, W. A.; Pierce, T.; Scholes, B.; Steinbrecher, R.; Tallamraju, R.; Taylor, J.; Zimmerman, P. A global model of natural volatile organic compound emissions. *J. Geophys. Res.* **1995**, *100*, 8873.

(21) Guenther, a.; Karl, T.; Harley, P.; Wiedinmyer, C.; Palmer, P. I.; Geron, C. Estimates of global terrestrial isoprene emissions using MEGAN (Model of Emissions of Gases and Aerosols from Nature). *Atmos. Chem. Phys. Discuss.* **2006**, *6*, 107–173.

(22) Kesselmeier, J.; Staudt, M. Biogenic Volatile Organic Compounds (VOC): An Overview on Emission , Physiology and Ecology. *J. Atmos. Chem.* **1999**, *33*, 23–88.

(23) Ervens, B.; Volkamer, R. Glyoxal processing by aerosol multiphase chemistry: towards a kinetic modeling framework of secondary organic aerosol formation in aqueous particles. *Atmos. Chem. Phys.* **2010**, *10*, 8219–8244.

(24) Levy, H. Normal atmosphere: large radical and formaldehyde concentrations predicted. *Science* **1971**, *173*, 141–3.

(25) Volkamer, R.; Platt, U.; Wirtz, K. Primary and Secondary Glyoxal Formation from Aromatics: Experimental Evidence for the Bicycloalkyl−Radical Pathway from Benzene, Toluene, and p -Xylene. *J. Phys. Chem. A* **2001**, *105*, 7865–7874.

(26) Volkamer, R.; San Martini, F.; Molina, L. T.; Salcedo, D.; Jimenez, J. L.; Molina, M. J. A missing sink for gas-phase glyoxal in Mexico City: Formation of secondary organic aerosol. *Geophys. Res. Lett.* **2007**, *34*, 1–5.

(27) Lim, H.-J.; Carlton, A. G.; Turpin, B. J. Isoprene Forms Secondary Organic Aerosol through Cloud Processing. *Environ. Sci. Technol.* **2005**, *39*, 4441–4446.

(28) Sorooshian, A.; Lu, M.-L.; Brechtel, F. J.; Jonsson, H.; Feingold, G.; Flagan, R. C.; Seinfeld, J. H. On the source of organic acid aerosol layers above clouds. *Environ. Sci. Technol.* **2007**, *41*, 4647–54.

(29) Tan, Y.; Carlton, A. G.; Seitzinger, S. P.; Turpin, B. J. SOA from methylglyoxal in clouds and wet aerosols: Measurement and prediction of key products. *Atmos. Environ.* **2010**, *44*, 5218–5226.

(30) Perri, M. J.; Seitzinger, S.; Turpin, B. J. Secondary organic aerosol production from aqueous photooxidation of glycolaldehyde: Laboratory experiments. *Atmos. Environ.* **2009**, *43*, 1487–1497.

(31) Altieri, K. E.; Seitzinger, S. P.; Carlton, a. G.; Turpin, B. J.; Klein, G. C.; Marshall, a. G. Oligomers formed through in-cloud methylglyoxal reactions: Chemical composition, properties, and mechanisms investigated by ultra-high resolution FT-ICR mass spectrometry. *Atmos. Environ.* **2008**, *42*, 1476–1490.

(32) Altieri, K. E.; Carlton, A. G.; Lim, H.-J.; Turpin, B. J.; Seitzinger, S. P. Evidence for oligomer formation in clouds: reactions of isoprene oxidation products. *Environ. Sci. Technol.* **2006**, *40*, 4956–60.

(33) Tan, Y.; Lim, Y. B.; Altieri, K. E.; Seitzinger, S. P.; Turpin, B. J. Mechanisms leading to oligomers and SOA through aqueous photooxidation: insights from OH radical oxidation of acetic acid and methylglyoxal. *Atmos. Chem. Phys.* **2012**, *12*, 801–813.

(34) Ervens, B.; Turpin, B. J.; Weber, R. J. Secondary organic aerosol formation in cloud droplets and aqueous particles (aqSOA): a review of laboratory, field and model studies. *Atmos. Chem. Phys.* **2011**, *11*, 11069–11102.

(35) Ervens, B.; Carlton, A. G.; Turpin, B. J.; Altieri, K. E.; Kreidenweis, S. M.; Feingold, G. Secondary organic aerosol yields from cloud-processing of isoprene oxidation products. *Geophys. Res. Lett.* **2008**, *35*, L02816.

(36) Chen, J.; Griffin, R. J.; Grini, a.; Tulet, P. Modeling secondary organic aerosol formation through cloud processing of organic compounds. *Atmos. Chem. Phys. Discuss.* **2007**, *7*, 8951–8982.

(37) Sareen, N.; Moussa, S. G.; McNeill, V. F. Photochemical aging of light-absorbing secondary organic aerosol material. *J. Phys. Chem. A* **2013**, *117*, 2987–96.

(38) Sareen, N.; Schwier, A. N.; Lathem, T. L.; Nenes, A.; McNeill, V. F. Surfactants from the gas phase may promote cloud droplet formation. *Proc. Natl. Acad. Sci. U. S. A.* **2013**, *110*, 2723–8.

(39) Surratt, J. D.; Lewandowski, M.; Offenberg, J. H.; Jaoui, M.; Kleindienst, T. E.; Edney, E. O.; Seinfeld, J. H. Effect of acidity on secondary organic aerosol formation from isoprene. *Environ. Sci. Technol.* **2007**, *41*, 5363–9.

(40) Surratt, J. D.; Kroll, J. H.; Kleindienst, T. E.; Edney, E. O.; Claeys, M.; Sorooshian, A.; Ng, N. L.; Offenberg, J. H.; Lewandowski, M.; Jaoui, M.; Flagan, R. C.; Seinfeld, J. H. Evidence for organosulfates in secondary organic aerosol. *Environ. Sci. Technol.* **2007**, *41*, 517–27.

(41) Gómez-González, Y.; Surratt, J. D.; Cuyckens, F.; Szmigielski, R.; Vermeylen, R.; Jaoui, M.; Lewandowski, M.; Offenberg, J. H.; Kleindienst, T. E.; Edney, E. O.; Blockhuys, F.; Van Alsenoy, C.; Maenhaut, W.; Claeys, M. Characterization of organosulfates from the photooxidation of isoprene and unsaturated fatty acids in ambient aerosol using liquid chromatography/(-) electrospray ionization mass spectrometry. *J. Mass Spectrom.* **2008**, *43*, 371–82.

(42) Surratt, J. D.; Gómez-González, Y.; Chan, A. W. H.; Vermeylen, R.; Shahgholi, M.; Kleindienst, T. E.; Edney, E. O.; Offenberg, J. H.; Lewandowski, M.; Jaoui, M.; Maenhaut, W.; Claeys, M.; Flagan, R. C.; Seinfeld, J. H. Organosulfate formation in biogenic secondary organic aerosol. *J. Phys. Chem. A* **2008**, *112*, 8345–78.

(43) Iinuma, Y.; Böge, O.; Kahnt, A.; Herrmann, H. Laboratory chamber studies on the formation of organosulfates from reactive uptake of monoterpene oxides. *Phys. Chem. Chem. Phys.* **2009**, *11*, 7759.

(44) Iinuma, Y.; Müller, C.; Berndt, T.; Böge, O.; Claeys, M.; Herrmann, H. Evidence for the existence of organosulfates from beta-pinene ozonolysis in ambient secondary organic aerosol. *Environ. Sci. Technol.* **2007**, *41*, 6678–83.

(45) Deno, N. C.; Newman, M. S. Mechanism of Sulfation of Alcohols. *J. Am. Chem. Soc.* **1950**, *72*, 3852–3856.

(46) Minerath, E. C.; Casale, M. T.; Elrod, M. J. Kinetics feasibility study of alcohol sulfate esterification reactions in tropospheric aerosols. *Environ. Sci. Technol.* **2008**, *42*, 4410–5.

(47) Minerath, E. C.; Elrod, M. J. Assessing the potential for diol and hydroxy sulfate ester formation from the reaction of epoxides in tropospheric aerosols. *Environ. Sci. Technol.* **2009**, *43*, 1386–92.

(48) Perri, M. J.; Lim, Y. B.; Seitzinger, S. P.; Turpin, B. J. Organosulfates from glycolaldehyde in aqueous aerosols and clouds: Laboratory studies. *Atmos. Environ.* **2010**, *44*, 2658–2664.

(49) Galloway, M. M.; Chhabra, P. S.; Chan, a. W. H.; Surratt, J. D.; Flagan, R. C.; Seinfeld, J. H.; Keutsch, F. N. Glyoxal uptake on ammonium sulphate seed aerosol: reaction products and reversibility of uptake under dark and irradiated conditions. *Atmos. Chem. Phys.* **2009**, *9*, 3331–3345.

(50) Surratt, J. D.; Chan, A. W. H.; Eddingsaas, N. C.; Chan, M.; Loza, C. L.; Kwan, A. J.; Hersey, S. P.; Flagan, R. C.; Wennberg, P. O.; Seinfeld, J. H. Reactive intermediates revealed in secondary organic aerosol formation from isoprene. *Proc. Natl. Acad. Sci. U. S. A.* **2010**, *107*, 6640–5.

(51) Paulot, F.; Crounse, J. D.; Kjaergaard, H. G.; Kürten, A.; St Clair, J. M.; Seinfeld, J. H.; Wennberg, P. O. Unexpected epoxide formation in the gas-phase photooxidation of isoprene. *Science* **2009**, *325*, 730–3.

(52) Hatch, L. E.; Creamean, J. M.; Ault, A. P.; Surratt, J. D.; Chan, M. N.; Seinfeld, J. H.; Edgerton, E. S.; Su, Y.; Prather, K. a Measurements of isoprene-derived organosulfates in ambient aerosols by aerosol time-of-flight mass spectrometry - part 1: single particle atmospheric observations in Atlanta. *Environ. Sci. Technol.* **2011**, *45*, 5105–11.

(53) Griffin, R. J.; Nguyen, K.; Dabdub, D. A Coupled Hydrophobic-Hydrophilic Model for Predicting Secondary Organic Aerosol Formation. *J. Atmos. Chem.* **2003**, *44*, 171–190.

(54) Pankow, J. F. An absorption model of gas/particle partitioning of organic compounds in the atmosphere. *Atmos. Environ.* **1994**, *28*, 185–188.

(55) Chen, J.; Griffin, R. Modeling secondary organic aerosol formation from oxidation of -pinene, -pinene, and -limonene. *Atmos. Environ.* **2005**, *39*, 7731–7744.

(56) Chen, J.; Mao, H.; Talbot, R. W.; Griffin, R. J. Application of the CACM and MPMPO modules using the CMAQ model for the eastern United States. *J. Geophys. Res.* **2006**, *111*, D23S25.

(57) Ervens, B. A modeling study of aqueous production of dicarboxylic acids: 1. Chemical pathways and speciated organic mass production. *J. Geophys. Res.* **2004**, *109*, D15205.

(58) Griffin, R. J.; Dabdub, D.; Seinfeld, J. H. Secondary organic aerosol 1. Atmospheric chemical mechanism for production of molecular constituents. *J. Geophys. Res.* **2002**, *107*, 4332.

(59) Carter, W. A detailed mechanism for the gas-phase atmospheric reactions of organic compounds. *Atmos. Environ.* **2007**, *41*, 80–117.

(60) Jenkin, M. E.; Saunders, S. M.; Wagner, V.; Pilling, M. J. Protocol for the development of the Master Chemical Mechanism, MCM v3 (Part B): tropospheric degradation of aromatic volatile organic compounds. *Atmos. Chem. Phys.* **2003**, *3*, 181–193.

(61) Saunders, S. M.; Jenkin, M. E.; Derwent, R. G.; Pilling, M. J. Protocol for the development of the Master Chemical Mechanism, MCM v3 (Part A): tropospheric degradation of non-aromatic volatile organic compounds. *Atmos. Chem. Phys.* **2003**, *3*, 161–180.

(62) Warneck, P. In-cloud chemistry opens pathway to the formation of oxalic acid in the marine atmosphere. *Atmos. Environ.* **2003**, *37*, 2423–2427.

(63) Aumont, B.; Madronich, S.; Bey, I.; Tyndall, G. S. Contribution of Secondary VOC to the Composition of Aqueous Atmospheric Particles : A Modeling Approach. *J. Atmos. Chem.* **2000**, *35*, 59–75.

(64) Schwartz, S. E. Mass-transport considerations pertinent to aqueous-phase reactions of gases in liquid-water clouds. In *Chemistry of Multiphase Atmospheric Systems*; Jaeschke, W., Ed.; Springer: New York, 1986.

(65) Hastings, W. P.; Koehler, C. a; Bailey, E. L.; De Haan, D. O. Secondary organic aerosol formation by glyoxal hydration and oligomer formation: humidity effects and equilibrium shifts during analysis. *Environ. Sci. Technol.* **2005**, *39*, 8728–35.

(66) Loeffler, K. W.; Koehler, C. a; Paul, N. M.; De Haan, D. O. Oligomer formation in evaporating aqueous glyoxal and methyl glyoxal solutions. *Environ. Sci. Technol.* **2006**, *40*, 6318–23.

(67) Otte, T. L.; Pouliot, G.; Pleim, J. E.; Young, J. O.; Schere, K. L.; Wong, D. C.; Lee, P. C. S.; Tsidulko, M.; McQueen, J. T.; Davidson, P.; Mathur, R.; Chuang, H.-Y.; DiMego, G.; Seaman, N. L. Linking the Eta Model with the Community Multiscale Air Quality (CMAQ) Modeling System to Build a National Air Quality Forecasting System. *Weather Forecast.* **2005**, *20*, 367–384.

(68) Carlton, A. G.; Bhave, P. V; Napelenok, S. L.; Edney, E. O.; Sarwar, G.; Pinder, R. W.; Pouliot, G. a; Houyoux, M. Model representation of secondary organic aerosol in CMAQv4.7. *Environ. Sci. Technol.* **2010**, *44*, 8553–60.

(69) Carlton, A. G.; Turpin, B. I.; Altieri, K. E.; Seitzinger, S. P.; Mathur, R.; Roselle, S. J.; Weber, R. J. CMAQ model performance enhanced when in-cloud secondary organic aerosol is included: comparisons of organic carbon predictions with measurements. *Environ. Sci. Technol.* **2008**, *42*, 8798–802.

(70) Henze, D. K.; Seinfeld, J. H.; Shindell, D. T. Inverse modeling and mapping US air quality influences of inorganic $PM_{2.5}$ precursor emissions using the adjoint of GEOS-Chem. *Atmos. Chem. Phys.* **2009**, *9*, 5877–5903.

(71) Corbett, J. J.; Winebrake, J. J.; Green, E. H.; Kasibhatla, P.; Eyring, V.; Lauer, A. Mortality from ship emissions: a global assessment. *Environ. Sci. Technol.* **2007**, *41*, 8512–8.

(72) Jaffe, D. Long-range transport of Siberian biomass burning emissions and impact on surface ozone in western North America. *Geophys. Res. Lett.* **2004**, *31*, L16106.

(73) Chung, S. H. Global distribution and climate forcing of carbonaceous aerosols. *J. Geophys. Res.* **2002**, *107*, 4407.

(74) Henze, D. K.; Seinfeld, J. H.; Ng, N. L.; Kroll, J. H.; Fu, T.-M.; Jacob, D. J.; Heald, C. L. Global modeling of secondary organic aerosol formation from aromatic hydrocarbons: high- vs. low-yield pathways. *Atmos. Chem. Phys.* **2008**, *8*, 2405–2420.

(75) Jimenez, J. L.; Canagaratna, M. R.; Donahue, N. M.; Prevot, A. S. H.; Zhang, Q.; Kroll, J. H.; DeCarlo, P. F.; Allan, J. D.; Coe, H.; Ng, N. L.; Aiken, A. C.; Docherty, K. S.; Ulbrich, I. M.; Grieshop, A. P.; Robinson, A. L.; Duplissy, J.; Smith, J. D.; Wilson, K. R.; Lanz, V. A.; Hueglin, C.; Sun, Y. L.; Tian, J.; Laaksonen, A.; Raatikainen, T.; Rautiainen, J.; Vaattovaara, P.; Ehn, M.; Kulmala, M.; Tomlinson, J. M.; Collins, D. R.; Cubison, M. J.; Dunlea, E. J.; Huffman, J. A.; Onasch, T. B.; Alfarra, M. R.; Williams, P. I.; Bower, K.; Kondo, Y.; Schneider, J.; Drewnick, F.; Borrmann, S.; Weimer, S.; Demerjian, K.; Salcedo, D.; Cottrell, L.; Griffin, R.; Takami, A.; Miyoshi, T.; Hatakeyama, S.; Shimono, A.; Sun, J. Y.; Zhang, Y. M.; Dzepina, K.; Kimmel, J. R.; Sueper, D.; Jayne, J. T.; Herndon, S. C.; Trimborn, A. M.; Williams, L. R.; Wood, E. C.; Middlebrook, A. M.; Kolb, C. E.; Baltensperger, U.; Worsnop, D. R. Evolution of organic aerosols in the atmosphere. *Science* **2009**, *326*, 1525–9.

(76) Nozière, B.; Esteve, W. Light-absorbing aldol condensation products in acidic aerosols: Spectra, kinetics, and contribution to the absorption index. *Atmos. Environ.* **2007**, *41*, 1150–1163.

(77) Nozière, B.; Córdova, A. A kinetic and mechanistic study of the amino acid catalyzed aldol condensation of acetaldehyde in aqueous and salt solutions. *J. Phys. Chem. A* **2008**, *112*, 2827–37.

(78) McNeill, V. F.; Sareen, N.; Schwier, A. N. Surface-Active Organics in Atmospheric Aerosols. *Top. Curr. Chem.* **2013**.

(79) Schwier, A. N.; Mitroo, D.; McNeill, V. F. Surface tension depression by low-solubility organic material in aqueous aerosol mimics. *Atmos. Environ.* **2012**, *54*, 490–495.

(80) McNeill, V. F.; Woo, J. L.; Kim, D. D.; Schwier, A. N.; Wannell, N. J.; Sumner, A. J.; Barakat, J. M. Aqueous-phase secondary organic aerosol and organosulfate formation in atmospheric aerosols: a modeling study. *Environ. Sci. Technol.* **2012**, *46*, 8075–81.

(81) Chan, M. N.; Surratt, J. D.; Claeys, M.; Edgerton, E. S.; Tanner, R. L.; Shaw, S. L.; Zheng, M.; Knipping, E. M.; Eddingsaas, N. C.; Wennberg, P. O.; Seinfeld, J. H. Characterization and quantification of isoprene-derived epoxydiols in ambient aerosol in the southeastern United States. *Environ. Sci. Technol.* **2010**, *44*, 4590–6.

(82) Hennigan, C. J.; Bergin, M. H.; Russell, A. G.; Nenes, A.; Weber, R. J. Gas/particle partitioning of water-soluble organic aerosol in Atlanta. *Atmos. Chem. Phys. Discuss.* **2009**, *9*, 635–671.

(83) Lin, Y.-H.; Zhang, Z.; Docherty, K. S.; Zhang, H.; Budisulistiorini, S. H.; Rubitschun, C. L.; Shaw, S. L.; Knipping, E. M.; Edgerton, E. S.; Kleindienst, T. E.; Gold, A.; Surratt, J. D. Isoprene epoxydiols as precursors to secondary organic aerosol formation: acid-catalyzed reactive uptake studies with authentic compounds. *Environ. Sci. Technol.* **2012**, *46*, 250–8.

(84) Köhler, H. The nucleus in and the growth of hygroscopic droplets. *Trans. Faraday Soc.* **1936**, *32*, 1152.

(85) Schwier, A. N.; Viglione, G. A.; Li, Z.; McNeill, V. F. Modeling the surface tension of complex, reactive organic-inorganic mixtures. *Atmos. Chem. Phys. Discuss.* **2013**, *13*, 549–580.

(86) Nozière, B.; Ekström, S.; Alsberg, T.; Holmström, S. Radical-initiated formation of organosulfates and surfactants in atmospheric aerosols. *Geophys. Res. Lett.* **2010**, *37*, n/a–n/a.

(87) Andreae, M. O.; Gelencsér, A. Black carbon or brown carbon? The nature of light-absorbing carbonaceous aerosols. *Atmos. Chem. Phys.* **2006**, *6*, 3131–3148.

(88)   Jacobson, M. Z. Isolating nitrated and aromatic aerosols and nitrated aromatic gases as sources of ultraviolet light absorption. *J. Geophys. Res.* **1999**, *104*, 3527–3542.

(89)   Herrmann, H.; Tilgner, a.; Barzaghi, P.; Majdik, Z.; Gligorovski, S.; Poulain, L.; Monod, a. Towards a more detailed description of tropospheric aqueous phase organic chemistry: CAPRAM 3.0. *Atmos. Environ.* **2005**, *39*, 4351–4363.

(90)   Whitby, K. The physical characteristics of sulfur aerosols. *Atmos. Environ.* **1978**, *12*, 135–159.

(91)   Wexler, A. S.; Clegg, S. L. Atmospheric aerosol models for systems including the ions H+, NH4+, Na+, SO42−, NO3−, Cl−, Br−, and H2O. *J. Geophys. Res. Atmos.* **2002**, *107*, ACH 14–1–ACH 14–14.

(92)   Hecobian, A.; Zhang, X.; Zheng, M.; Frank, N.; Edgerton, E. S.; Weber, R. J. Water-Soluble Organic Aerosol material and the light-absorption characteristics of aqueous extracts measured over the Southeastern United States. *Atmos. Chem. Phys.* **2010**, *10*, 5965–5977.

(93)   Tanner, R. L.; Olszyna, K. J.; Edgerton, E. S.; Knipping, E.; Shaw, S. L. Searching for evidence of acid-catalyzed enhancement of secondary organic aerosol formation using ambient aerosol data. *Atmos. Environ.* **2009**, *43*, 3440–3444.

(94)   Jimenez, J. L. L.; Jayne, J. T.; Shi, Q.; Kolb, C. E.; Worsnop, D. R.; Yourshaw, I.; Seinfeld, J. H.; Flagan, R. C.; Zhang, X.; Smith, K. A.; Morris, J. W.; Davidovits, P. Ambient aerosol sampling using the Aerodyne Aerosol Mass Spectrometer. *J. Geophys. Res.* **2003**, *108*, 8425.

(95)   Langmuir, I. The shapes of group molecules forming the surfaces of liquids. *Proc. Natl. Acad. Sci. U. S. A.* **1917**, *3*, 251–257.

(96)   Henning, S.; Rosenørn, T.; D'Anna, B.; Gola, A. A.; Svenningsson, B.; Bilde, M. Cloud droplet activation and surface tension of mixtures of slightly soluble organics and inorganic salt. *Atmos. Chem. Phys.* **2005**, *5*, 575–582.

(97)   Paredes-Miranda, G.; Arnott, W. P.; Jimenez, J. L.; Aiken, A. C.; Gaffney, J. S.; Marley, N. A. Primary and secondary contributions to aerosol light scattering and absorption in Mexico City during the MILAGRO 2006 campaign. *Atmos. Chem. Phys.* **2009**, *9*, 3721–3730.

(98)   Nguyen, T. B.; Lee, P. B.; Updyke, K. M.; Bones, D. L.; Laskin, J.; Laskin, A.; Nizkorodov, S. A. Formation of nitrogen- and sulfur-containing light-absorbing compounds accelerated by evaporation of water from secondary organic aerosols. *J. Geophys. Res.* **2012**, *117*, D01207.

(99) Bones, D. L.; Henricksen, D. K.; Mang, S. A.; Gonsior, M.; Bateman, A. P.; Nguyen, T. B.; Cooper, W. J.; Nizkorodov, S. A. Appearance of strong absorbers and fluorophores in limonene-O 3 secondary organic aerosol due to NH 4 + -mediated chemical aging over long time scales. *J. Geophys. Res.* **2010**, *115*, D05203.

(100) Pitts, J. N.; Van Cauwenberghe, K. A.; Grosjean, D.; Schmid, J. P.; Fitz, D. R.; Belser Jr., W. L.; Knudson, G. B.; Hynds, P. M. Atmospheric Reactions of Polycyclic Aromatic Hydrocarbons : Facile Formation of Mutagenic Nitro Derivatives. *Science (80-.).* **1978**, *202*, 515–519.

(101) Zhang, X.; Lin, Y.-H.; Surratt, J. D.; Zotter, P.; Prévôt, A. S. H.; Weber, R. J. Light-absorbing soluble organic aerosol in Los Angeles and Atlanta: A contrast in secondary organic aerosol. *Geophys. Res. Lett.* **2011**, *38*, n/a–n/a.

(102) Miles, N. L.; Verlinde, J.; Clothiaux, E. E. Cloud Droplet Size Distributions in Low-Level Stratiform Clouds. *J. Atmos. Sci.* **2000**, *57*, 295–311.

(103) Feingold, G.; Kreidenweis, S. M.; Zhang, Y. Stratocumulus processing of gases and cloud condensation nuclei: 1. Trajectory ensemble model. *J. Geophys. Res.* **1998**, *103*, 19527.

(104) Surratt, J. D.; Murphy, S. M.; Kroll, J. H.; Ng, N. L.; Hildebrandt, L.; Sorooshian, A.; Szmigielski, R.; Vermeylen, R.; Maenhaut, W.; Claeys, M.; Flagan, R. C.; Seinfeld, J. H. Chemical composition of secondary organic aerosol formed from the photooxidation of isoprene. *J. Phys. Chem. A* **2006**, *110*, 9665–90.

(105) Sorooshian, A.; Varutbangkul, V.; Brechtel, F. J.; Ervens, B.; Feingold, G.; Bahreini, R.; Murphy, S. M.; Holloway, J. S.; Atlas, E. L.; Buzorius, G.; Jonsson, H.; Flagan, R. C.; Seinfeld, J. H. Oxalic acid in clear and cloudy atmospheres: Analysis of data from International Consortium for Atmospheric Research on Transport and Transformation 2004. *J. Geophys. Res.* **2006**, *111*, D23S45.

(106) Yu, G.; Bayer, A. R.; Galloway, M. M.; Korshavn, K. J.; Fry, C. G.; Keutsch, F. N. Glyoxal in aqueous ammonium sulfate solutions: products, kinetics and hydration effects. *Environ. Sci. Technol.* **2011**, *45*, 6336–6342.

(107) Minerath, E. C.; Schultz, M. P.; Elrod, M. J. Kinetics of the reactions of isoprene-derived epoxides in model tropospheric aerosol solutions. *Environ. Sci. Technol.* **2009**, *43*, 8133–9.

(108) Eddingsaas, N. C.; VanderVelde, D. G.; Wennberg, P. O. Kinetics and products of the acid-catalyzed ring-opening of atmospherically relevant butyl epoxy alcohols. *J. Phys. Chem. A* **2010**, *114*, 8106–13.

(109) Crahan, K. K.; Hegg, D.; Covert, D. S.; Jonsson, H. An exploration of aqueous oxalic acid production in the coastal marine atmosphere. *Atmos. Environ.* **2004**, *38*, 3757–3764.

(110) Galloway, M. M.; Loza, C. L.; Chhabra, P. S.; Chan, a. W. H.; Yee, L. D.; Seinfeld, J. H.; Keutsch, F. N. Analysis of photochemical and dark glyoxal uptake: Implications for SOA formation. *Geophys. Res. Lett.* **2011**, *38*, n/a–n/a.

(111) Volkamer, R.; Ziemann, P. J.; Molina, M. J. Secondary Organic Aerosol Formation from Acetylene (C_2H_2): seed effect on SOA yields due to organic photochemistry in the aerosol aqueous phase. *Atmos. Chem. Phys.* **2009**, *9*, 1907–1928.

(112) Hatch, L. E.; Creamean, J. M.; Ault, A. P.; Surratt, J. D.; Chan, M. N.; Seinfeld, J. H.; Edgerton, E. S.; Su, Y.; Prather, K. a Measurements of isoprene-derived organosulfates in ambient aerosols by aerosol time-of-flight mass spectrometry-part 2: temporal variability and formation mechanisms. *Environ. Sci. Technol.* **2011**, *45*, 8648–55.

(113) Froyd, K. D.; Murphy, S. M.; Murphy, D. M.; Gouw, J. A. De; Eddingsaas, N. C.; Wennberg, P. O. Contribution of isoprene-derived organosulfates to free tropospheric aerosol mass. *Proc. Natl. Acad. Sci. U. S. A.* **2010**, *107*, 21360–21365.

(114) Goldstein, A. H.; Schade, G. W. Quantifying biogenic and anthropogenic contributions to acetone mixing ratios in a rural environment. *Atmos. Environ.* **2000**, *34*, 4997–5006.

(115) König, G.; Brunda, M.; Puxbaum, H.; Hewitt, C. N.; Duckham, S. C.; Rudolph, J. Relative contribution of oxygenated hydrocarbons to the total biogenic VOC emissions of selected mid-European agricultural and natural plant species. *Atmos. Environ.* **1995**, *29*, 861–874.

(116) Chan, A. W. H.; Galloway, M. M.; Kwan, A. J.; Chhabra, P. S.; Keutsch, F. N.; Wennberg, P. O.; Flagan, R. C.; Seinfeld, J. H. Photooxidation of 2-methyl-3-Buten-2-ol (MBO) as a potential source of secondary organic aerosol. *Environ. Sci. Technol.* **2009**, *43*, 4647–4652.

(117) Rudich, Y.; Talukdar, R.; Burkholder, J. B.; Ravishankara, A. R. Reaction of Methylbutenol with the OH Radical: Mechanism and Atmospheric Implications. *J. Phys. Chem.* **1995**, *99*, 12188–12194.

(118) Zhang, H.; Worton, D. R.; Lewandowski, M.; Ortega, J.; Rubitschun, C. L.; Park, J.-H.; Kristensen, K.; Campuzano-Jost, P.; Day, D. a; Jimenez, J. L.; Jaoui, M.; Offenberg, J. H.; Kleindienst, T. E.; Gilman, J.; Kuster, W. C.; de Gouw, J.; Park, C.; Schade, G. W.; Frossard, A. a; Russell, L.; Kaser, L.; Jud, W.; Hansel, A.; Cappellin, L.; Karl, T.; Glasius, M.; Guenther, A.; Goldstein, A. H.; Seinfeld, J. H.; Gold, A.; Kamens, R. M.; Surratt, J. D. Organosulfates as tracers for secondary organic aerosol (SOA) formation from 2-methyl-3-buten-2-ol (MBO) in the atmosphere. *Environ. Sci. Technol.* **2012**, *46*, 9437–46.

(119) Steiner, A. L.; Tonse, S.; Cohen, R. C.; Goldstein, A. H.; Harley, R. a. Biogenic 2-methyl-3-buten-2-ol increases regional ozone and HO x sources. *Geophys. Res. Lett.* **2007**, *34*, L15806.

(120) Lal, V.; Khalizov, A. F.; Lin, Y.; Galvan, M. D.; Connell, B. T.; Zhang, R. Heterogeneous reactions of epoxides in acidic media. *J. Phys. Chem. A* **2012**, *116*, 6078–90.

(121) Eddingsaas, N. C.; Loza, C. L.; Yee, L. D.; Seinfeld, J. H.; Wennberg, P. O. α-pinene photooxidation under controlled chemical conditions – Part 1: Gas-phase composition in low- and high-NO$_x$ environments. *Atmos. Chem. Phys.* **2012**, *12*, 6489–6504.

(122) Drozd, G. T.; Woo, J. L.; McNeill, V. F. Self-limited uptake of α-pinene oxide to acidic aerosol: the effects of liquid–liquid phase separation and implications for the formation of secondary organic aerosol and organosulfates from epoxides. *Atmos. Chem. Phys.* **2013**, *13*, 8255–8263.

(123) Ito, A.; Penner, J. E. Historical emissions of carbonaceous aerosols from biomass and fossil fuel burning for the period 1870-2000. *Global Biogeochem. Cycles* **2005**, *19*, n/a–n/a.

(124) Hawthorne, S. B.; Krieger, M. S.; Miller, D. J.; Mathiason, M. B. Collection and quantitation of methoxylated phenol tracers for atmospheric pollution from residential wood stoves. *Environ. Sci. Technol.* **1989**, *23*, 470–475.

(125) Berndt, T.; Böge, O. Formation of phenol and carbonyls from the atmospheric reaction of OH radicals with benzene. *Phys. Chem. Chem. Phys.* **2006**, *8*, 1205–14.

(126) Ofner, J.; Krüger, H.-U.; Grothe, H.; Schmitt-Kopplin, P.; Whitmore, K.; Zetzsch, C. Physico-chemical characterization of SOA derived from catechol and guaiacol – a model substance for the aromatic fraction of atmospheric HULIS. *Atmos. Chem. Phys.* **2011**, *11*, 1–15.

(127) Yee, L. D.; Kautzman, K. E.; Loza, C. L.; Schilling, K. a.; Coggon, M. M.; Chhabra, P. S.; Chan, M. N.; Chan, a. W. H.; Hersey, S. P.; Crounse, J. D.; Wennberg, P. O.; Flagan, R. C.; Seinfeld, J. H. Secondary organic aerosol formation from biomass burning intermediates: phenol and methoxyphenols. *Atmos. Chem. Phys.* **2013**, *13*, 8019–8043.

(128) Berndt, T.; Böge, O. Gas-phase reaction of OH radicals with phenol. *Phys. Chem. Chem. Phys.* **2003**, *5*, 342–350.

(129) Birdsall, A. W.; Andreoni, J. F.; Elrod, M. J. Investigation of the role of bicyclic peroxy radicals in the oxidation mechanism of toluene. *J. Phys. Chem. A* **2010**, *114*, 10655–63.

(130) Sun, Y. L.; Zhang, Q.; Anastasio, C.; Sun, J. Insights into secondary organic aerosol formed via aqueous-phase reactions of phenolic compounds based on high resolution mass spectrometry. *Atmos. Chem. Phys.* **2010**, *10*, 4809–4822.

(131) Kampf, C. J.; Jakob, R.; Hoffmann, T. Identification and characterization of aging products in the glyoxal/ammonium sulfate system – implications for light-absorbing material in atmospheric aerosols. *Atmos. Chem. Phys.* **2012**, *12*, 6323–6333.

(132) Aregahegn, K. Z.; Nozière, B.; George, C. Organic aerosol formation photo-enhanced by the formation of secondary photosensitizers in aerosols. *Faraday Discuss.* **2013**.

(133) Thornton, J. a.; Jaeglé, L.; McNeill, V. F. Assessing known pathways for HO 2 loss in aqueous atmospheric aerosols: Regional and global impacts on tropospheric oxidants. *J. Geophys. Res.* **2008**, *113*, D05303.

(134) Iraci, L. T.; Baker, B. M.; Tyndall, G. S.; Orlando, J. J. Measurements of the Henry ' s Law Coefficients of 2-Methyl-3-buten-2-ol , Methacrolein , and Methylvinyl Ketone. *J. Atmos. Chem.* **1999**, *33*, 321–330.

(135) Betterton, E. A.; Hoffmann, M. R. Henry's Law Constants of Some Environmentally Important Aldehydes. *Environ. Sci. Technol.* **1988**, *22*, 1415–1418.

(136) Kroll, J. H.; Ng, N. L.; Murphy, S. M.; Varutbangkul, V.; Flagan, R. C.; Seinfeld, J. H. Chamber studies of secondary organic aerosol growth by reactive uptake of simple carbonyl compounds. *J. Geophys. Res.* **2005**, *110*, D23207.

(137) Lind, J. a.; Kok, G. L. Henry's law determinations for aqueous solutions of hydrogen peroxide, methylhydroperoxide, and peroxyacetic acid. *J. Geophys. Res.* **1986**, *91*, 7889.

(138) Davidovits, P.; Kolb, C. E.; Williams, L. R.; Jayne, J. T.; Worsnop, D. R. Mass accommodation and chemical reactions at gas-liquid interfaces. *Chem. Rev.* **2006**, *106*, 1323–54.

(139) Khan, I.; Brimblecombe, P.; Clegg, S. L. Solubilities of pyruvic acid and the lower (C1-C6) carboxylic acids. Experimental determination of equilibrium vapour pressures above pure aqueous and salt solutions. *J. Atmos. Chem.* **1995**, *22*, 285–302.

(140) Davidovits, P.; Hu, J. H.; Worsnop, D. R.; Zahniser, M. S.; Kolb, C. E. Entry of gas molecules into liquids. *Faraday Discuss.* **1995**, *100*, 65.

(141) Ip, H. S. S.; Huang, X. H. H.; Yu, J. Z. Effective Henry's law constants of glyoxal, glyoxylic acid, and glycolic acid. *Geophys. Res. Lett.* **2009**, *36*, L01802.

(142) Saxena, P.; Hildemann, L. M. Water-soluble organics in atmospheric particles: A critical review of the literature and application of thermodynamics to identify candidate compounds. *J. Atmos. Chem.* **1996**, *24*, 57–109.

(143) Yaws, C. L. *Yaw's Handbook of Thermodynamic and Physical Properties of Chemical Compounds*; Knovel, 2003.

(144) Technology, N. I. of S. and *NIST Chemistry WebBook, NIST Standard Reference Database Number 69*; Linstrom, P. J.; Mallard, W. G., Eds.; Gaithersburg, MD, 2013.

(145) Sander, R.; Crutzen, P. J. Model study indicating halogen activation and ozone destruction in polluted air masses transported to the sea. *J. Geophys. Res.* **1996**, *101*, 9121.

(146) Lelieveld, J.; Crutzen, P. J. The Role of Clouds in Tropospheric Photochemistry. *J. Atmos. Chem.* **1991**, *12*, 229–267.

(147) Kolb, C. E.; Cox, R. a.; Abbatt, J. P. D.; Ammann, M.; Davis, E. J.; Donaldson, D. J.; Garrett, B. C.; George, C.; Griffiths, P. T.; Hanson, D. R.; Kulmala, M.; McFiggans, G.; Pöschl, U.; Riipinen, I.; Rossi, M. J.; Rudich, Y.; Wagner, P. E.; Winkler, P. M.; Worsnop, D. R.; O' Dowd, C. D. An overview of current issues in the uptake of atmospheric trace gases by aerosols and clouds. *Atmos. Chem. Phys.* **2010**, *10*, 10561–10605.

(148) Becker, K. H.; Kleffmann, J.; Martin Negri, R.; Wiesen, P. Solubility of nitrous acid (HONO) in ammonium sulfate solutions. *J. Chem. Soc. Faraday Trans.* **1998**, *94*, 1583–1586.

(149) Hilal, S. ?H.; Karickhoff, S. ?W.; Carreira, L. ?a. Prediction of the Solubility, Activity Coefficient and Liquid/Liquid Partition Coefficient of Organic Compounds. *QSAR Comb. Sci.* **2004**, *23*, 709–720.

(150) Warneck, P. The relative importance of various pathways for the oxidation of sulfur dioxide and nitrogen dioxide in sunlit continental fair weather clouds. *Phys. Chem. Chem. Phys.* **1999**, *1*, 5471–5483.

(151) DeMore, W. B.; Sander, R.; Golden, D. M.; Hampson, R. F.; Kurylo, M. J.; Howard, C. J.; Ravishankara, A. R.; Kolb, C. E.; Molina, M. J. *Chemical Kinetics and Photochemical Data for Use in Stratospheric Modeling*; 12th ed.; National Aeronautics and Space Administration Jet Propulsion Laboratory: Pasadena, CA, 1997; p. 182.

(152) Paulot, F.; Crounse, J. D.; Kjaergaard, H. G.; Kroll, J. H.; Seinfeld, J. H.; Wennberg, P. O. Isoprene photooxidation: new insights into the production of acids and organic nitrates. *Atmos. Chem. Phys.* **2009**, *9*, 1479–1501.

(153) Atkinson, R. Gas-phase tropospheric chemistry of organic compounds: A review. *Atmos. Environ. Part A. Gen. Top.* **1990**, *24*, 1–41.

(154) Atkinson, R. Kinetics and Mechanisms of the Gas-phase reactions of the OH radical with organic compounds under atmospheric conditions.pdf. *Chem. Rev.* **1986**, *86*, 69–201.

(155) Zimmermann, J.; Poppe, D. A supplement for the RADM2 chemical mechanism: The photooxidation of isoprene. *Atmos. Environ.* **1996**, *30*, 1255–1269.

(156) Stockwell, W. R.; Middleton, P.; Chang, J. S.; Tang, X. The second generation regional acid deposition model chemical mechanism for regional air quality modeling. *J. Geophys. Res.* **1990**, *95*, 16343.

(157) Wagner, V.; Jenkin, M. E.; Saunders, S. M.; Stanton, J.; Wirtz, K.; Pilling, M. J. Modelling of the photooxidation of toluene: conceptual ideas for validating detailed mechanisms. *Atmos. Chem. Phys.* **2003**, *3*, 89–106.

(158) LaFranchi, B. W.; Wolfe, G. M.; Thornton, J. a.; Harrold, S. a.; Browne, E. C.; Min, K. E.; Wooldridge, P. J.; Gilman, J. B.; Kuster, W. C.; Goldan, P. D.; de Gouw, J. a.; McKay, M.; Goldstein, a. H.; Ren, X.; Mao, J.; Cohen, R. C. Closing the peroxy acetyl nitrate budget: observations of acyl peroxy nitrates (PAN, PPN, and MPAN) during BEARPEX 2007. *Atmos. Chem. Phys.* **2009**, *9*, 7623–7641.

(159) Tan, Y.; Perri, M. J.; Seitzinger, S. P.; Turpin, B. J. Effects of precursor concentration and acidic sulfate in aqueous glyoxal-OH radical oxidation and implications for secondary organic aerosol. *Environ. Sci. Technol.* **2009**, *43*, 8105–12.

(160) Ervens, B. Kinetic laboratory investigations of the atmospheric chemistry of SO4- and Cl2- radical anions in aqueous solution, Institute of Physical and Theoretical Stuffing, Universitat Essen, 1997.

(161) Jiang, P.-Y.; Katsumura, Y.; Nagaishi, R.; Domae, M.; Ishikawa, K.; Ishigure, K.; Yoshida, Y. Pulse radiolysis study of concentrated sulfuric acid solutions. Formation mechanism, yield and reactivity of sulfate radicals. *J. Chem. Soc. Faraday Trans.* **1992**, *88*, 1653.

(162) Tang, Y.; Thorn, R. P.; Mauldin, R. L.; Wine, P. H. Kinetics and spectroscopy of the SO4− radical in aqueous solution. *J. Photochem. Photobiol. A Chem.* **1988**, *44*, 243–258.

(163) Bielski, R. Reactivity of HO2-O2 radicals in aqueous solution. *J. Phys. Chem. Ref. Data* **1985**, *14*, 1041–1100.

(164) Manion, J. A. *NIST Chemical Kinetics Database, NIST Standard Reference Database 17*; 7.0 ed.; National Institute of Standards and Technology: Gaithersburg, MD, 2008.

(165) Buxton, G. V.; Malone, T. N.; Arthur Salmon, G. Oxidation of glyoxal initiated by OH in oxygenated aqueous solution. *J. Chem. Soc. Faraday Trans.* **1997**, *93*, 2889–2891.

(166) Stefan, M. I.; Bolton, J. R. Reinvestigation of the Acetone Degradation Mechanism in Dilute Aqueous Solution by the UV/H 2 O 2 Process. *Environ. Sci. Technol.* **1999**, *33*, 870–873.

(167) Monod, a.; Doussin, J. F. Structure-activity relationship for the estimation of OH-oxidation rate constants of aliphatic organic compounds in the aqueous phase: alkanes, alcohols, organic acids and bases. *Atmos. Environ.* **2008**, *42*, 7611–7622.

(168) Vel Leitner, N. K.; Doré, M. Mecanisme d'action des radicaux OH sur les acides glycolique, glyoxylique, acetique et oxalique en solution aqueuse: Incidence sur la consammation de peroxyde d'hydrogene dans les systemes H2O2UV et O3H2O2. *Water Res.* **1997**, *31*, 1383–1397.

(169) Huang, D.; Zhang, X.; Chen, Z. M.; Zhao, Y.; Shen, X. L. The kinetics and mechanism of an aqueous phase isoprene reaction with hydroxyl radical. *Atmos. Chem. Phys.* **2011**, *11*, 7399–7415.

(170) Guzman, M. I.; Colussi, a J.; Hoffmann, M. R. Photoinduced oligomerization of aqueous pyruvic acid. *J. Phys. Chem. A* **2006**, *110*, 3619–26.

(171) Carter, W. P. L.; Darnall, K. R.; Graham, R. A.; Winer, A. M.; Pitts, J. N. Reactions of C2 and C4 .alpha.-hydroxy radicals with oxygen. *J. Phys. Chem.* **1979**, *83*, 2305–2311.

(172) Ervens, B.; Gligorovski, S.; Herrmann, H. Temperature-dependent rate constants for hydroxyl radical reactions with organic compounds in aqueous solutions. *Phys. Chem. Chem. Phys.* **2003**, *5*, 1811–1824.

(173) George, C.; Rassy, H. El; Chovelon, J.-M. Reactivity of selected volatile organic compounds (VOCs) toward the sulfate radical (SO4?). *Int. J. Chem. Kinet.* **2001**, *33*, 539–547.

(174) Wine, P. H.; Tang, Y.; Thorn, R. P.; Wells, J. R.; Davis, D. D. Kinetics of aqueous phase reactions of the SO 4 − radical with potential importance in cloud chemistry. *J. Geophys. Res.* **1989**, *94*, 1085.

(175) Kanakidou, M.; Bonsang, B.; Roulley, J. C. Le; Lambert, G.; Martin, D.; Sennequier, G. Marine source of atmospheric acetylene. *Nature* **1988**, *333*, 51–52.

(176) Krizner, H. E.; De Haan, D. O.; Kua, J. Thermodynamics and kinetics of methylglyoxal dimer formation: a computational study. *J. Phys. Chem. A* **2009**, *113*, 6994–7001.

(177) Darer, A. I.; Cole-Filipiak, N. C.; O'Connor, A. E.; Elrod, M. J. Formation and stability of atmospherically relevant isoprene-derived organosulfates and organonitrates. *Environ. Sci. Technol.* **2011**, *45*, 1895–902.

APPENDIX A

A.1 – Detailed GAMMA Mechanism Information

Table A-1 – List of gas-phase species in GAMMA

Species Name	GAMMA Codifier	Index		Molecular Formula
		Lo	**Hi**	
Acetic Acid	[ACETIC] (gas)	55	23	C2H4O2
Acetaldehyde, higher order aldehydes	[ALD] (gas)	112	61	C2H4O
Higher order acyl peroxy nitrates	[APN] (gas)	132	66	
Aromatic ketones from aromatic oxidation	[AROMATIC_KETONES] (gas)	139	56	
Acetylene	[C2H2] (gas)	110	52	C2H2
Acetyl peroxy radical	[CH3CO3] (gas)	94	26	C2H3O3
Methoxy radical	[CH3O] (gas)	114		CH3O
Methyl hydrogen peroxide	[CH3O2H] (gas)	118	160	CH4O2
Methanol	[CH3OH] (gas)	117	159	CH4O
Methyl peroxy radical	[CH3OO] (gas)	96	28	CH3O2
Carbon Monoxide	[CO] (gas)	12	12	CO
Cresol	[CSL] (gas)	128	54	C7H8O
Unsaturated dicarbonyls	[DCB] (gas)	119		
Dihydroxybutanone nitrate	[DHBN] (gas)		45	C4H9NO7
2,4-dihydroxy-2-methyl-3-oxobutanal	[DHMOB] (gas)		41	C5H8O4
Dibble peroxy radical	[DIBOO] (gas)		40	C5H9O4
C4-epoxy dials	[EPXC4DIAL] (gas)	143	63	C4H4O3
Methyl C4-epoxy dials	[EPXC4MDIAL] (gas)	144	76	C5H5O3
Ethanal Nitrate	[ETHLN] (gas)		48	C2H3NO4
Peroxyradicals from ketone photolysis	[ETHP] (gas)	136	64	
Formaldehyde	[FORM] (gas)	15	15	CH2O
Formic Acid	[FORMIC] (gas)	16	16	CH2O2
Furanones from aromatic oxidation	[FURANONES] (gas)	138	55	
Glyoxylic Acid	[GLYAC] (gas)	52	20	C2H2O3
Glycolaldehyde	[GLYC] (gas)	9	9	C2H4O2
Glycolic Acid	[GLYCAC] (gas)	51	19	C2H4O3
Glyoxal	[GLYX] (gas)	10	10	C2H2O2
Hydrogen Peroxide	[H2O2] (gas)	13	13	H2O2

Hydroxy acetone	[HAC] (gas)	17	17	C3H6O2
Peroxyradicals from OP2, OH	[HC3P] (gas)	126	69	
C4 alkanes	[HC4] (gas)		43	C4H10
4-hydroxy-2-methyl-but-2-enal	[HC5] (gas)	18	18	C5H8O2
4-hydroxy-2-methyl-but-2-enal peroxy radical	[HC5OO] (gas)	97	29	C5H7O4
Nitric Acid	[HNO3] (gas)	102	34	HNO3
Pernitric Acid	[HNO4] (gas)	104	36	HNO4
Hydroperoxyl radical	[HO2] (gas)	3	3	HO2
Nitrous Acid	[HONO] (gas)	103	35	HNO2
Isoprene-derived dihydroxy epoxide	[IEPOX] (gas)	7		C5H10O3
IEPOX-derived peroxyradical	[IEPOXOO] (gas)	8		C5H10O5
Isoprene	[ISOP] (gas)	1	1	C5H10
Isoprene nitrate	[ISOPNb] (gas)		7	C5H9NO4
Isoprene nitrate	[ISOPNd] (gas)		4	C5H9NO4
Peroxyradicals formed via ISOPNb	[ISOPNOOb] (gas)		49	C5H9O7
Peroxyradicals formed via ISOPNd	[ISOPNOOd] (gas)		44	C5H9O7
Isoprene hydroxy hydroperoxyl radical	[ISOPOO] (gas)	2	2	C5H9O3
Isoprene hydroxy hydroperoxide	[ISOPOOH] (gas)	4		C5H10O3
Misc. ketones (Lim)	[KET] (gas)	116	72	
Peroxyradicals from ketones	[KETP] (gas)	124	71	
Methacrolein peroxy radical	[MACP] (gas)	93	25	C4H5O3
Methacrolein	[MACR] (gas)	5	5	C4H6O
Methacrolein nitrate	[MACRN] (gas)		50	C4H7NO5
Dimethyl phenols (methylcresols)	[MCSL] (gas)	141	74	
Methylfuran	[MF] (gas)		8	C5H6O
Methylglyoxal	[MGLY] (gas)	11	11	C3H4O2
2-methyl-4-oxobut-2-enoic acid	[MOBA] (gas)		42	C5H6O3
Peroxyradicals formed from MOBA	[MOBAOO] (gas)		51	C5H5O5
Methyl vinyl ketone	[MVK] (gas)	6	6	C4H56O
Methyl vinyl ketone nitrate	[MVKN] (gas)		47	C4H7NO5
Methyl vinyl ketone peroxy radical	[MVKP] (gas)	95	27	C4H5O3
Dinitrogen pentoxide	[N2O5] (gas)	101	33	N2O5
Nitrogen monoxide radical	[NO] (gas)	98	30	NO

Nitrogen dioxide	[NO2] (gas)	99	31	NO2
Nitrate radical	[NO3] (gas)	100	32	NO3
1D oxygen atom	[O1D] (gas)	106	38	O
Ozone	[O3] (gas)	105	37	O3
3P oxygen atom	[O3P] (gas)	107	39	O
Hydroxide Radical	[OH] (gas)	14	14	OH
Internal alkenes	[OLI] (gas)	120		
Peroxyradicals from internal alkenes	[OLIP] (gas)	123		
Terminal alkenes (values for 1-butene)	[OLT] (gas)	111	60	C4H8
Peroxyradicals from terminal alkenes	[OLTP] (gas)	122	68	C4H8O2
Organonitrates	[ONIT] (gas)	137	70	
Higher order peroxides (values for 1-butene-OO)	[OP2] (gas)	113	62	C4H8O2
Oxalic Acid	[OXLAC] (gas)	54	22	C2H2O4
Peroxyacetyl nitrate	[PAN] (gas)	121	65	C2H3NO5
Polyfunctional aromatic species	[POLY_FXNAL_AROMATIC] (gas)	142	59	
Propanone nitrate	[PROPNN] (gas)		46	C3H5NO4
Pyruvic Acid	[PYRAC] (gas)	53	21	C3H4O3
Sulfur Dioxide	[SO2] (gas)	56	24	SO2
Peroxyradicals from dicarbonyl photolysis	[TCO3] (gas)	125	67	
Toluene	[TOL] (gas)	127	53	C7H8
Toluene-based epoxides	[TOL_EPOX] (gas)	130	57	
Unsaturated aldehydes from aromatic oxidation	[UNSAT_ALDEHYDES] (gas)	140	58	
Order peroxides (Lim) (values for 1-butene-OO)	[XO2] (gas)		115	C4H8
Xylenes	[XYL] (gas)	129	73	C8H10
Xylene-based epoxides	[XYL_EPOX] (gas)	131	75	

Table A-2 – List of aqueous-phase species in GAMMA

Species Name	GAMMA Codifier	Index		Molecular Formula
		Lo	Hi	
Acetaldehyde, higher-order aldehydes	[ALD] (aq)	133	151	C2H4O
Bisulfate ion	[BISULFATE] (aq)	35	92	HO4S
Hydroxymethyl radical	[CH2OH] (aq)	83	132	CH3O
Acetate ion	[CH3CO2-] (aq)	50	105	C2H3O2
Acetic Acid	[CH3CO2H] (aq)	49	104	C2H4O2
Methyl hydroperoxide	[CH3O2H] (aq)	135	162	CH4O2
Methanol	[CH3OH] (aq)	134	161	CH4O
Hydrated formaldehyde radical	[CHOHOH] (aq)	72	121	CH3O2
Carbon monoxide	[CO] (aq)	85	134	CO
Carbon dioxide	[CO2] (aq)	57		CO2
Carbon dioxide anion	[CO2-] (aq)	86	135	CO2
Carbonate radical	[CO3-] (aq)	91	140	CO3
Carbonate (II) ion	[CO3--] (aq)	90	139	CO3
Carboxyl radical	[COOH] (aq)	78	127	CHO2
C4-epoxy dial derived diols	[EPXC4DIAL diol] (aq)	149	149	C4H6O4
C4-epoxy dial derived organosulfates	[EPXC4DIAL OS] (aq)	150	150	C4H6O7S
C4-epoxy dials	[EPXC4DIAL] (aq)	148	148	C4H4O3
Methyl C4-epoxy dial-derived diols	[EPXC4MDIAL diol] (aq)	155	157	C5H8O4
Methyl C4-epoxy dial-derived organosulfates	[EPXC4MDIAL OS] (aq)	156	158	C5H8O7S
Methyl C4-epoxy dial	[EPXC4MDIAL] (aq)	154	156	C5H6O3
Formaldehyde	[FORM] (aq)	28	85	CH2O
Formic acid	[FORMIC] (aq)	43	98	CH2O2
Formate ion	[FORMIC-] (aq)	44	99	CHO2
Glyoxylic acid	[GLYAC] (aq)	29	86	C2H2O3
Glyoxylate ion	[GLYAC-] (aq)	31	88	C2HO3
Glyoxylic acid derived organosulfates	[GLYACOS] (aq)	39	96	C2H2O7S
Glyoxylic acid radical	[GLYACR] (aq)	61	110	C2HO3
Glyoxylate radical	[GLYACR-] (aq)	62	111	C2O3
Glyoxalic acid peroxy radical	[GLYACRO2] (aq)	87	136	C2HO5
Glyoxalate peroxy radical	[GLYACRO2-] (aq)	88	137	C2H5
Glycolaldehyde	[GLYC] (aq)	23	80	C2H4O2
Glycolic Acid	[GLYCAC] (aq)	45	100	C2H4O3
Glycolate ion	[GLYCAC-] (aq)	46	101	C2H3O3
Glyoxylic acid-derived	[GLYCACOS] (aq)	69	118	C2H4O7S

organosulfates				
Glycolic acid radical	[GLYCACR] (aq)	65	114	C2H3O3
Glycolate radical	[GLYCACR-] (aq)	66	115	C2H2O3
Glycolic acid peroxy radical	[GLYCACRO2] (aq)	84	133	C2H3O5
Glycolaldehyde-derived organosulfates	[GLYCOS] (aq)	68	117	C2H4O6S
Glycolaldehyde radical 1	[GLYCR1] (aq)	63	112	C2H3O2
Glycolaldehyde peroxy radical 1	[GLYCR1O2] (aq)	81	130	C2H3O4
Glycolaldehyde radical 2	[GLYCR2] (aq)	64	113	C2H3O2
Glycolaldehyde peroxy radical 2	[GLYCR2O2] (aq)	82	131	C2H3O4
Glyoxal-derived organosulfates	[GLYOS] (aq)	67	116	C2H2O6S
Glyoxal radical	[GLYR] (aq)	60	109	C2H5O4
Glyoxal peroxy radical	[GLYRO2] (aq)	71	120	C2H5O6
Glyoxal	[GLYX] (aq)	24	81	C2H2O2
Hydrogen peroxide	[H2O2] (aq)	26	83	H2O2
Sulfuric acid	[H2SO4] (aq)	38	95	H2O4S
Bicarbonate (I) ion	[HCO3-] (aq)	89	138	CHO3
Hydroperoxyl radical	[HO2] (aq)	19	77	HO2
Bisulfate radical	[HSO4rad] (aq)	58	107	HO4S
Isoprene-derived dihydroxy epoxide	[IEPOX] (aq)	22		C5H10O3
IEPOX-derived organosulfates	[IEPOXOS] (aq)	41		C5H12O7S
Isoprene	[ISOP] (aq)	59	108	C5H10
Methacrolein	[MACR] (aq)	20	78	C4H6O
Malonic acid	[MALONIC] (aq)	73	122	C3H4O4
Malonic acid radical	[MArad] (aq)	76	125	C3H3O4
Malonic acid peroxy radical	[MAradO2] (aq)	77	126	C3H3O6
Methylglyoxal	[MGLY] (aq)	25	82	C3H3O6
Methyl vinyl ketone	[MVK] (aq)	21	79	C4H6O
Nitrite (I) ion	[NO2-] (aq)	109	143	NO2
Nitrate (I) ion	[NO3-] (aq)	108	142	NO3
Superoxide	[O2-] (aq)	34	91	O2
Hydroxide radical	[OH] (aq)	27	84	HO
Oxalic acid	[OXLAC] (aq)	30	87	C2H2O4
Oxalate (I) ion	[OXLAC-] (aq)	32	89	C2HO4
Oxalate (II) ion	[OXLAC--] (aq)	33	90	C2O4
Light-absorbing aldehyde derived oligmers	[Pald] (aq)	152	158	
Light-absorbing poly-glyoxal oligomers	[Pgly] (aq)	40	97	

Light-absorbing poly-methylglyoxal oligomers	[Pmgly] (aq)	92	141	
Pyruvic acid	[PYRAC] (aq)	47	102	C3H4O3
Pyruvate ion	[PYRAC-] (aq)	48	103	C3H3O3
Succinic acid radical	[SArad] (aq)	74	123	C4H5O4
Succinic acid peroxy radical	[SAradO2] (aq)	75	124	C4H5O6
Sulfur dioxide	[SO2] (aq)		106	O2S
Sulfate radical	[SO4-] (aq)	37	94	O4S
Succinic acid	[SUCCINIC] (aq)	70	119	C4H6O4
Sulfate ion	[SULFATE] (aq)	36	93	O4S
2-Methyl tetrol	[tetrol] (aq)	42		C5H12O4
Toluene-based epoxide-derived diols	[TOL_EPOX diol] (aq)	146	145	C7H8O4
Toluene-based epoxide-derived organosulfates	[TOL_EPOX OS] (aq)	147	146	C7H8O7S
Toluene-based epoxides	[TOL_EPOX] (aq)	145	144	C7H6O3
Unsaturated aldehydes	[unsaturated_aldehydes] (aq)	157	147	
Malonic acid oxidation products	[X] (aq)	79	128	
Xylene-based epoxide-derived diols	[XYL_EPOX diol] (aq)	152	154	C8H12O4
Xylene-based epoxide-derived organosulfates	[XYL_EPOX OS] (aq)	153	155	C8H12O7S
Xylene-based epoxides	[XYL_EPOX] (aq)	151	153	C8H10O3
Succinic acid oxidation products	[Y] (aq)	80	129	

Table A-3 – Effective Henry's Law constants (H*) and accommodation coefficients (α)

Species	H* (M/atm)	α	Reference
HO2	$H^* = exp\left(-\frac{\Delta G}{RT}\right) * \left(1 + \frac{2.05 \times 10^{-5}}{10^{-pH}}\right)$ $\Delta G = -4.19 + 0.023 * (298 - T)$ kcal/mol	1	*(64, 133)*
MACR	6.5	0.02	*(134)* a
MVK	41	0.02	*(134)* a
IEPOX	1.9e7	0.02	*(81)* a
GLYC	4.14e4	0.023	*(27, 135)* g
GLYX	1e8	0.023	*(89, 136)*
MGLY	3.71e3	0.023	*(27, 135)* g
H2O2	exp(6621/T-11.0)	0.11	*(89, 137)*
OH	29.7	0.05	*(89, 138)*
FORM	2.97e3	0.02	*(89, 135)*
FORMIC	5530	0.012	*(89, 139, 140)*

GLYCAC	2.83e4	0.019	(*27, 141*) b
GLYAC	1e4	0.019	(*27, 141*) b
PYRAC	exp(-4.41706+5087.92/T)	0.019	(*27, 139*) b
OXLAC	5e8	0.019	(*27, 142*) b
ACETIC	5500	0.019	(*89, 139, 140*)
CO2	4.58e-2	2e-4	(*89, 143*)
CH3OH	220	0.015	(*89, 140, 144*)
CH3OOH	300	0.0038	(*89, 140, 144*)
ISOP	0.028	1e-4	(*144*)a
N2O5	1.4e10	0.005	(*27, 78, 145*)
HNO3	2.1e5	0.2	(*89, 146, 147*)
HONO	50	0.0028	(*89, 138, 148*)
HNO4	1e5	0.2	(*89*) c
TOL_EPOX	2.5e5	0.02	(*149*) a,d
UNSAT_ALDEHYDES	2.5e4	0.02	(*149*) a,e
EPXC4DIAL	1.4e5	0.02	(*22*) a,d
ALD	11.4	0.03	(*89, 135*)f
XYL_EPOX	1.09e5	0.02	(*149*) a,d
EPXC4MDIAL	2.478e4	0.02	(*149*) a,d

a. Estimated accommodation coefficient
b. Assume accommodation coefficient same as acetic acid
c. Assume accommodation coefficient same as HNO3
d. Henry's law constant estimated using SPARC (*149*)
e. Henry's law constant estimated based on O=CC=CC(=O)C using SPARC (*149*)
f. Henry's law, accommodation coefficient values for acetaldehyde.
g. Assume accommodation coefficient same as glyoxal

Table A-4- Gas-phase photolysis reactions

Reaction	k (s^{-1}) [a]	Note[b]
H2O2 + hn → 2 OH	7.66e-6	
O3 + hn → O1D + O2	3.55e-5	
O3 + hn → O3P + O2	2.08e-4	
NO2 + hn → NO + O3P	8.79e-3	
NO3 + hn → NO2 + O3P	1.53e-1	
NO3 + hn → NO + O2	2.21e-2	
HNO3 + hn → NO2 + OH	6.56e-7	
HONO + hn → NO + OH	1.95e-3	

Reaction	ka	Ref
N2O5 + hn → NO2 + NO3	2.54e-5	
FORM + hn → H2 + CO	4.85e-5	
FORM + hn → 2 HO2 + CO	3.16e-5	c
GLYX + hn → 0.13 FORM + 1.87 CO	5.55e-5	c
GLYX + hn → 0.45 FORM + 1.55 CO + 0.80 HO2	2.71e-5	c
MGLY + hn → CH3CO3 + CO + HO2	1.24e-4	c
GLYC + hn → FORM + CO + 2 HO2	1.93e-5	c
ALD + hn → CH3OO + HO2 + CO	4.62e-6	c, d
HC5 + hn → CH3CO3 + GLYC + HO2 + CO	8.30e-6	
HC5 + hn → OP2 + HO2	8.30e-6	
MACR + hn → 1.65 CO + HO2 + 0.35 CH3CO3 + FORM + 0.65 CH3OO	8.30e-6	e
MACR + hn → OP2 + HO2	8.30e-6	
MVK + hn → 0.5 CH3CO3 + 0.5 HCHO + 0.5 HO2 + CO + 0.5C3H6	2.68e-5	
HAC + hn → CH3CO3 + HCHO + HO2	3.83e-6	
OP2 + hn → ALD + HO2 + OH	9.26e-6	
KET + hn → CH3CO3 + ETHP	1.40e-6	
DCB + hn → 0.98HO2 + TCO3 + 0.02CH3CO3	6.04e-4	L
organic nitrates (ISOPNd+ISOPNb+ISOPNOOd+DHBN+PROPNN+ MVKN+ETHLN+ISOPNOOb+MACRN+ONIT) + hn → 0.2 ALD + 0.8 KET + HO2 + NO2	1.47e-6	
MOBA + hn → GLYAC + HO2 + CO +CH3O2	8.30e-6	H
TOL_EPOX + hn → 0.5 EPXC4DIAL + 0.5 UNSAT_ALDEHYDES + 0.5 CH3CO3 + CO + HO2	8.8e-4	f
EPXC4DIAL + hn → ALD + CO + HO2	1.07e-4	f
XYL_EPOX + hn → 0.5 EPXC4MDIAL + 0.5 UNSAT_ALDEHYDES + 0.5 CH3CO3 + CO + HO2	8.8e-4	f
EPXC4MDIAL + hn → ALD + CO + HO2	1.07e-4	f

a. Maximum (noon) photolysis rate calculated following Saunders et al. (2003) for June 21, Atlanta, GA (SZA = 13.5) listed. Sinusoidal dependence on time of day assumed.
b. L = Low-NOx scheme only, H = high-NOx scheme only
c. Products from Lim et al. (2005)
d. Rate for acetaldehyde
e. Assuming fast decomposition of peroxy radical intermediate
f. Condensed from the Master Chemical Mechanism (MCM)

Table A-5 – Aqueous-phase photolysis reactions

Reaction	ka (s^{-1}) ^{a}	Reference
H2O2 + hn → 2 OH	3.77e-6	(*27, 137*)

a. Maximum (noon) photolysis rate from reference is listed. Sinusoidal dependence on time of day assumed.

Table A-6 – Aqueous-phase equilibrium reactions

Reaction	k_a (M^{1-n} s^{-1})	k_r (M^{1-n} s^{-1})	Ref.
HO2 ↔ H+ + O2-	8e5	5e10	(*27, 150*)
GLYAC ↔ GLYAC- + H+	6.94e6	2e10	(*89*)
OXLAC ↔ OXLAC- + H+	2.835e9	5e10	(*89*)
OXLAC- ↔ OXLAC-- + H+	2.71e6	5e10	(*89*)
H2SO4 ↔ bisulfate + H+	5e13	5e10	(*89*)
bisulfate ↔ sulfate + H+	1.02e9	1e11	(*89*)
FORMIC ↔ FORMIC- + H+	8.85e6	5e10	(*27, 150*)
GLYCAC ↔ GLYCAC- + H+	6.94e6	2e10	(*27*)
ACETIC ↔ ACETIC- + H+	8.75e5	5e10	(*89*)
PYRAC ↔ PYRAC- + H+	6.4e7	2e10	(*27*)
CO2 + H2O ↔ H+ + HCO3-	5.6e4	0.024	(*27, 145*)
HCO3- ↔ H+ + CO3-2	5e10	2.345	(*89*)

Table A-7 – Gas-phase thermal reactions

Reaction	k ((molec cm^{-3})$^{1-n}$ s^{-1})	Ref.	Note [a]
O1D + N2 → O3P + N2	1.8e-11*exp(100/T)	(*27, 151*)	
O1D + O2 → O3P + O2	3.2e-11*exp(70/T)	(*27, 151*)	
O3P + O2 + M → O3 + M	6e-34*(T/300)^(-2.3)	(*27, 151*)	
O1D + H2O → 2OH	2.2e-10	(*27, 151*)	
O3 + OH → HO2 + O2	1.6e-12*exp(-940/T)	(*27, 151*)	
O3 + HO2 → OH + 2O2	1.1e-14*exp(-500/T)	(*27, 151*)	
NO + OH (+M) → HONO(+M)	7.6e-12	(*27, 151*)	
O3 + NO → NO2 + O2	2e-12*exp(-1400/T)	(*27, 151*)	
O3 + NO2 → NO3 + O2	1.2e-13*exp(-2450/T)	(*27, 151*)	
NO + NO3 → 2 NO2	1.5e-11*exp(170/T)	(*27, 151*)	
NO2 + NO3 (+M) → N2O5(+M)	1.3e-12	(*27, 151*)	
N2O5(+M) → NO2 + NO3 (+M)	6.8e-2*exp(-11080/T)	(*27, 150*)	
NO2 + OH (+M)→ HNO3(+M)	9.7e-12	(*27, 151*)	
NO2 + HO2 (+M) → HNO4(+M)	1.5e-12	(*27, 151*)	
HNO4 (+M)→ NO2 + HO2(+M)	7.7e-12*exp(-10420/T)	(*27, 150*)	
CO + OH → CO2 + HO2	1.5e-13	(*15, 27*)	
HO2 + HO2 → H2O2 + O2	2.3e-13*exp(600/T) + 1.7e-33*2.46e19*298.15/T*exp(1000/T)	(*15, 27*)	
H2O2 + OH → HO2 + H2O	2.9e-12*exp(-160/T)	(*27, 151*)	
HO2 + NO → NO2 + OH	3.5e-12*exp(250/T)	(*15*)	
HO2 + OH → H2O + O2	4.8e-11*exp(250/T)	(*27, 151*)	
SO2 + OH → SO3 + HO2	4.8e-13	(*27, 151*)	

ISOP + OH → ISOPOO	2.7e-11*exp(390/T)	(*51, 152*)	
ISOPOOH + OH → IEPOX + OH	1.9e-11*exp(390/T)	(*51*)	L
ISOPOOH + OH → 0.7 ISOPOO + 0.3 HC5 + 0.3 OH	0.38e-11*exp(200/T)	(*51*)	L
IEPOX + OH → IEPOXOO	5.78e-11*exp(-400/T)	(*51*)	L
FORM + OH → HO2 + CO + H2O	1.20e-14*T*exp(287/T)	(*15*)	
FORMIC + OH → HO2 + CO2 + H2O	4.5e-13	(*15*)	
GLYX + OH → HO2 + 2CO + H2O	11.4e-12	(*15*)	
MGLY + OH → CH3CO3 + CO + H2O	17.2e-12	(*15*)	
MACR + OH → 0.47 MACP + 0.53 CH3CO3	2.95e-11	(*51*)	
MVK + OH → MVKP	1.75e-11	(*51*)	
GLYC + OH → 0.71 FORM + 0.16 FORMIC + 0.35 CO2 + 0.52 CO + 0.13 GLYX + 0.75 HO2 + 0.25 OH	0.8e-11	(*51*)	
HAC + OH → 0.75 MGLY + 0.825 HO2 + 0.125 FORMIC + 0.1 OH + 0.125 CH3OO + 0.20 CO2 + 0.05 CO + 0.125 ACETIC	0.6e-11	(*51*)	
HC5 + OH → HC5OO	11e-11	(*51*)	
GLYC + OH → GLYX + HO2	2.5e-12	(*153*)	
C2H2 + OH → GLYX + OH	8.8e-13*0.636	(*154*)	
C2H2 + OH → FORMIC + CO + HO2	8.8e-13*0.364	(*154*)	
CH4 + OH → CH3OO + H2O	2.45e-12*exp(-1775/T)	(*27, 151*)	
ALD + OH → CH3CO3 + H2O	6.87e-12*exp(256/T)	(*155*)	
CH3OH + OH → FORM + HO2 + H2O	6.7e-12*exp(-600/T)	(*27, 151*)	
CH3O2H + OH → 0.3 FORM + 0.3 OH + 0.7 CH3OO + H2O	3.8e-12*exp(200/T)	(*27, 151*)	
ACETIC, GLYCAC, GLYAC, PYRAC + OH → CH3OO	4e-13*exp(200/T)	(*27, 151*)	
OLT + OH → OLTP	5.32e-12*exp(504/T)	(*27, 156*)	
OP2 + OH → 0.5 HC3P + 0.5 ALD + 0.5 OH	1e-11	(*27, 156*)	
OLI + OH → OLIP	1.07e-11*exp(549/T)	(*27, 156*)	L
KET + OH → KETP + H2O	1.2e-11*exp(-745/T)	(*27, 156*)	
DCB + OH → TCO3 + H2O	2.8e-11	(*27, 156*)	L
DHMOB + OH → 1.5 CO + 0.5 HO2+ 0.5 HAC + 0.5 HC4	1e-11	(*152*)	H
MOBA + OH → MOBAOO	0.3e-11	(*152*)	H
TOL + OH → 0.20 CSL + 0.238 GLYX + 0.238 MGLY + 0.198 TOL_FURANONES + 0.106 AROMATIC_KETONES + 0.20 TOL_EPOX + 0.277 UNSAT_ALDEHYDES	1.81e-12*exp(338/T)	(*74, 157*)	
XYL + OH → 0.937 HO2 +	1.43e-11	(*60*)	c

0.09 AROMATIC_KETONES + 0.16 MCSL + 0.09 POLY_FXNAL_AROMATIC + 0.21 XYL_EPOX + 0.317 UNSAT_ALDEHYDES + 0.247 GLYX + 0.14 MGLY + 0.07 FURANONES			
CSL + OH → 0.13 GLYX + 0.13 UNSAT_ALDEHYDES + 0.93 HO2 + 0.86 POLY_FXNAL_AROMATIC + 0.68 NO2	4.65e-11	(*60*)	L, c
CSL + OH → 0.13 GLYX + 0.13 UNSAT_ALDEHYDES + 0.93 HO2 + 0.86 POLY_FXNAL_AROMATIC + 0.93 NO2 + 0.01 OP2	4.65e-11	(*60*)	H, c
MCSL + OH → 0.14 MGLY + 0.14 UNSAT_ALDEHYDES + 0.93 HO2 + 0.86 POLY_FXNAL_AROMATIC + 0.68 NO2	8e-11	(*60*)	L, c
MCSL + OH → 0.10 MGLY + 0.10 UNSAT_ALDEHYDES + 0.87 HO2 + 0.79 POLY_FXNAL_AROMATIC + 0.28 NO2 + 0.11 OP2	8e-11	(*60*)	H, c
TOL_EPOX + OH → 0.38 EPXC4DIAL + 0.31 UNSAT_ALDEHYDES + 0.070 CH3CO3 + 0.31 MGLY + 0.10 CO + 0.38 HO2 + 1.32 NO2 + 0.61 ALD	7.99e-11	(*60*)	L, c
TOL_EPOX + OH → 0.28 EPXC4DIAL + 0.31 UNSAT_ALDEHYDES + 0.05 CH3CO3 + 0.22 MGLY + 0.14 CO + 0.28 HO2 + 1.37 NO2 + 0.45 ALD + 0.01 OH + 0.19 OP2	7.99e-11	(*60*)	H, c
XYL_EPOX + OH → 0.41 EPXC4MDIAL + 0.26 UNSAT_ALDEHYDES + 0.08 CH3CO3 + 0.33 MGLY + 0.10 CO + 0.40 HO2 + 1.27 NO2 + 0.66 ALD	7.88e-11	(*60*)	L, c
XYL_EPOX + OH → 0.31 EPXC4MDIAL + 0.26 UNSAT_ALDEHYDES + 0.06 CH3CO3 + 0.25 MGLY + 0.13 CO + 0.30 HO2 + 1.29 NO2 +0.50 ALD + 0.01 OH + 0.19 OP2	7.88e-11	(*60*)	H, c
EPXC4DIAL + OH → ALD + NO2	4.32e-11	(*60*)	L, c
EPXC4DIAL + OH → ALD + 0.92 NO2 + 0.01 HO2 + 0.07 OH + 0.02 O3	4.32e-11	(*60*)	H, c
EPXC4MDIAL + OH → ALD + NO2	4.32e-11	(*60*)	L, c
EPXC4MDIAL + OH → 0.01 HO2 + ALD + 0.92NO2 + 0.07 OH + 0.02 O3	4.32e-11	(*60*)	H, c
ONIT + OH → HC3P + NO2	1.55e-11*exp(-540/T)	(*27*)	

ISOPNd + OH → ISOPNOOd	9.5e-11	(*152*)	H
ISOPNb + OH → ISOPNOOb	1.3e-11	(*152*)	H
MVKN + OH → 0.65*(FORMIC + MGLY) + 0.35*(FORM + PYRAC) + NO3	0.56e-11	(*152*)	H
MACRN + OH → 0.08*(ACETIC + FORM + NO3) + 0.07*(FORMIC + NO3 + MGLY) + 0.85*(HAC + NO2) + 0.93 CO2	5e-11	(*152*)	H
ETHLN + OH → FORM + CO2 + NO2	1e-11	(*152*)	H
ISOP + O3 → 0.55 MACR + 0.21 MVK + 0.3 O3P + 0.5 OH + 0.89 FORM + 0.11 HO2 + 0.18 CO + 0.07 OLT + 0.15 ACETIC + 0.07 FORMIC + 0.09 CH3OO + 0.01 GLYX	1.23e-14*exp(-2013/T)	(*27, 155*)	
MACR + O3 → 0.76 MGLY + 0.23 O3P + 0.46 OH + 0.7 FORM + 0.11 FORMIC + 0.23 ACETIC	4.4e-15*exp(-2500/T)	(*27, 155*)	
MVK + O3 → 0.76 MGLY + 0.23 O3P + 0.46 OH + 0.7 FORM + 0.11 FORMIC + 0.24 CH3OO + 0.24 CO	4e-15*exp(-2000/T)	(*27, 155*)	
OLT + O3 → 0.53 FORM + 0.5 ALD + 0.33 CO + 0.2 FORMIC + 0.2 ACETIC + 0.23 HO2 + 0.22 CH3OO + 0.1 OH + 0.06 CH4	1.32e-14*exp(-2105/T)	(*27, 156*)	
TOL_EPOX + O3 → EPXC4DIAL + 0.70 CH3CO3 + 0.31 MGLY + 0.57 CO + 0.13 HO2 + 0.18 NO2	5e-18	(*60*)	c
XYL_EPOX + O3 → EPXC4MDIAL + 0.70 CH3CO3 + 0.30 MGLY + 0.57 CO + 0.13 HO2 + 0.18 NO2	5e-18	(*60*)	c
FORM + NO3 → HNO3 + HO2 + CO	5.8e-16	(*27, 151*)	
MVK + NO3 → NO2 + CH3OO + MGLY	6e-14	(*155*)	
MACR + NO3 → 0.5 HNO3 + 0.5 NO2 + 0.8 CH3CO3 + 0.5 MGLY	1e-14	(*155*)	
ALD + NO3 → CH3CO3 + HNO3	1.4e-12*exp(-1900/T)	(*27*)	
GLYX + NO3 → HO2 + HNO3 + 2 CO	6e-13*exp(-2058/T)	(*27*)	
MGLY + NO3 → CH3CO3 + HNO3 + CO	1.4e-12*exp(-1900/T)	(*27*)	
CSL + NO3 → 0.57 GLYX + 0.57 UNSAT_ALDEHYDES + 0.1 HO2 + 0.4 POLY_FXNAL_AROMATIC + 0.49 HNO3 + 3.69 NO2 + 0.02 OP2	1.4e-11	(*60*)	L, c
CSL + NO3 → 0.57 GLYX + 0.57 UNSAT_ALDEHYDES + 0.1 HO2 + 0.40 POLY_FXNAL_AROMATIC + 0.49 HNO3 + 5.03 NO2 + 0.03 OP2	1.4e-11	(*60*)	H, c
MCSL + NO3 → 0.57 MGLY + 0.57 UNSAT_ALDEHYDES + 0.1 HO2 + 0.40 POLY_FXNAL_AROMATIC +	3.48e-11	(*60*)	L, c

0.49 HNO3 + 3.76 NO2 + 0.02 OP2			
MCSL + NO3 → 0.42 MGLY + 0.42 UNSAT_ALDEHYDES + 0.07 HO2 + 0.12 POLY_FXNAL_AROMATIC + 0.49 HNO3 + 1.58 NO2+0.46 OP2	3.48e-11	(*60*)	H, c
TOL_EPOX + NO3 → UNSAT_ALDEHYDES + HNO3 + 0.10 CO + 2.05 NO2	2.7254e-15	(*60*)	L, c
TOL_EPOX + NO3 → UNSAT_ALDEHYDES + HNO3 + 0.28 CO + 2.81 NO2 + 0.04 OH	2.7254e-15	(*60*)	H, c
EPXC4DIAL + NO3 → ALD + HNO3 + NO2	2.18e-14	(*60*)	L, c
EPXC4DIAL + NO3 → ALD + HNO3 + 0.92 NO2 + 0.07 OH + 0.02 O3	2.18e-14	(*60*)	H, c
XYL_EPOX + NO3 → UNSAT_ALDEHYDES + HNO3 + 0.1 CO + 2.05 NO2	1.16e-14	(*60*)	L, c
XYL_EPOX + NO3 → UNSAT_ALDEHYDES + HNO3 + 0.28 CO + 2.82 NO2 + 0.04 OH + 0.01 O3	1.16e-14	(*60*)	H, c
EPXC4MDIAL + NO3 → ALD + HNO3 + NO2	4.63e-14	(*60*)	L, c
EPXC4MDIAL + NO3 → ALD + HNO3 + 0.92NO2 + 0.07 OH + 0.02 O3	4.63e-14	(*60*)	H, c
CH3OO + HO2 → CH3O2H + O2	3.8e-13*exp(800/T)	(*27, 151*)	
ISOPOO + HO2 → 0.880 ISOPOOH + 0.120 OH + 0.047 MACR + 0.073 MVK + 0.120 HO2 + 0.120 FORM	0.074e-11*exp(700/T)	(*51*)	L
IEPOXOO + HO2 → 0.725 HAC + 0.275 GLYC + 0.275 GLYX + 0.275 MGLY + 1.125 OH + 0.825 HO2 + 0.200 CO2 + 0.375 FORM + 0.074 FORMIC + 0.251 CO	0.074e-11*exp(700/T)	(*51*)	L
All other peroxyradicals + HO2 → OP2	7.7e-14*exp(1300/T)	(*27, 155*)	
CH3OO + NO (+O2) → FORM + HO2 + NO2	3e-12*exp(280/T)	(*27, 151*)	
DIBOO + NO → NO2 + HO2 + 0.52*(GLYC + MGLY) + 0.48*(GLYX + HAC)	0.81e-11	(*152*)	H
MVKP + NO → 0.625*(GLYC + CH3CO3) + 0.265*(MGLY + FORM + HO2)+ 0.11 MVKN +0.89 NO2	0.81e-11	(*152*)	
MACP + NO → 0.85*(NO2 + HO2) + 0.425*(HAC + CO) + 0.425*(FORM + MGLY) + 0.15 MACRN	0.81e-11	(*152*)	
TCO3 + NO → 0.89 GLY + 0.11 MGLY +	4.2e-12*exp(180/T)	(*27, 156*)	

0.05 CH3CO3 + 0.95 CO + 2 XO2 + NO2 + 0.92 HO2			
OLTP + NO → ALD + FORM + NO2 + HO2	4.2e-12*exp(180/T)	(*27*)	
HC3P + NO → 0.75 ALD + 0.25 KET + 0.09 FORM + 0.036 ONIT + 0.964 NO2 + 0.964 HO2	4.2e-12*exp(180/T)	(*27*)	
KETP + NO → MGLY + NO2 + HO2	4.2e-12*exp(180/T)	(*27*)	
ETHP + NO → ALD + HO2 + NO2	4.2e-12*exp(180/T)	(*27*)	
CH3CO3 + NO → NO2 + CO + CO2 + FORM + CH3OO	2.1e-11	(*152*)	
MOBAOO + NO → HC4 + CO2 + HO2 + NO2	0.8e-11	(*152*)	H
ISOPNOOb + NO → 0.6*(GLYC + HAC)+0.4*(FORM + HO2)+0.26 MACRN + 0.14 MVKN + 1.6 NO2	0.81e-11	(*152*)	H
ISOPNOOd + NO → 0.34 DHBN + 0.15 PROPNN + 0.44 HAC + 0.07 MVKN + 0.13 ETHLN + 0.31 FORMIC + 0.31 NO3 + 0.72 FORM + 0.15 GLYC + 1.34 NO2 + 0.35 HO2	0.81e-11	(*152*)	H
ISOPOO + NO → 0.26 MACR + 0.40 MVK + 0.883 NO2 + 0.66 FORM +0.07 ISOPNd + 0.047 ISOPNb + 0.10 HC5 + 0.043 MF + 0.08 DIBOO + 0.803 HO2	0.81e-11	(*152*)	H
HC5OO + NO → NO2 + 0.234*(GLYC + MGLY) + 0.216*(GLYX + HAC) + 0.29 DHMOB + 0.17 MOBA + 0.09 HC4 + 0.09 CO + HO2	0.81e-11	(*152*)	H
MVKP or MACP + ISOPOO → 0.3 MACR + 0.3 MVK + 0.6 MGLY + FORM + 1.2 HO2 + 0.1 DCB + 0.4 OLT + 0.3 OLI	3.5e-15	(*27, 51, 155*)	L, b
ISOPOO + ISOPOO → 0.34 MACR + 0.42 MVK + 0.3 OLT + 0.06 DCB + 0.1 OLI + 1.3 HO2 + 0.55 FORM + 0.1 MGLY	7e-16	(*27, 51, 155*)	L, b
CH3CO3 + NO2 → PAN	2.8e-12*exp(181/T)	(*27, 156*)	
PAN → CH3CO3 + NO2	1.95e16*exp(-13543/T)	(*27, 156*)	
PAN + OH → FORM + NO2 + CO	3e-14	(*61*)	
HC5OO, MOBAOO, TCO3 + NO2 → APN	1e-11	(*158*)	
APN → HC5OO, MOBAOO, TCO3 + NO2	4.6e-4	(*158*)	
APN + OH → ALD + NO2 + CO	3.2e-11	(*158*)	

    a. L = Low-NOx scheme only, H = high-NOx scheme only

    b. Rate adjusted to improve agreement with Paulot et al. (2009) gas-phase chamber data

    c. Condensed from The Master Chemical Mechanism (MCMv3.2) (*60, 61*)

Table A-8 – Aqueous-phase thermal reactions

Reaction	Rate $(M^{1-n} s^{-1})$	Ref.	Note[a]
OH + H2O2 → HO2 + H2O	2.7e7	(*27, 150*)	
HO2 + H2O2 → OH + H2O + O2	3.7	(*159*)	
HO2 + HO2 → H2O2 + O2	8.3e5	(*27, 62, 159*)	
OH + HO2 → H2O + O2	7.1e9	(*27, 150*)	
SO4- + SO4- → S2O8-	6.1e8	(*89, 160*)	
SO4- + H2O2 → sulfate + H+ + HO2	1.7e7	(*89*)	CAPRAM average value
SO4- + HO2 → sulfate + H+ + O2	3.5e9	(*89, 161*)	
SO4- + O2- → sulfate + O2	3.5e9	(*89*)	
bisulfate + OH → SO4- + H2O	3.5e5	(*89, 162*)	
HO2 + O2- →H2O2 + O2	9.7e7	(*89, 163*)	
OH + OH → H2O2	5.5e9	(*150*)	
OH + O2- → OH- + O2	1.0e10	(*150*)	
H2SO4 + OH → HSO4rad + H2O	1.4e7	(*48, 162*)	
CO2- + O2 → O2- + CO2	2.4e9	(*159*)	
HCO3- + OH → H2O + CO3-	1e7	(*27, 150, 164, 165*)	
CO3- + O2- → O2 + CO3-2	6.5e8	(*27, 150, 163, 164*)	
CO3- + H2O2 → HCO3- + HO2	8e5	(*159*)	
CO3- + FORMIC- → HCO3- + CO2-	1.5e5	(*27, 150, 164*)	
GLYX + OH → GLYR + H2O	1.1e9	(*27, 159, 165*)	
FORMIC + OH (+O2) → COOH + H2O	1e8	(*48, 159*)	
MGLY + OH → 0.92 PYRAC- + 0.08 GLYAC- + HO2 + H2O	7e8	(*27, 166*)	
GLYC + OH (+O2) → GLYCR1 + H2O	5e8	(*48, 62*)	
GLYC + OH (+O2) → GLYCR2 + H2O	1e9	(*48, 62*)	
FORMIC- + OH (+O2) → H2O + CO2-	3.1e9*exp(-1240/T)	(*27, 165*)	
OXLAC + OH → COOH + CO2 + 2H2O	1.4e6	(*48, 159*)	
OXLAC- + OH → COOH + CO2- + 2H2O	2e7	(*27, 62, 159*)	
OXLAC-- + OH → COOH + CO2- + OH-	4e7	(*27, 62, 159*)	
GLYAC + OH → GLYACR + H2O	3.62e8	(*27, 159, 166*)	
GLYAC- + OH → GLYACR- + H2O	2.9e9	(*27, 62, 159*)	
GLYCAC + OH (+O2) → GLYCACR + H2O	6e8	(*48, 167*)	
GLYCAC- + OH (+O2) → GLYCACR- + H2O	8.6e8	(*27, 150*)	
PYRAC + OH → ACETIC + HO2 +	6e7	(*27, 166*)	

CO2			
PYRAC- + OH → ACETIC- + HO2 + CO2	6e7	(*27, 166*)	
ACETIC + OH → 0.85 GLYAC + 0.15 FORM	1.6e7	(*27, 168*)	
ACETIC- + OH → 0.85 GLYAC- + 0.15 FORM	8.5e7	(*27, 168*)	
ISOP + OH → 0.241 MVK + 0.109 MACR + 0.114 MGLY + 0.038 GLYX + 0.262 OXALIC + (oligomers)	1.2e10	(*169*)	
c2rad (GLYR+GLYACR+GLYACR- +GLYCR1+GLYCR2+GLYCACR+GL YCACR-) + c2rad → SUCCINIC	1.3e9	(*48, 170*)	
c1rad (CHOHOH+COOH+CH2OH) + c2rad → MALONIC	1.3e9	(*48, 170*)	
GLYCR1 + O2 → GLYCR1O2	1e6	(*48, 170*)	
GLYCR2 + O2 → GLYCR2O2	1e6	(*48, 170*)	
GLYCR1O2 → GLYCAC + HO2	50	(*48, 171*)	
GLYCR2O2 → GLY + HO2	50	(*48, 171*)	
GLYCR1O2 + GLYCR1O2 → CH2OH + CO2	3e8	(*48*)	
MALONIC + OH → MArad + H2O	3e8	(*48, 172*)	
MArad + O2 → MAradO2	1e6	(*48, 170*)	
MAradO2 → X + HO2	50	(*48, 171*)	
MAradO2 + MAradO2 → 2 COOH + 2 GLYAC	3e8	(*48*)	
SUCCINIC + OH → SArad + H2O	1.1e8	(*48, 172*)	
SArad + O2 → SAradO2	1e6	(*48, 170*)	
SAradO2 → Y + HO2	50	(*48, 171*)	
SAradO2 + SAradO2 → 2 GLYAC	3e8	(*48*)	
CHOHOH + COOH → GLYAC	1.3e9	(*48, 170*)	
COOH + COOH → OXLAC	1.3e9	(*48, 170*)	
GLYCR2O2 + GLYCR2O2 → GLY + GLYAC + FORMIC + CHOHOH	3e8	(*48*)	
GLYCACR + O2 → GLYCACRO2	1e6	(*48, 170*)	
GLYR + O2 → GLYRO2	1e6	(*48, 170*)	
GLYRO2 → GLYAC + HO2	50	(*48, 171*)	
GLYRO2 + GLYRO2 → 2CHOHOH + 2 CO2 + O2 + 2 H2O	3e8	(*48*)	
CHOHOH + O2 → FORMIC + HO2	5e6	(*48, 171*)	
GLYCACRO2 → GLYAC + HO2	50	(*48, 171*)	
CH2OH + O2 → CO + HO2	1e6	(*48, 171*)	
CHOHOH + CHOHOH → GLYX	1.3e9	(*48, 170*)	
GLYACR + O2 → GLYACRO2	1e6	(*48, 170*)	
GLYACRO2 → OXLAC + HO2	50	(*48, 171*)	

GLYACRO2 + GLYACRO2 → 2 CO2 + 2 COOH	3e8	(*48*)	
COOH + O2 → CO2 + HO2	5e6	(*48, 170*)	
GLYACR- + O2 → GLYACRO2-	1e6	(*48, 170*)	
GLYACRO2- → OXLAC- + HO2	50	(*48, 171*)	
GLYACRO2- + GLYACRO2- → 2 CO2- + 2 COOH	3e8	(*48*)	
FORM + SO4- → HO2 + CO + bisulfate	1.4e7	(*173*)	
FORMIC +SO4- (+O2) → bisulfate + COOH	1.4e6	(*27, 150, 174*)	
FORMIC- +SO4- (+O2) → bisulfate + CO2-	1.1e8	(*27, 150, 174*)	
GLYX + SO4- → GLYR + bisulfate	2.4e7	(*173*)	
GLYAC + SO4- → GLYACR + bisulfate	7.9e6	(*48*)	c
GLYACR + SO4- → GLYACOS	1e8	(*48*)	b
GLYAC- + SO4- → GLYACR- + bisulfate	6.3e7	(*48*)	c
GLYACR- + SO4- → GLYACOS	1e8	(*48*)	b
GLYR + SO4- → GLYOS	1e8	(*48*)	b
GLYCR1 + SO4- → GLYCOS	1e8	(*48*)	b
GLYCR2 + SO4- → GLYCOS	1e8	(*48*)	b
GLYCACR + SO4- → GLYCACOS	1e8	(*48*)	b
GLYCACR- + SO4- → GLYCACOS	1e8	(*48*)	b
ISOP + SO4- → ISOPOS	1e8	(*48, 86*)	d
MVK + SO4- → MVKOS	1e8	(*48, 86*)	d
MACR+ SO4- → MACROS	1e8	(*48, 86*)	d
GLYR + HSO4rad → GLYOS	1e8	(*48*)	
GLYCR1 + HSO4rad → GLYCOS	1e8	(*48*)	
GLYCR2 + HSO4rad → GLYCOS	1e8	(*48*)	
GLYCACR + HSO4rad → GLYCACOS	1e8	(*48*)	
GLYCACR- + HSO4rad → GLYCACOS	1e8	(*48*)	
IEPOX + sulfate → IEPOXOS	(5e-2*aH +2e-4 *[sulfate]*aH +7.3e-4*[bisulfate]) * BETA	(*108*)	L
IEPOX + H2O → tetrol	(5e-2*aH +2e-4 *[sulfate]*aH +7.3e-4*[bisulfate])	(*108*)	L

	* (1-BETA)		
TOL_EPOX + sulfate → TOL_EPOX OS	(5e-2*aH +2e-4 *[sulfate]*aH +7.3e-4*[bisulfate]) * BETA	(*108*)	e
TOL_EPOX + H2O → TOL_EPOX diol	(5e-2*aH +2e-4 *[sulfate]*aH +7.3e-4*[bisulfate]) * (1-BETA)	(*108*)	e
EPXC4DIAL + sulfate → EPXC4DIALOS	(5e-2*aH +2e-4 *[sulfate]*aH +7.3e-4*[bisulfate]) * BETA	(*108*)	e
EPXC4DIAL + H2O → EPXC4DIAL_diol	(5e-2*aH +2e-4 *[sulfate]*aH +7.3e-4*[bisulfate]) * (1-BETA)	(*108*)	e
XYL_EPOX + sulfate → XYL_EPOX OS	(5e-2*aH +2e-4 *[sulfate]*aH +7.3e-4*[bisulfate]) * BETA	(*108*)	e
XYL_EPOX + H2O → XYL_EPOX diol	(5e-2*aH +2e-4 *[sulfate]*aH +7.3e-4*[bisulfate]) * (1-BETA)	(*108*)	e
EPXC4MDIAL + sulfate → EPXC4DIAL OS	(5e-2*aH +2e-4 *[sulfate]*aH +7.3e-4*[bisulfate]) * BETA	(*108*)	e

EPXC4MDIAL + H2O → EPXC4DIAL_diol	(5e-2*aH +2e-4 *[sulfate]*aH +7.3e-4*[bisulfate]) * (1-BETA)	(*108*)	e

a. L = Low-NOx scheme only, H = high-NOx scheme only
b. Assume same mechanism, rate as HSO4rad
c. Assume the same ratio as glyoxal for the rates of H abstraction by SO4- vs. OH
d. Mechanism from Noziere et al. (2010), assuming rate following Perri et al. (2010)
e. Assuming same mechanism, rate as IEPOX

Table A-9 - Model Initial Conditions.

For all gas-phase species not listed here, initial concentration = 0. Values adopted from CAPRAM 3.0 (*89*) except as noted.

Species	Low-NOx (ppb)	High-NOx (ppb)	Note
Isoprene	1	0.1	
Glyoxal	0.1	0.1	
Methylglyoxal	0.1	0.1	
CO	150	200	
HOOH	1	1	
OH	4e-5	4e-5	estimate
Formaldehyde	0.5	0.1	
Acetic acid	0.001	0.001	
SO2	1	10	
NO2	0.3	4.5	
HNO3	0.3	1	
O3	40	90	
C2H2	0.5	3	(*175*)
OLT	0.1	0.1	
ALD	0.1	0.1	
OP2	0.01	0.01	
KET	0.1	0.1	
CH3OH	2	5	
CH3O2H	0.01	0.01	
PAN	0.01	0.01	
APN	0.001	0.001	Estimate
Toluene	0.01	0.1	
Cresol	0.001	0.001	
Xylenes	0.01	0.1	
CO2	3.57e5	5e5	
CH4	1700	1700	
H2O	Calculated based on specified RH		

Table A-10 – Emission Rates

All values adopted from CAPRAM 3.0 (*89*). Assumes mixing height of 10^5 cm.

Species	Low-NOx ($cm^{-2} s^{-1}$)	High-NOx ($cm^{-2} s^{-1}$)	Note
Isoprene	1.5e6	1.54e5	= 0 at nighttime
CO	3.7e6	8.99e7	
Formaldehyde	3028	2.58e5	
Acetic acid	3350	8.44e4	
SO2	2.91e5	3.27e7	
NO	2.86e5	1.01e7	
OLT	7950	4.94e5	
ALD	3171	5.93e5	
KET	8920	9.9e5	
CH3OH	1.07e4	1.16e6	
CH3OOH	3350	8.44e4	Assumed same as acetic acid
Toluene	2.108e4	1.7e6	
Cresol	2.88e4	1.82e6	
Xylenes	1.13e4	9.88e5	

Table A-11 – Deposition Rates

All values adopted from CAPRAM 3.0 (*89*). Assumes mixing height of 10^5 cm.

Species	Deposition rate (s^{-1})
CO	1e-6
HOOH	1e-5
Formaldehyde	1e-5
Formic acid	1e-5
SO2	1e-5
NO2	4e-6
N2O5	2e-5
HNO3	2e-5
O3	4e-6
CH3OH	1e-5
CH3O2H	5e-6

Table A-12 – List of SOA molecular weights, O:C ratios, and H:C ratios

Species Name	Abbreviation	Formula	Molecular Weight	O:C	H:C
2-methyl tetrol	[tetrol]	C5H12O4	136.15	0.8	2.4
Formic acid	[FORMIC]	CH2O2	46.03	2	2
Formate ion	[FORMIC-]	CHO2	45.02	2	1

Glycolic acid	[GLYCAC]	$C_2H_4O_3$	76.05	1.5	2
Glycolate (I) ion	[GLYCAC-]	$C_2H_3O_3$	75.04	1.5	1.5
Pyruvic acid	[PYRAC]	$C_3H_4O_3$	88.06	1	1.33
Pyruvate (I) ion	[PYRAC-]	$C_3H_3O_3$	87.05	1	1
Acetic acid	[CH3CO2H]	$C_2H_4O_2$	60.05	1	2
Acetate ion	[CH3CO2-]	$C_2H_3O_2$	59.04	1	1.5
Carbon dioxide	[CO2]	CO_2	44.01	2	0
Isoprene	[ISOP]	C_5H_8	68.12	0	1.6
Glyoxal-derived organosulfate	[GLYOS]	$C_2H_2O_6S$	122.03	3	1
Glycolaldehyde-derived organosulfate	[GLYCOS]	$C_2H_4O_6S$	124.05	3	2
Glyoxylic acid-derived organosulfate	[GLYCACOS]	$C_2H_4O_7S$	140.05	3.5	2
Succinic acid	[SUCCINIC]	$C_4H_6O_4$	118.09	1	1.5
Malonic acid	[MALONIC]	$C_3H_4O_4$	104.06	1.33	1.33
Carbon monoxide	[CO]	CO	28.01	1	0
Carbon dioxide anion	[CO2-]	CO_2-	44.01	2	0
Bicarbonate (I) ion	[HCO3-]	HCO_3-	61.02	3	1
Carbonate (II) ion	[CO3--]	CO_3--	60.01	3	0
Carbonate radical	[CO3-]	CO_3--	60.01	3	0
2,3-epoxy-6-oxo-heptanal	TOL_EPOX	$C_7H_6O_3$	138.06	0.43	0.86
2,3-epoxy-6-oxo-heptanal derived diols	TOL_EPOX diol	$C_7H_8O_4$	156.08	0.57	1.14
2,3-epoxy-6-oxo-heptanal derived organosulfates	TOL_EPOX OS	$C_7H_8O_7S$	239.08	1	1.14
Unsaturated aldehydes[a]	ALD	n/a	97.4	0.43	1.27
C4-epoxy-dial	EPXC4DIAL	$C_4H_4O_3$	100.04	0.75	1
C4-epoxy-dial-derived diols	EPXC4DIAL diol	$C_4H_6O_4$	118.06	1	1.5
C4-epoxy-dial-derived organosulfates	EPXC4DIAL OS	$C_4H_6O_7S$	201.06	1.75	1.5
Xylene-derived epoxide	XYL_EPOX	$C_8H_{10}O_3$	154.1	0.38	1.25
Xylene-derived epoxide diols	XYL_EPOX_DIOL	$C_8H_{12}O_4$	172.12	0.5	1.5
Xylene-derived epoxide organosulfates	XYL_EPOX_OS	$C_8H_{12}O_7S$	255.12	0.88	1.5
Methyl-C4-epoxy-dial	EPX4MDIAL	$C_5H_6O_3$	114.06	0.6	1.2
Methyl-C4-epoxy-dial diols	EPX4MDIAL_DIOL	$C_5H_8O_4$	132.08	0.8	1.6
Methyl-C4-epoxy-dial organosulfate	EPX4MDIAL_OS	$C_5H_8O_7S$	215.08	1.4	1.6

[a]Average of values considered.

A.2 – Density functional theory calculations

Ab initio calculations were used to analyze the reaction pathways for the hydrolysis and reaction with HSO_4^- for TOL_EPOX, XYL_EPOX, EPXC4DIAL, and EPXMC4DIAL. Geometry optimizations, transition state searches, and energy calculations were performed using Jaguar 7.0 (Schrödinger). Density functional theory (DFT) with the B3LYP functional and 6-31G** basis set was used. These ab initio calculations were performed for gas phase species. Including Poisson-Boltzmann solvation with a water solvent did not significantly impact the calculation results (*4, 176*).

Rate constants were calculated from the output of the Jaguar calculations using transition state theory as follows:

$$k = L^{\ddagger} \frac{k_B T}{h} \frac{Q^{\ddagger}}{Q_A Q_B} \exp\left(-\frac{\Delta E_0}{k_B T}\right) \tag{A-1}$$

where $L^{\ddagger}$ is a symmetry correction factor, k_B is Boltzman's constant, T is absolute temperature, h is Planck's constant, and ΔE_0 is the change in zero point energy. Q_A, Q_B, and $Q^{\ddagger}$ are the overall partition functions for the reactants and the transition state.
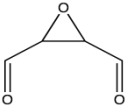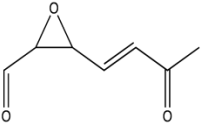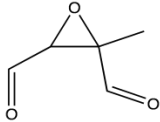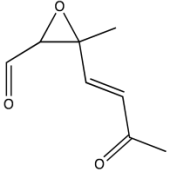
Our results show that hydrolysis and organosulfate formation are thermodynamically favorable for each of the epoxide precursors studied. Changes in Gibbs free energy for the reactions are summarized in Table S12. All of the reactions are exothermic. The rate determining step for each reactive system was found to be the attack of the nucleophile (HSO_4^- or H_2O) on the protonated epoxide. Note that the ΔG values reported for the hydrolysis reactions in Table S12 do not take into account deprotonation of the hydrolysis product after H_2O addition. This step was found to be endothermic, with ΔG ranging from +22 to +33 kcal mol^{-1}, in our gas-phase

calculations. Despite the endothermic nature of this step, the overall ΔG including deprotonation is still negative for each of the hydrolysis pathways studied. The deprotonation step would likely be facilitated in an aqueous environment as compared to our gas-phase calculations.

Using the data for the rate determining transition states, we calculated the rate constants for each reaction. These results are also summarized in Table A-13. Each of the reactions are predicted to have large rate constants relative to those that have been recently measured for the IEPOX hydrolysis and organosulfate reactions (*108*, *177*). Significant uncertainty exists in predictions of rate constants using density functional theory, so for the purposes of GAMMA we have assumed that each of these reactions proceeded at the observed rates for IEPOX.

Taken together, our calculations predict that the formation of SOA and organosulfates from TOL_EPOX, XYL_EPOX, EPXC4DIAL, and EPXMC4DIAL should be thermodynamically and kinetically favorable. These predictions should be confirmed experimentally, and rate constants for these processes should be measured.

Table A-133 – Calculated overall free energy changes and rate constants for aqueous aerosol-phase reactions of toluene and xylene-derived epoxides

Epoxide precursor	Reaction	ΔG (kcal mol^{-1})	Rate Constant k (M^{-1} s^{-1})
EPXC4DIAL	Protonation	-5.56	
	Hydrolysis	-35.22	2.95E+04
	HSO$_4^-$ addition	-155.99	6.43E+03
TOL_EPOX	Protonation	-24.47	
	Hydrolysis	-29.20	1.02E+03
	HSO$_4^-$ addition	-149.88	1.12E+01
EPXMC4DIAL	Protonation	-7.37	
	Hydrolysis	-39.67	2.14E+03
	HSO$_4^-$ addition	-151.88	4.03E+02
XYL_EPOX	Protonation	-38.97	
	Hydrolysis	-42.02	5.38E+05
	HSO$_4^-$ addition	-148.79	1.17E+01

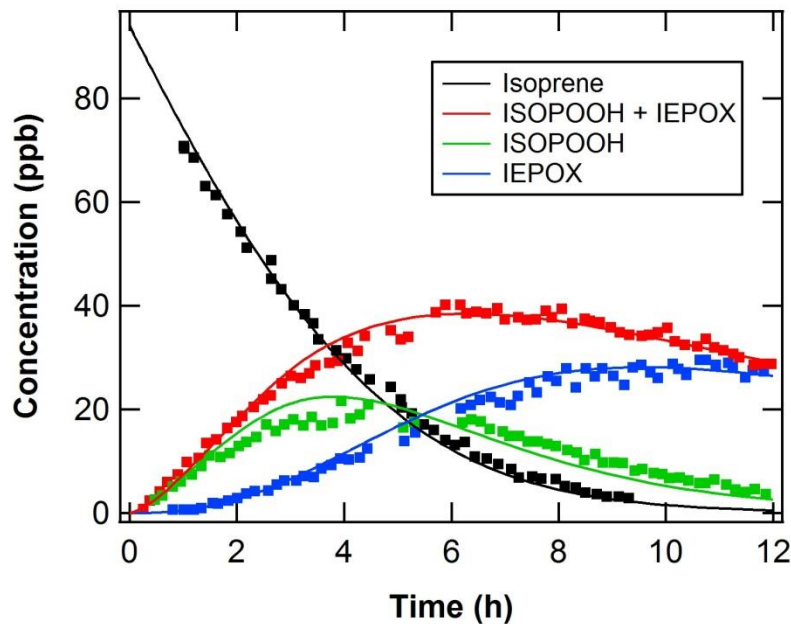**A.3 – Model comparison with experiments of Paulot et al. (2009a)**

Figure A-1 – Comparison of low-NOx model output (curves) with experimental data from Paulot et al. (2009a) (points).

A.4 – Light Absorption Module Detailed Information

Table A-14 – List of UV-visible spectra followed by GAMMA absorption module.

Species Name	Detection Range	Reference
Glyoxal oligomer, [PGly]	190-800	(*5*)
Methylglyoxal oligomer, [PMgly]	190-800	(*5*)
Oxalic Acid [OXLAC]	275-305	(*95*)
Succinic Acid [SUCCINIC]	265-400	(*96*)
Acetaldehyde oligomer, [PAld][a]	190-800	(*7*)

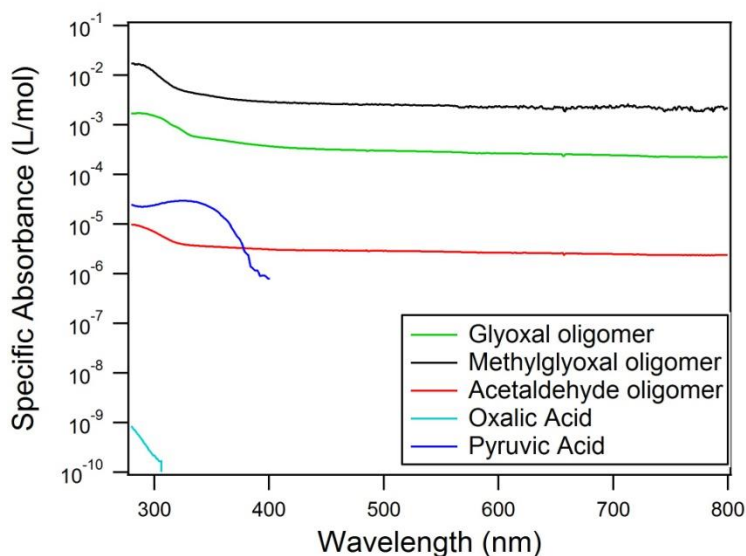*[a] Acetaldehyde treated as a proxy for all multicarbon (C>2) aldehydes.*

Figure A-2 – Specific absorbances used for calculation of composite absorption spectra in Chapter 3. Data unavailable for oxalic acid for λ > 305nm, and for pyruvic acid for λ > 400nm

A.5 – MAE Calculations

Mass absorption efficiency was calculated from model output following Hecobian et al. (*92*) as follows:

$$MAE = \frac{E_{365} - E_{700}}{c_{org}} \qquad \text{(A-2)}$$

Where c_{org} is the calculated organic aerosol loading, in g-C/m^3. E_λ is given by:

$$E_\lambda = \sum_i \varepsilon_{\lambda,i} c_i \qquad \text{(A-3)}$$

Where $\varepsilon_{i,\lambda}$ is the molar absorptivity of species *I* of wavelength λ in L/mol-m, and c_i is its corresponding in-particle concentration in mol/L.